

Synthesis and application of ruthenium(II) alkenyl complexes with perylene fluorophores for the detection of toxic vapours and gases

José García-Calvo,^[a] Jonathan A. Robson,^[b] Tomás Torroba*^[a]
and James D. E. T. Wilton-Ely*^[b]

[a] *Dr. J. García-Calvo, Prof. Dr. T. Torroba*
Department of Chemistry, Faculty of Science, University of Burgos, 09001
Burgos (Spain)
E-mail: ttorroba@ubu.es

[b] *Dr. J. A. Robson, Prof. Dr. J. D. E. T. Wilton-Ely*
Department of Chemistry, Imperial College London,
Molecular Sciences Research Hub, White City Campus, London W12 0BZ
(UK).
E-mail: j.wilton-ely@imperial.ac.uk

Keywords

Ruthenium, vinyl, perylene, sensing

Abstract

A series of new ruthenium(II) vinyl complexes has been prepared incorporating perylenemonoimide (PMI) units. This fluorogenic moiety was functionalised with terminal alkyne or pyridyl groups, allowing attachment to the metal either as a vinyl ligand or through the pyridyl nitrogen. The inherent low solubility of the perylene compounds was improved through the design of poly-PEGylated (PEG = polyethylene glycol) units bearing a terminal alkyne or a pyridyl group. By absorbing the compounds on silica, vapours and gases could be detected in the solid state. The reaction of the complexes $[\text{Ru}(\text{CH}=\text{CH}-\text{Per}^{\text{Im}})\text{Cl}(\text{CO})(\text{py}-3\text{PEG})(\text{PPh}_3)_2]$ and $[\text{Ru}(\text{CH}=\text{CH}-3\text{PEG})\text{Cl}(\text{CO})(\text{py}-\text{Per}^{\text{Im}})(\text{PPh}_3)_2]$ with carbon monoxide, isonitrile or cyanide was found to result in modulation of the fluorescence behaviour. The complexes were observed to display solvatochromic effects and the interaction of the complexes with a wide range of other species was also studied. The study suggests that such complexes have potential for the detection of gases or vapours that are toxic to humans.

Introduction

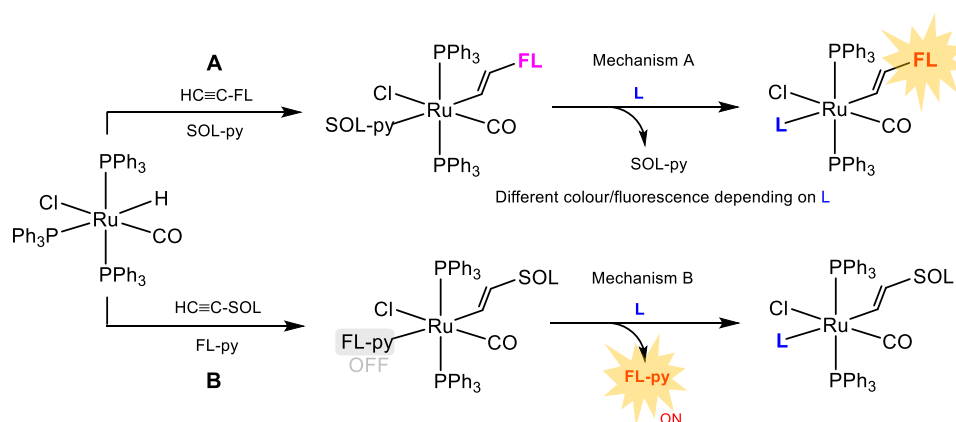
The growth in interest in vinyl complexes of the heavier congeners of group 8 started around 30 years ago¹⁻⁹ and, since then, these versatile complexes have attracted much attention. Although other approaches are known, the most widely used route to ruthenium vinyl complexes, such as the 5-coordinate compounds $[\text{Ru}(\text{CR}=\text{CHR}')\text{Cl}(\text{CO})(\text{PR}_3)_2]$ ($\text{R} = \text{Ph}, \text{Pr}^i$), is through the hydrometallation of alkynes by the compounds $[\text{RuHCl}(\text{CO})(\text{PPh}_3)_3]$ ^{1a} and $[\text{RuHCl}(\text{CO})(\text{PPr}^i_3)_2]$.^{3a} Harris and Hill reported a modification of this approach to yield the triphenylphosphine derivatives, which avoided contamination with tris(phosphine) side products by using $[\text{RuHCl}(\text{CO})(\text{BSD})(\text{PPh}_3)_2]$ as the precursor.^{10a} The labile 2,1,3-benzoselenadiazole (BSD) ligand permitted insertion of alkynes into the Ru-H bond to yield the coordinatively-saturated products $[\text{Ru}(\text{CR}=\text{CHR}')\text{Cl}(\text{CO})(\text{BSD})(\text{PPh}_3)_2]$ ($\text{R}, \text{R}' = \text{H}$ or alkyl/aryl substituents).^{10a} Our work has focused on the analogous 2,1,3-benzothiadiazole (BTD) complexes, including osmium examples,^{10b} which use the cheaper BTD heterocycle. Through the lability of the chloride and phosphine ligands (and BTD/BSD, if present), mono-,^{11,12} bi-^{13,14,15} and tridentate¹⁶ donors can be coordinated to these vinyl compounds. This provides ample demonstration of the reactivity at the metal centre, however, the installation of the vinyl ligand through facile reaction with terminal alkynes (also internal alkynes under more forcing conditions) allows the incorporation of further functionality that can be influenced by the metal centre.¹⁷ Our recent work has demonstrated the potential of this approach through the selective detection of very low concentrations of carbon monoxide both in air^{12a,b} and in cells,^{12c,d} following work by others in the area.^{12e-t} Among other features, this contribution provides an illustration of the versatility of such ruthenium vinyl complexes to install a fluorophore either through coordination to the metal centre or as the substituent of the vinyl itself.

Perylenemonoimide (PMI) compounds have been demonstrated to be effective fluorescent signalling units for use in fluorogenic sensors.¹⁸ They possess many advantages with respect to other more classical and widely-used fluorescent molecules, such as BODIPY (boron dipyrromethene) derivatives. For example, they display excitation/emission wavelengths in the visible and near-IR regions of the spectrum, which offer substantial advantages in terms of biological imaging. As well as excellent thermal and photo-stability, PMI compounds are tolerant towards a wide range of different reagents and are easily functionalised, for example by bromination followed by Suzuki coupling.¹⁹ All the above characteristics are exploited here to allow the incorporation of PMI units into divalent ruthenium vinyl complexes for application in the

detection of a range of analytes. The use of silica supports in this work provides an illustration of the use of these inorganic materials as an inexpensive and efficient method for enhancing the application of colorimetric or fluorogenic chemosensors.^{12,19}

Results and Discussion

Two different approaches were used to incorporate fluorescent units into ruthenium vinyl complexes.¹² The two designs are shown in Scheme 1 and involve the fluorophore as either the vinyl substituent or the ligand directly attached to the metal centre.

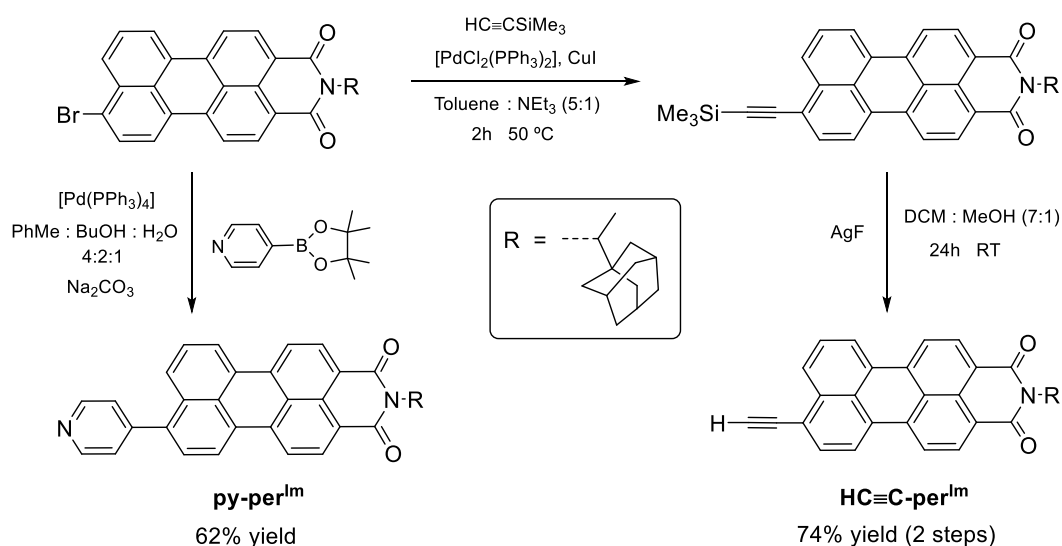


Scheme 1. Two approaches to functionalising ruthenium vinyl complexes with fluorogenic units. FL = fluorophore, SOL = solubilizing unit.

The benefits of mechanism **A** include the fact that the fluorophore is retained within the metal complex, ensuring that the metal complex is located where fluorescence is observed. The fluorogenic response originates from the electronic changes caused by displacement of the ligand *trans* to the vinyl group by the analyte (L). This also leads to a modulation of the colour observed in many cases. However, mechanism **B** can often result in a greater fluorescence revival as the fluorophore is completely detached from the metal centre, allowing the quenching (heavy atom effect²⁰) to be fully removed, resulting in a turn-ON fluorescence response.²¹ A possible disadvantage of mechanism **B** is that premature displacement of the fluorophore is more likely and that, once displacement occurs, the fluorophore and the metal complex may not remain co-localised. However, this design does allow the facile addition of other functional units (e.g., to enhance solubility or cellular targeting) to the vinyl ligand through use of a functionalised terminal alkyne.

Synthesis of fluorophores and solubilizing units

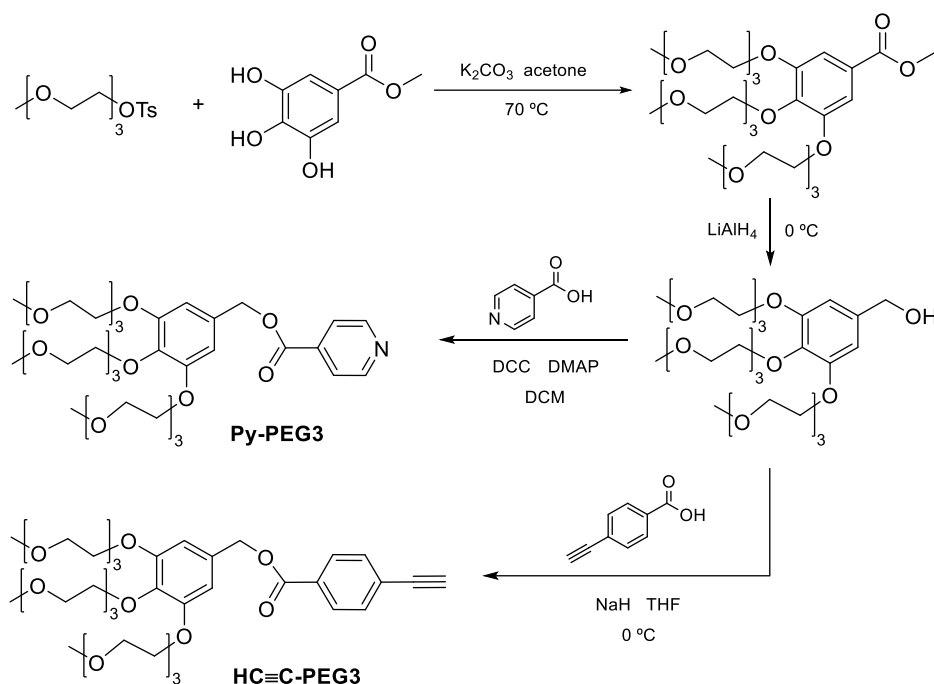
In order to explore both sensing mechanisms shown in Scheme 1, two new PMI derivatives, **py-per^{lm}** and **HC≡C-per^{lm}**, were prepared with ethynyl and pyridyl functionality. This was achieved starting from the 9-bromo derivative, as shown in Scheme 2:



Scheme 2. Synthesis of new perylene monoimide derivatives.

The synthesised compounds, **py-per^{lm}** and **HC≡C-per^{lm}**, were fully characterised using ¹H and ¹³C{¹H} NMR and infrared spectroscopies and mass spectrometry. Both compounds possess an imide group with a bulky aliphatic group (1-adamantylethylamine) to increase solubility and were synthesised using palladium-catalysed C-C coupling approaches. A Suzuki reaction was used to prepare **py-per^{lm}** while **HC≡C-per^{lm}** was obtained as the product of a Sonogashira coupling after a deprotection step. Both compounds were purified using column chromatography (silica gel) and were obtained as red solids in good yields (further details in Supporting Information).

Perylenemonoimide compounds often suffer from poor solubility and it was considered likely that this characteristic would also be imparted to their metal complexes. It was therefore decided to devise a solubilizing unit that could be used with both designs shown in Scheme 1. This led to the synthesis of a structure with three polyethylene glycol chains and this was used to generate two new pyridyl (**py-PEG3**) and alkynyl (**HC≡C-PEG3**) derivatives (Scheme 3).



Scheme 3. Synthesis of PEGylated units suitable for use in aqueous and polar solvents.

These solubilizing units, **py-PEG3** and **HC≡C-PEG3**, were fully characterised by ^1H , $^{13}\text{C}\{^1\text{H}\}$ NMR and infrared spectroscopies and mass spectrometry. Both **py-PEG3** and **HC≡C-PEG3**, were obtained as pale yellow oils after purification by column chromatography in DCM : MeOH mixtures. Characteristic signals were observed, such as the 5.26 ppm singlet attributed to the terminal alkyne in the ^1H NMR spectrum (see Supporting Information).

With the perylenemonoimide fluorophores and the complementary PEGylated solubilizing units prepared, the focus moved to the synthesis of the ruthenium vinyl complexes.

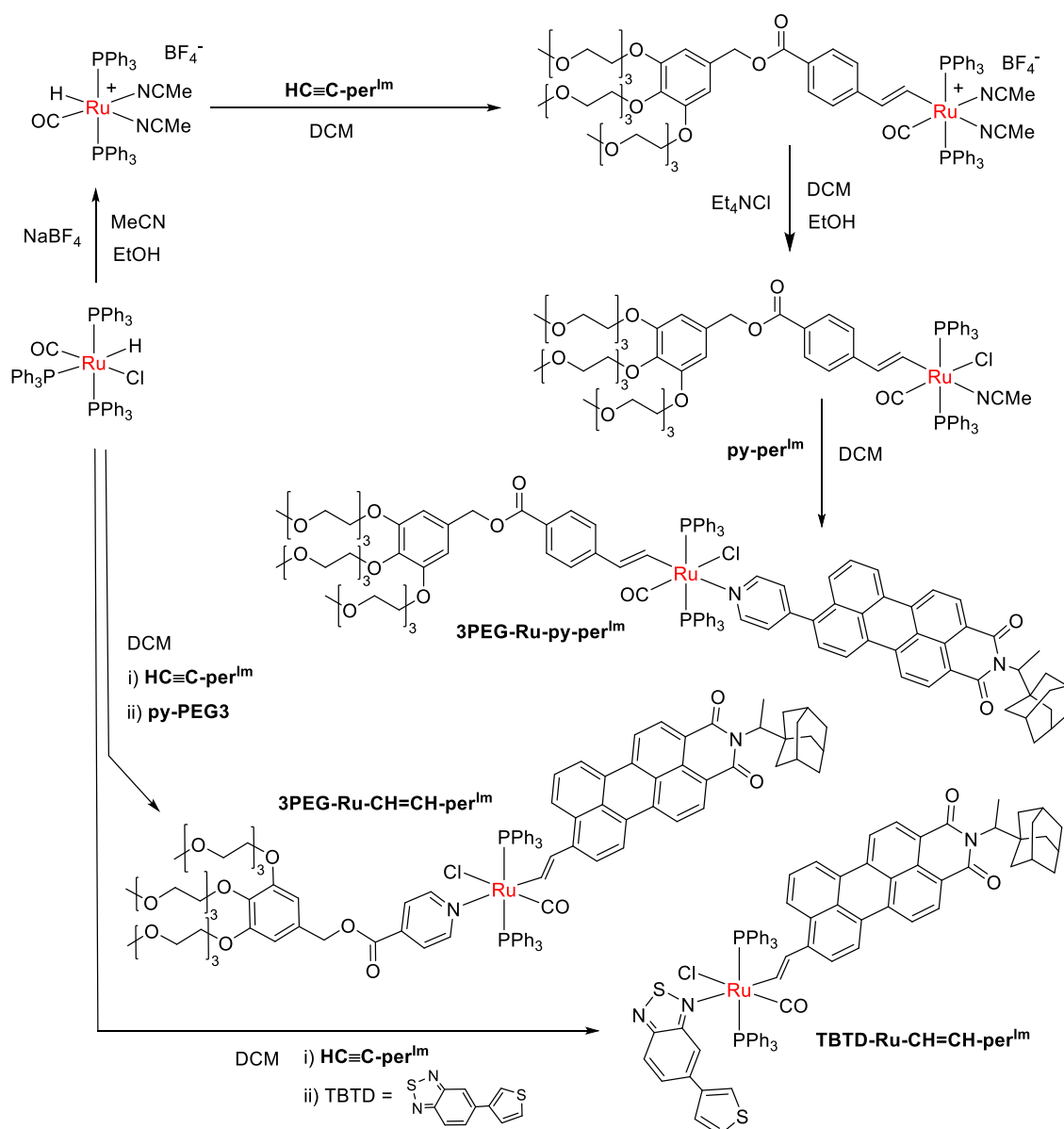
Ruthenium vinyl complexes

Two approaches were employed to synthesise the new ruthenium vinyl complexes reported in this contribution. The most straightforward approach utilises the 5-coordinate triphenylphosphine compounds first reported by Santos and co-workers,^{1a} $[\text{Ru}(\text{CH}=\text{CHR})\text{Cl}(\text{CO})(\text{PPh}_3)_2]$, which are formed by the hydrometallation of alkynes by the commercially-available tris(phosphine) compound, $[\text{RuHCl}(\text{CO})(\text{PPh}_3)_3]$. The second approach takes this hydride compound and converts it to the cationic bis(acetonitrile)

adduct, $[\text{RuH}(\text{CO})(\text{NCMe})_2(\text{PPh}_3)_2]^+$,^{2e,22} which reacts with alkynes to form $[\text{Ru}(\text{CH}=\text{CHR})(\text{CO})(\text{NCMe})_2(\text{PPh}_3)_2]^+$ ^{2e} before halide addition yields the neutral compound $[\text{Ru}(\text{CH}=\text{CHR})\text{Cl}(\text{CO})(\text{NCMe})(\text{PPh}_3)_2]$, in which the labile acetonitrile ligand can be readily substituted.

Reaction of $[\text{RuHCl}(\text{CO})(\text{PPh}_3)_3]$ with **HC≡C-per^{lm}** in dichloromethane solution generated the 5-coordinate $[\text{Ru}(\text{CH}=\text{CH-per}^{\text{lm}})\text{Cl}(\text{CO})(\text{PPh}_3)_2]$ *in situ*. Addition of **py-PEG3** led to formation of the dark blue complex $[\text{Ru}(\text{CH}=\text{CH-per}^{\text{lm}})\text{Cl}(\text{CO})(\text{py-PEG3})(\text{PPh}_3)_2]$ (**3PEG-Ru-CH=CH-per^{lm}**) in 84% yield (Scheme 4). A singlet in the $^{31}\text{P}\{^1\text{H}\}$ NMR spectrum at 26.2 ppm indicated the presence of mutually *trans* phosphine ligands. In the ^1H NMR spectrum, the retention of the vinyl ligand was confirmed by characteristic doublets ($J_{\text{HH}} = 16.3$ Hz) for the H α and H β protons at 9.59 and 6.96 ppm, respectively. Characteristic resonances for the perylene unit were observed between 8.02 - 8.39 ppm (aromatic) and 1.63 - 1.98 ppm (adamantyl), with a diagnostic resonance at 5.09 ppm for the CH(Me)Ad proton. Pyridyl resonances were observed at 7.66 and 8.74 ppm, confirming the presence of the water-solubilizing unit. The carbonyl groups were clearly visible in the $^{13}\text{C}\{^1\text{H}\}$ NMR spectrum at 203.6 ppm (RuCO), and between 166.0 - 164.6 ppm (amide and ester groups). The carbon monoxide ligand bonded to the metal gave rise to an absorption at 1926 cm^{-1} while the ester and amide carbonyls contributed to a broader resonance at 1734 cm^{-1} . The overall composition was confirmed by mass spectrometry data and good agreement between calculated and measured elemental analysis values.

The bis(acetonitrile) cation, $[\text{RuH}(\text{CO})(\text{NCMe})_2(\text{PPh}_3)_2]\text{BF}_4$ reacted with **HC≡C-per^{lm}** in dichloromethane solution to initially yield $[\text{Ru}(\text{CH}=\text{CH-PEG3})(\text{CO})(\text{NCMe})_2(\text{PPh}_3)_2]\text{BF}_4$, before addition of $[\text{NEt}_4]\text{Cl}$ gave the neutral $[\text{Ru}(\text{CH}=\text{CH-PEG3})\text{Cl}(\text{CO})(\text{NCMe})(\text{PPh}_3)_2]$ (Scheme 4). The labile acetonitrile ligand was readily displaced by **py-per^{lm}** to yield the red complex, $[\text{Ru}(\text{CH}=\text{CH-PEG3})\text{Cl}(\text{CO})(\text{py-per}^{\text{lm}})(\text{PPh}_3)_2]$ (**3PEG-Ru-py-per^{lm}**) in 65% overall yield. The purity of the product was indicated by the presence of only one singlet at 26.7 ppm in the $^{31}\text{P}\{^1\text{H}\}$ NMR spectrum, while the vinyl ligand gave rise to two doublets ($J_{\text{HH}} = 16.8$ Hz) at 9.35 and 6.00 ppm for the H α and H β protons, with the lower field resonance displaying broadening due to coupling with the mutually *trans* phosphines. The presence of the py-per^{lm} unit was indicated by pyridyl resonances at 7.85 and 8.76 ppm as well as a diagnostic quartet at 5.10 ppm for the CH(Me)Ad proton. Good agreement between calculated and determined elemental analysis values confirmed the overall composition, along with MALDI mass spectrometry data (Supporting Information).



Scheme 4. Synthesis of ruthenium vinyl complexes.

There is considerable interest in ratiometric probes in which two fluorophores are combined within the same molecule.²³ This allows detection of an analyte through two different emission responses. Previously, we have used the 5-(3-thienyl)-2,1,3-benzothiadiazole (TBTD) fluorophore ($\lambda_{\text{exc}} = 355 \text{ nm}$, $\lambda_{\text{em}} = 500 \text{ nm}$) to detect carbon monoxide in cells and in a mouse model of inflammation.^{12c,d} This fluorophore could also be excited under two-photon conditions^{12c} at 715 nm to allow detection of endogenous CO at extremely low probe concentrations. It was therefore decided to explore the installation of both the perylenemonoimide (PMI) and TBTD fluorophores within the same complex. Treatment of $[\text{RuHCl}(\text{CO})(\text{PPh}_3)_3]$ with $\text{HC}\equiv\text{C-per}^{\text{Im}}$ in dichloromethane led to *in situ* generation of $[\text{Ru}(\text{CH}=\text{CH-per}^{\text{Im}})\text{Cl}(\text{CO})(\text{PPh}_3)_n]$ ($n = 2$ or 3) before addition of the

TBTD ligand, which provided the dark blue compound [Ru(CH=CH-per^{lm})Cl(CO)(TBTD)(PPh₃)₂] (**TBTD-Ru-CH=CH-per^{lm}**) in 71% overall yield. The ¹H NMR spectrum was again the most diagnostic characterisation method, displaying clear resonances for the CH=CH-per^{lm} unit at 9.41 (H α), 6.94 (H β) and 5.08 (CH(Me)adamantyl) ppm as well as features between 1.5 - 2.0 ppm for the adamantyl unit. In the same spectrum, the TBTD ligand gave rise to resonances at 7.63, 7.74 and 7.86 ppm. The overall composition was supported by MALDI data and satisfactory elemental analysis values for the dichloromethane solvate. Substantial effort was invested in attempts to grow single crystals of all ruthenium complexes suitable for a structural determination, but without success. The difficulty in obtaining structural data on PMI derivatives has been remarked upon previously.¹⁸ However, the presence of characteristic features in the NMR and IR spectra and the many established examples of ruthenium vinyl complexes of this type ensure that there is little doubt as to the composition of these complexes.

Photophysical characterisation

The absorbance and fluorescence properties of the synthesised compounds were investigated in solution (Table 1). All of the PMI derivatives displayed high molar extinction coefficients and around three times greater quenching of the fluorescence for the complexes compared to the ligands **HC \equiv C-per^{lm}** and **py-per^{lm}**. It was also found that the fluorescence lifetime decay values increased by 0.12 ns in the complexes over those measured for the ligands.

Compound	log ϵ (λ_{\max}) (CHCl₃)	Φ, % ($\pm 2\%$) (CH₂Cl₂)	τ (ns) (CH₂Cl₂)	χ
HC\equivC-per^{lm}	(500 nm) 4.7	90	4.62	1.085
py-per^{lm}	(500 nm) 4.5	91	4.45	1.116
3PEG-Ru-CH=CH-per^{lm}	(575 nm) 4.7	38	4.74	1.078
3PEG-Ru-py-per^{lm}	(500 nm) 4.7	29	4.57	1.098

Table 1. Photophysical parameters of the different PMI derivatives synthesised.

The absorption and fluorescence studies also showed that **3PEG-Ru-CH=CH-per^{lm}** displayed a remarkable bathochromic shift with polarity. It was also noted that the absorption bands were broader than in the free perylenemonoimides, partly overlapping

with the emission bands. The absorption and fluorescence of **3PEG-Ru-py-per^{lm}** was found to depend on the solvent in the same way as its perylenemonoimide precursor **py-per^{lm}**. Complexation to a metal served to increase its solubility, rendering it slightly soluble in organic:water mixtures, however, the fluorescence was found to be quenched under these conditions.

In general, it was found that there was little difference in the absorption and fluorescence behaviour of **3PEG-Ru-CH=CH-per^{lm}** and **TBTD-Ru-CH=CH-per^{lm}**. The only exception to this was the observation of an absorption in the region 300-400 nm, attributed to the absorption of the TBTD fluorophore (Fig. S4.2 in Supporting Information).

After this initial evaluation of the photophysical parameters, a solvatochromic (Figs. S2.16, S2.21, S2.26 and S2.31 in the Supporting Information) and solubility study led to acetone being chosen as the optimal solvent for testing the response to other analytes (Supporting Information).

The coordinated PMI complexes were screened against a series of 16 different cations (Section S4.4 in Supporting Information). For **3PEG-Ru-CH=CH-per^{lm}**, little change was observed apart from in the presence of Cu^{2+} when irradiated with UV light (Fig. S4.12 in ESI). The effect of different pH conditions was also investigated with this PMI compound, which revealed little change until a highly basic aqueous solution (pH 12.3) was reached, likely due to chemical modification of the complex itself (Fig. S4.13. in ESI). For **3PEG-Ru-py-per^{lm}** there was no significant change in the fluorescence properties except with Au^{3+} cations (Fig. S4.14), which could be a result of the acidity of the HAuCl_4 used.

Eleven different anions were screened for interactions with the perylene moiety in the complexes. In almost all cases, little significant change was observed. An exception was a colour change to pale blue and the observation of a red emission for **3PEG-Ru-CH=CH-per^{lm}** with cyanide ions (Fig. S4.15). This was attributed to the π -acid cyanide forming a complex with the ruthenium compound in a similar way to that found with carbon monoxide.¹² This result led to an investigation of the sensing potential of the complexes with a series of π -acid analytes. It was of particular interest to explore the detection of toxic substances found as gases or vapours as the risk of exposure is particularly great. The detection of carbon monoxide (CO), cyanide (CN⁻) and a representative isonitrile (*t*BuNC) was studied. Accordingly, it was found that 5 μM solutions of the probes **3PEG-Ru-CH=CH-per^{lm}** and **3PEG-Ru-py-per^{lm}** displayed changes in presence of these analytes (Figures 1 and 2).

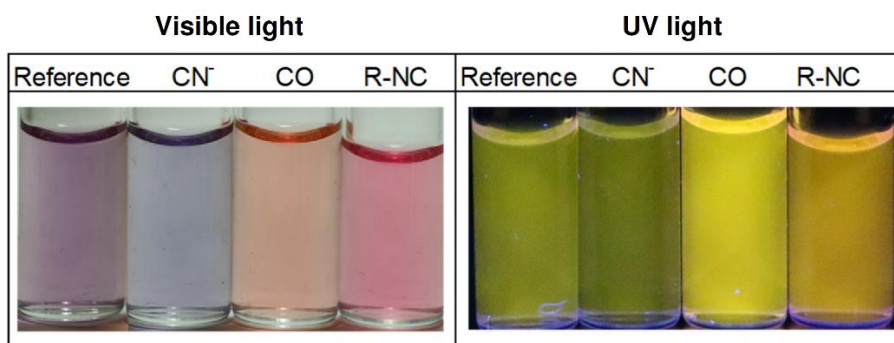


Figure 1. Colour (left) and fluorescence (right) responses of **3PEG-Ru-CH=CH-per^{lm}** (5 μ M) to NBu₄CN (50 μ M), CO (bubbled for 2 minutes) and *t*BuNC (50 μ M) in acetone solution. Reference = acetone solution of the original complex.

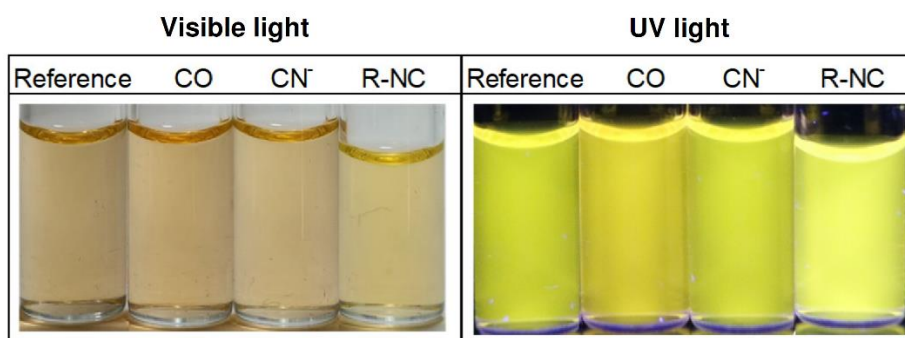


Figure 2. Colour (left) and fluorescence (right) responses of **3PEG-Ru-py-per^{lm}** (5 μ M) to NBu₄CN (50 μ M), CO (bubbled for 2 minutes) and *t*BuNC (50 μ M) in acetone solution. Reference = acetone solution of the original complex.

In contrast, acetone solutions of **3PEG-Ru-py-per^{lm}** produces an increase in fluorescence for all three analytes ([NBu₄]CN, CO and *t*BuNC), with little differentiation between them. The drastic colour and fluorescence changes displayed by **3PEG-Ru-CH=CH-per^{lm}** depending on the analyte are reflected in the quantitative data shown in Figure 3.

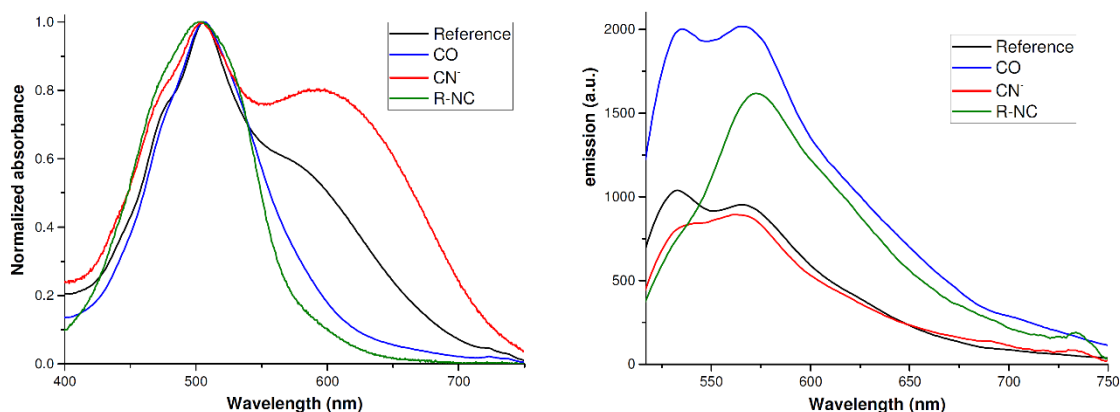


Figure 3. Absorbance (left) and fluorescence (right) spectra of **3PEG-Ru-CH=CH-per^{Im}** (5 μ M) with [NBu₄]CN (50 μ M), CO (bubbled for 2 minutes) and *t*BuNC (50 μ M) in acetone solution.

Using the absorbance and fluorescence data, several titrations were carried out, which allowed calculations to be performed to determine the limit of detection (LOD) in solution for cyanide and *t*BuNC.²⁴ A limit of detection of 0.29 μ M (7.55 μ g/L) was recorded for cyanide with probe **3PEG-Ru-CH=CH-per^{Im}** while the corresponding value for **3PEG-Ru-py-per^{Im}** was 0.41 μ M (10.7 μ g/L). For the isonitrile *t*BuNC, the LOD was measured to be 0.29 μ M (24.1 μ g/L) for **3PEG-Ru-CH=CH-per^{Im}** and 0.12 μ M (10 μ g/L) for **3PEG-Ru-py-per^{Im}**. Across all experiments, the results showed a very high sensitivity for both cyanide and isocyanide as analytes (Section S4.5 in Supporting Information).

Silica immobilisation of the complexes

Detection of analytes, such as cyanide, in solution is important due to its common occurrence as an environmental pollutant in ground water.²⁵ Such applications, where measurement is often undertaken by non-specialists, are served best by simple, low-cost and easily-used systems, such as colorimetric methods.²³ The use of colour strips has been investigated in our earlier work on carbon monoxide detection and this approach proved successful,^{12a,b} whether analysis was performed by the naked eye or by an optoelectronic device.²⁶ With this in mind, the compounds **3PEG-Ru-CH=CH-per^{Im}** and **3PEG-Ru-py-per^{Im}** were immobilised on a silica support backed by an aluminium sheet (TLC, silica gel 60, Merck). The absorption was performed by dissolving the compound (2 mg) in toluene (25 mL) and then submerging the TLC plates (5 \times 5 cm) in the solution overnight at 60 $^{\circ}$ C. The solution became colourless and successful

immobilisation of the compound on the silica was confirmed by the bright colours observed for the plates (Figure 4).

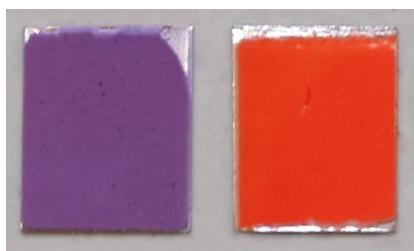


Figure 4. Image of the TLC plates with absorbed **3PEG-Ru-CH=CH-per^{lm}** (left) and **3PEG-Ru-py-per^{lm}** (right).

In a similar way to the behaviour observed in solution, the immobilised complexes gave rise to fluorescence changes after short periods in an atmosphere with CO gas or when isonitrile or BrCN vapours were present. Using the apparatus shown in Figure 5, these gases/vapours were found to lead to distinct changes in colour/fluorescence for each analyte without the need for any solvent.

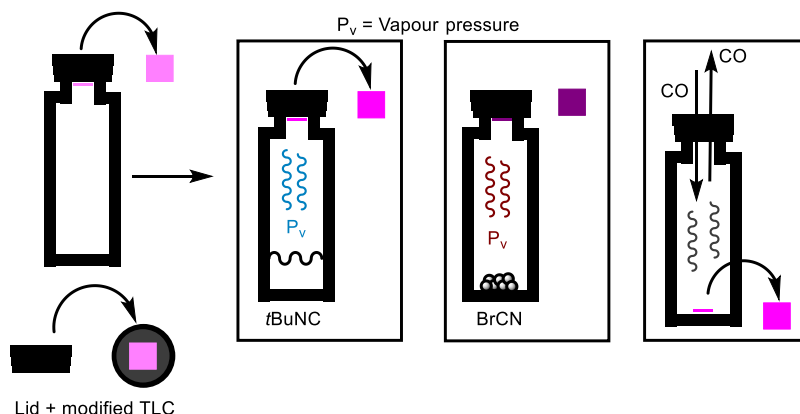


Figure 5. Representation of the method employed to expose the modified TLCs to different vapours or gas.

The experiments were performed for both the modified TLC plates based on **3PEG-Ru-CH=CH-per^{lm}** and **3PEG-Ru-py-per^{lm}** (See Section S4.5 in Supporting Information). In order to measure the colour changes on reaction with the analyte, the immobilised compounds were exposed to a constant stream of CO to saturate the chamber and the changes were then studied over time. In a similar process, the TLC plates were placed in sealed 15 mL vials with 20 μ L of *t*BuNC or 5 mg of BrCN at room temperature. The response observed depended on the vapour pressure of the compound and the interaction with the supported probe, as can be seen in Figure 6.

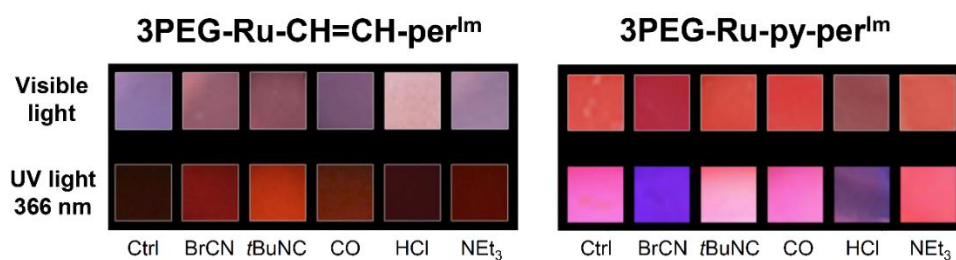


Figure 6. Qualitative response of the TLC plates modified with **3PEG-Ru-CH=CH-per^{lm}** (left) and **3PEG-Ru-py-per^{lm}** (right) in the presence of different vapours/gases with measurement after 6 hours.

At constant vapour pressure, the changes of colour and fluorescence of the immobilised compounds were found to depend on time. When studying the response to *t*BuNC, it was enough to wait for only 30 minutes to observe a significant increase in fluorescence, with both probes reaching the saturation point after 2-3 hours (Figure 7).

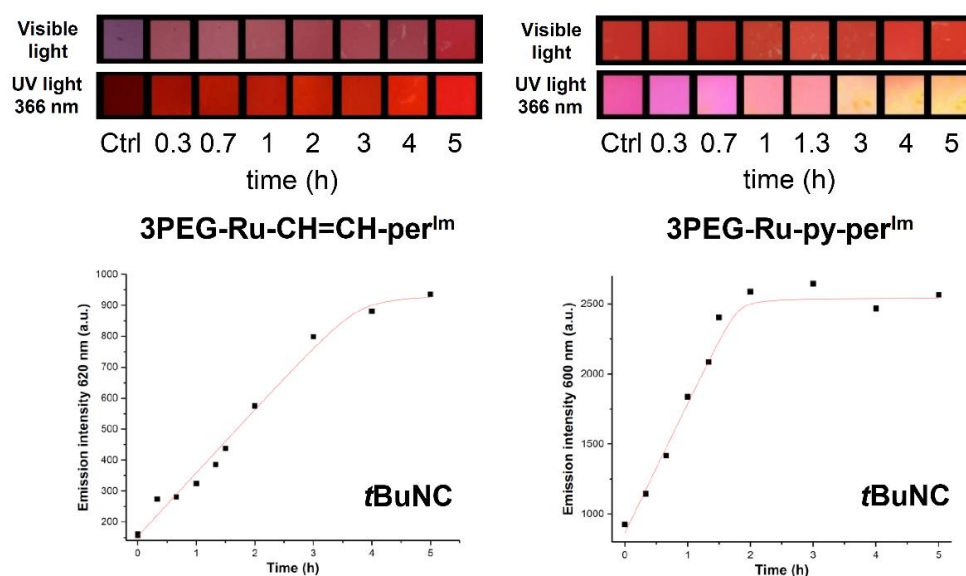


Figure 7. Colour and fluorescence responses of immobilised **3PEG-Ru-CH=CH-per^{lm}** (left) and **3PEG-Ru-py-per^{lm}** (right) to *t*BuNC vapour over time, based on the emission at 620 nm ($\lambda_{exc} = 515$ nm).

In contrast, the response was completely different when evaluating the response to BrCN, which produced only a small increase in fluorescence for the supported probe **3PEG-Ru-CH=CH-per^{lm}**, reaching a maximum after 2-3 hours (Figure 8, left). However, in contact with BrCN vapour, the fluorescence of immobilised **3PEG-Ru-py-per^{lm}** was almost totally quenched after one hour (Figure 8, right).

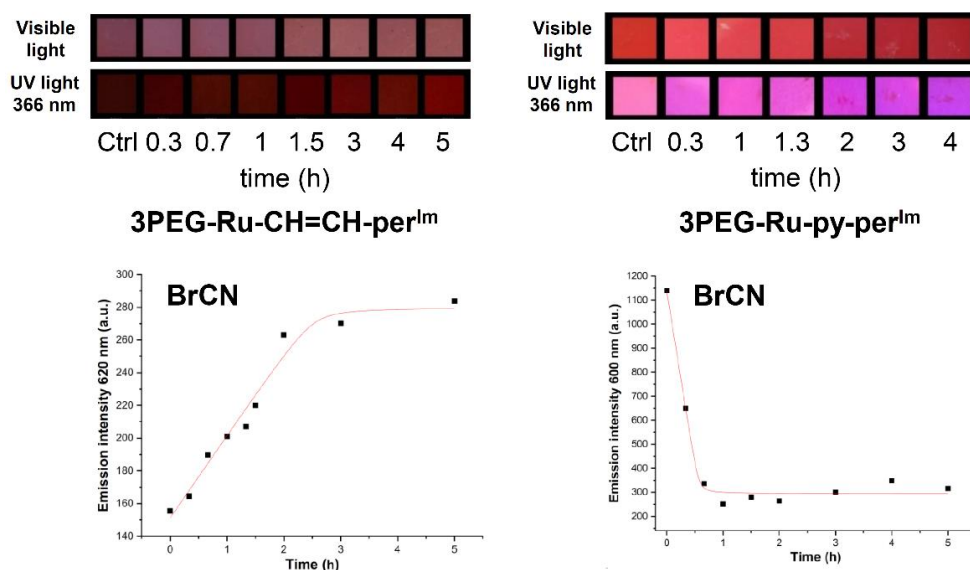


Figure 8. Colour and fluorescence responses of immobilised 3PEG-Ru-CH=CH-per^{lm} (left) and 3PEG-Ru-py-per^{lm} (right) to BrCN vapour over time, based on the emission at 620 nm ($\lambda_{\text{exc}} = 515$ nm).

The behaviour of the immobilised probes with CO were found to be very similar to those obtained in solution, with the fluorescence increasing rapidly in the presence of a constant stream of CO (saturated atmosphere). Saturation occurs in less than 30 minutes and the response is similar to that observed with *t*BuNC vapour, although with a smaller increase in fluorescence for both of the immobilised systems (Figure 9 and Figures 1 and 2).

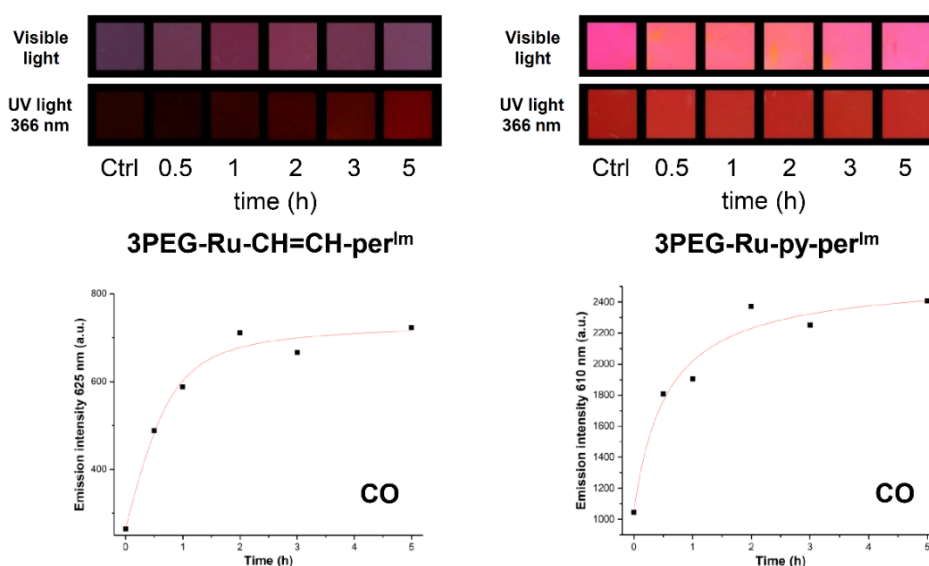


Figure 9. Colour and fluorescence responses of immobilised 3PEG-Ru-CH=CH-per^{lm} (left) and 3PEG-Ru-py-per^{lm} (right) to a stream of CO over time, based on the emission at 625 nm ($\lambda_{\text{exc}} = 515$ nm).

Conclusions

The first fluorescent ruthenium(II) vinyl complexes based on the perylenemonoimide (PMI) fluorophore have been synthesised and characterised and their photophysical properties investigated. While one ruthenium example based on a perylenebisimide design has been reported (as a photosensitizer for photodynamic therapy),²⁷ these solvatochromic compounds represent the first examples of ruthenium with PMI-based ligands. Using the inherent versatility of these compounds, both the vinyl substituent and the coordination site at the metal centre were used to introduce the PMI fluorophore. In order to increase the solubility and stability of the complexes in solution, two new water-solubilizing moieties were designed and introduced through either the vinyl ligand or a pyridyl unit. The two designs allowed sensing mechanisms based on a) modulation of the fluorescence of the retained fluorophore through ligand substitution (**3PEG-Ru-CH=CH-per^{lm}**) and b) displacement of the fluorophore to be investigated (**3PEG-Ru-py-per^{lm}**). In acetone solution, the compounds displayed a particular affinity for the π -acid species investigated. This led to preliminary studies in which the probes proved effective for the detection of several toxic analytes (isonitrile, cyanide and carbon monoxide), not only in solution but supported on silica. In particular, the probes showed very low limits of detection (LOD) for cyanide (0.29 μM) and tertiarybutylisonitrile (0.12 μM) in solution and sensitive detection of these analytes as vapours in less than an hour when the probes were immobilized on silica.

Conflicts of interest

The authors declare no conflicts of interest.

Acknowledgements

We gratefully acknowledge financial support from the Ministerio de Economía y Competitividad, Spain (Project CTQ2015-71353-R) and Junta de Castilla y León, Consejería de Educación y Cultura y Fondo Social Europeo (Project BU263P18). J. G.-C. thanks the Ministerio de Economía y Competitividad for his predoctoral FPU fellowship and J. A. R. is grateful to the Engineering and Physical Sciences Research Council (UK) for a DTP Studentship.

Supporting Information

Supporting Information (consisting of synthetic procedures, characterisation data and the results of absorbance and fluorescence measurements) are available on the WWW at <http://>.

References

1. a) M. R. Torres, A. Vegas, A. Santos, J. Ros, *J. Organomet. Chem.* **1986**, 309, 169–177; b) M. R. Torres, A. Santos, J. Ros, X. Solans, *Organometallics*, **1987**, 6, 1091–1095; c) M. R. Torres, A. Vegas, A. Santos, J. Ros, *J. Organomet. Chem.* **1987**, 326, 413–421;
2. a) A. M. Castaño, A. M. Echavarren, J. López, A. Santos, *J. Organomet. Chem.* **1989**, 379, 171–175; b) J. Montoya, A. Santos, A. M. Echavarren, J. Ros, *J. Organomet. Chem.* **1990**, 390, C57–C60; c) H. Loumrhari, J. Ros, M. R. Torres, A. Santos, A. M. Echavarren, *J. Organomet. Chem.* **1991**, 411, 255–261; d) J. Montoya, A. Santos, J. López, A. M. Echavarren, J. Ros, A. Romero, *J. Organomet. Chem.* **1992**, 426, 383–398; e) J. López, A. Romero, A. Santos, A. Vegas, A. M. Echavarren, P. Noheda, *J. Organomet. Chem.* **1989**, 373, 249–258; f) A. M. Echavarren, J. López, A. Santos, J. Montoya, *J. Organomet. Chem.* **1991**, 414, 393–400; g) A. Santos, J. Lopez, L. Matas, J. Ros, A. Galan, A. M. Echavarren, *Organometallics* **1993**, 12, 4215–4218.
3. a) H. Werner, M. A. Esteruelas, H. Otto, *Organometallics* **1986**, 5, 2295–2299; b) S. Jung, K. Ilg, C. D. Brandt, J. Wolf, H. Werner, *Eur. J. Inorg. Chem.* **2004**, 469–480; c) S. Jung, C. D. Brandt, J. Wolf, H. Werner, *Dalton Trans.* **2004**, 375–383; d) H. Werner, S. Jung, P. Gonzalez-Herrero, K. Ilg, J. Wolf, *Eur. J. Inorg. Chem.* **2001**, 1957–1961; e) S. Jung, K. Ilg, J. Wolf, H. Werner, *Organometallics* **2001**, 20, 2121–2123; f) H. Werner, W. Stüer, S. Jung, B. Weberndörfer, J. Wolf, *Eur. J. Inorg. Chem.* **2002**, 1076–1080; g) H. Werner, A. Stark, P. Steinert, C. Grunwald, J. Wolf, *Chem. Ber.* **1995**, 128, 49–62.
4. a) M. A. Esteruelas, A. M. López, E. Oñate, *Organometallics* **2007**, 26, 3260–3263; b) T. Bolano, R. Castarlenas, M. A. Esteruelas, E. Oñate, *J. Am. Chem. Soc.* **2006**, 128, 3965–3973; c) B. Eguillar, M. A. Esteruelas, M. Oliván, E. Oñate, *Organometallics* **2005**, 24, 1428–1438; d) R. Castarlenas, M. A. Esteruelas, E. Oñate, *Organometallics* **2001**, 20, 3283–3292; e) R. Castarlenas, M. A. Esteruelas, E. Oñate, *Organometallics* **2001**, 20, 2294–2302; f) M. A. Esteruelas, C. García-Yebra, M. Oliván, E. Oñate, M. Tajada, *Organometallics* **2000**, 19, 5098–5106; g) R. Castarlenas, M. A. Esteruelas, E. Oñate, *Organometallics* **2000**, 19, 5454–5463; h) M. L. Buil, M. A. Esteruelas, C. García-Yebra, E. Gutiérrez-Puebla, M. Oliván, *Organometallics* **2000**, 19, 2184–2193; i) C. Bohanna, M. L. Buil, M. A. Esteruelas, E. Oñate, C. Valero, *Organometallics* **1999**, 18, 5176–5179; j) C. Bohanna, B. Callejas, A. Edwards, M. A. Esteruelas, F. J. Lahoz, L. A. Oro, N. Ruiz, C. Valero, *Organometallics* **1998**, 17, 373–381; k) M. A. Esteruelas, A. V.

- Gómez, A. M. López, E. Oñate, *Organometallics* **1998**, *17*, 3567–3573; l) M. A. Esteruelas, F. Liu, E. Oñate, E. Sola, B. Zeier, *Organometallics* **1997**, *16*, 2919–2928; m) M. L. Buil, S. Elipe, M. A. Esteruelas, E. Oñate, E. Peinado, N. Ruiz, *Organometallics* **1997**, *16*, 5748–5755; n) M. A. Esteruelas, F. J. Lahoz, E. Oñate, L. A. Oro, E. Sola, *J. Am. Chem. Soc.* **1996**, *118*, 89–99; o) C. Bohanna, M. A. Esteruelas, J. Herrero, A. M. López, L. A. Oro, *J. Organomet. Chem.* **1995**, *498*, 199–206; p) C. Bohanna, M. A. Esteruelas, F. J. Lahoz, E. Oñate, L. A. Oro, E. Sola, *Organometallics* **1995**, *14*, 4825–4831; q) C. Bohanna, M. A. Esteruelas, F. J. Lahoz, E. Oñate, L. A. Oro, *Organometallics* **1995**, *14*, 4685–4696; r) P. Crochet, M. A. Esteruelas, A. M. López, M.-P. Martínez, M. Oliván, E. Oñate, N. Ruiz, *Organometallics* **1998**, *17*, 4500–4509; s) M. A. Esteruelas, F. J. Lahoz, E. Oñate, L. A. Oro, C. Valero, B. Zeier, *J. Am. Chem. Soc.* **1995**, *117*, 7935–7942.
5. a) A. F. Hill, R. P. Melling, *J. Organomet. Chem.* **1990**, *396*, C22–C24; b) A. F. Hill, M. C. J. Harris, R. P. Melling, *Polyhedron* **1992**, *11*, 781–787; c) R. B. Bedford, A. F. Hill, A. R. Thompsett, A. J. P. White, D. J. Williams, *Chem. Commun.* **1996**, 1059–1060; d) A. F. Hill, C. T. Ho, J. D. E. T. Wilton-Ely, *Chem. Commun.* **1997**, 2207–2208.
6. a) M. El Guaouzi, J. Ros, X. Solans, M. Font-Bardía, *Inorg. Chim. Acta* **1995**, *231*, 181–186; b) L. Matas, J. Muniente, J. Ros, A. Alvarez-Larena, J. F. Piniella, *Inorg. Chem. Comm.* **1999**, *2*, 364–367; c) M. El Guaouzi, R. Yáñez, J. Ros, A. Alvarez-Larena, J. F. Piniella, *Inorg. Chem. Comm.* **1999**, *2*, 288–291; d) M. R. Torres, A. Perales, H. Loumrhari, J. Ros, *J. Organomet. Chem.* **1990**, *385*, 379–386; e) L. Matas, I. Moldes, J. Soler, J. Ros, A. Alvarez-Larena, J. F. Piniella, *Organometallics* **1998**, *17*, 4551–4555; f) H. Loumrhari, J. Ros, M. R. Torres, A. Perales, *Polyhedron* **1990**, *9*, 907–911; g) H. Loumrhari, J. Ros, R. Yanez, M. R. Torres, *J. Organomet. Chem.* **1991**, *408*, 233–239.
7. a) S. M. Maddock, C. E. F. Rickard, W. R. Roper, L. J. Wright, *Organometallics* **1996**, *15*, 1793–1803; b) S. S. Deshpande, S. Gopinathan, C. Gopinathan, *J. Organomet. Chem.* **1991**, *415*, 265–270.
8. a) J. Maurer, R. F. Winter, B. Sarkar, J. Fiedler, S. Zálíš, *Chem. Commun.* **2004**, 1900–1901; b) J. Maurer, B. Sarkar, B. Schwederski, W. Kaim, R. F. Winter, S. Zálíš, *Organometallics* **2006**, *25*, 3701–3712; c) J. Maurer, B. Sarkar, W. Kaim, R. F. Winter, S. Zálíš, *Chem. Eur. J.* **2007**, *13*, 10257–10272; d) J. Maurer, M. Linseis, B. Sarkar, B. Schwederski, M. Niemeyer, W. Kaim, S. Zálíš, C. Anson, M. Zabel, R. F. Winter, *J. Am. Chem. Soc.* **2008**, *130*, 259–268; e) S. Zálíš, R. F. Winter, W. Kaim, *Coord. Chem. Rev.* **2010**, *254*, 1383–1396; f) P. Mücke, M. Linseis, S. Zálíš, R. F. Winter, *Inorg. Chim. Acta* **2011**, *374*, 36–50; g) S. Zálíš, R. F. Winter, W.

- Kaim, *Coord. Chem. Rev.* **2010**, *254*, 1383–1396; h) S. Scheerer, N. Rotthowe, O. S. Abdel-Rahman, X. He, S. Rigaut, H. Kvapilová, S. Záliš, R. F. Winter, *Inorg. Chem.* **2015**, *54*, 3387-3402.
9. a) S. H. Liu, Y. Chen, K. L. Wan, T. B. Wen, Z. Zhou, M. F. Lo, I. D. Williams, G. Jia, *Organometallics* **2002**, *21*, 4984–4992; b) S. H. Liu, H. Xia, T. B. Wen, Z. Zhou, G. Jia, *Organometallics* **2003**, *22*, 737–743; c) S. H. Liu, Q. Y. Hu, P. Xue, T. B. Wen, I. D. Williams, G. Jia, *Organometallics* **2005**, *24*, 769–772; d) S. H. Liu, H. Xia, K. L. Wan, R. C. Y. Yeung, Q. Y. Hu, G. Jia, *J. Organomet. Chem.* **2003**, *683*, 331–336; e) H. Xia, T. B. Wen, Q. Y. Hu, X. Wang, X. Chen, L. Y. Shek, I. D. Williams, K. S. Wong, G. K. L. Wong, G. Jia, *Organometallics* **2005**, *24*, 562–569.
10. a) M. C. J. Harris, A. F. Hill, *Organometallics* **1991**, *10*, 3903–3906; b) A. F. Hill, J. D. E. T. Wilton-Ely, *J. Chem. Soc., Dalton Trans.* **1998**, 3501–3510.
11. a) A. Romero, A. Santos, J. López, A. M. Echavarren, *J. Organomet. Chem.* **1990**, *391*, 219–223; b) A. Romero, A. Santos, A. Vegas, *J. Organometallics* **1988**, *7*, 1988–1993.
12. a) M. E. Moragues, A. Toscani, F. Sancenón, R. Martínez-Mañez, A. J. P. White, J. D. E. T. Wilton-Ely, *J. Am. Chem. Soc.* **2014**, *136*, 11930–11933; b) A. Toscani, C. Marín-Hernández, M. E. Moragues, F. Sancenón, P. Dingwall, N. J. Brown, R. Martínez-Mañez, A. J. P. White, J. D. E. T. Wilton-Ely, *Chem. Eur. J.* **2015**, *21*, 14529 – 14538; c) C. de la Torre, A. Toscani, C. Marín-Hernández, J. A. Robson, M. C. Terencio, A. J. P. White, M. J. Alcaraz, J. D. E. T. Wilton-Ely, R. Martínez-Mañez, F. Sancenón, *J. Am. Chem. Soc.* **2017**, *139*, 18484-18487; d) A. Toscani, C. Marín-Hernández, J. A. Robson, E. Chua, P. Dingwall, A. J. P. White, F. Sancenón, R. Martínez-Mañez, J. D. E. T. Wilton-Ely, *Chem. Eur. J.* **2019**, *25*, 2069 – 2081; e) J. Wang, J. Karpus, B. S. Zhao, Z. Luo, P. R. Chen, C. He, *Angew. Chem. Int. Ed.*, **2012**, *51*, 9652-9656; f) B. W. Michel, A. R. Lippert, C. J. Chang, *J. Am. Chem. Soc.*, **2012**, *134*, 15668-15671; g) K. Zheng, W. Lin, L. Tan, H. Chen, H. Cui, *Chem. Sci.*, **2014**, *5*, 3439-3448; h) S. Pal, M. Mukherjee, B. Sen, S. K. Mandal, S. Lohar, P. Chattopadhyay, K. Dhara, *Chem. Commun.*, **2015**, *51*, 4410-4413; i) Y. Cao, D.-W. Li, L.-J. Zhao, X.-Y. Liu, X.-M. Cao, Y.-T. Long, *Anal. Chem.*, **2015**, *87*, 9696-9701; j) W. Feng, D. Liu, S. Feng, G. Feng, *G. Anal. Chem.*, **2016**, *88*, 10648-10653; k) Z. Xu, J. Yan, J. Li, P. Yao, J. Tan, L. Zhang, *Tetrahedron Lett.*, **2016**, *57*, 2927-2930; l) W. Feng, D. Liu, Q. Zhai, G. Feng, *Sens. Act. B*, **2017**, *240*, 625-630; m) W. Feng, J. Hong, G. Feng, *Sens. Actuators, B*, **2017**, *251*, 389-395; n) S. Feng, D. Liu, W. Feng, G. Feng, *G. Anal. Chem.*, **2017**, *89*, 3754-3760; o) K. Dhara, B. S. Lohar, A. Patra, P. Roy, S. K. Saha, G. C. Sadhukhan, P. Chattopadhyay, *Anal. Chem.* **2018**, *90*, 2933-2938; p) B. Das, S. Lohar, A. Patra,

- E. Ahmmed, S. K. Mandal, J. N. Bhakta, K. Dhara, P. Chattopadhyay, *New J. Chem.*, **2018**, *42*, 13497-13502; q) Z. Wang, Z. Geng, Z. Zhao, W. Sheng, C. Liu, X. Lv, Q. He, B. Zhu, *New J. Chem.* **2018**, *42*, 14417-14423; r) W. Feng, G. Feng, *Sens. Actuators B*, **2018**, *255*, 2314-2320; s) S. Gong, S. J. Hong, E. Zhou, G. Feng, *Talanta*, **2019**, *201*, 40-45; t) S. Xu, H. W. Liu, X. Yin, L. Yuan, S. Y. Huan, X. B. Zhang, *Chem. Sci.*, **2019**, *10*, 320-325.
13. a) Y. H. Lin, N. H. Leung, K. B. Holt, A. L. Thompson, J. D. E. T. Wilton-Ely, *Dalton Trans.* **2009**, 7891-7901; b) S. Naeem, A. L. Thompson, L. Delaude, J. D. E. T. Wilton-Ely, *Chem. Eur. J.* **2010**, *16*, 10971-10974; c) S. Naeem, A. L. Thompson, A. J. P. White, L. Delaude, J. D. E. T. Wilton-Ely, *Dalton Trans.* **2011**, *40*, 3737-3747; d) P. Patel, S. Naeem, A. J. P. White, J. D. E. T. Wilton-Ely, *RSC Adv.* **2012**, *2*, 999-1008; e) M. J. Macgregor, G. Hogarth, A. L. Thompson, J. D. E. T. Wilton-Ely, *Organometallics* **2009**, *28*, 197-208; f) S. Naeem, E. Ogilvie, A. J. P. White, G. Hogarth, J. D. E. T. Wilton-Ely, *Dalton Trans.* **2010**, *39*, 4080-4089; g) S. Naeem, A. J. P. White, G. Hogarth, J. D. E. T. Wilton-Ely, *Organometallics* **2010**, *29*, 2547-2556; h) S. Naeem, A. J. P. White, G. Hogarth, J. D. E. T. Wilton-Ely, *Organometallics* **2011**, *30*, 2068-2069; i) G. Jia, W. F. Wu, R. C. Y. Yeung, H. P. Xia, *J. Organomet. Chem.* **1997**, *539*, 53-59; j) S. Sung, H. Holmes, L. Wainwright, A. Toscani, G. J. Stasiuk, A. J. P. White, J. D. Bell, J. D. E. T. Wilton-Ely, *Inorg. Chem., Inorg. Chem.* **2014**, *53*, 1989-2005; k) R. B. Bedford, C. S. J. Cazin, *J. Organomet. Chem.* **2000**, *598*, 20-23; l) J. D. E. T. Wilton-Ely, M. Wang, D. Benoit, D. A. Tocher, *Eur. J. Inorg. Chem.* **2006**, 3068-3078; m) J. D. E. T. Wilton-Ely, P. J. Pogorzelec, S. J. Honarkhah, D. A. Tocher, *Organometallics* **2005**, *24*, 2862-2874; n) J. D. E. T. Wilton-Ely, M. Wang, S. J. Honarkhah, D. A. Tocher, *Inorg. Chim. Acta.* **2005**, *358*, 3218-3226; o) A. R. Cowley, A. L. Hector, A. F. Hill, A. J. P. White, D. J. Williams, J. D. E. T. Wilton-Ely, *Organometallics* **2007**, *26*, 6114-6125.
14. a) A. Toscani, E. K. Heliövaara, J. B. Hena, A. J. P. White, J. D. E. T. Wilton-Ely, *Organometallics* **2015**, *34*, 494-505; b) Y. H. Lin, L. Duclaux, F. González de Rivera, A. L. Thompson, J. D. E. T. Wilton-Ely *Eur. J. Inorg. Chem.* **2014**, 2065-2072; c) S. Naeem, A. Ribes, A. J. P. White, M. N. Haque, K. B. Holt, J. D. E. T. Wilton-Ely, *Inorg. Chem.* **2013**, *52*, 4700-4713; d) K. A. Jantan, J. A. McArdle, L. Mognon, V. Fiorini, L. A. Wilkinson, A. J. P. White, S. Stagni, N. J. Long, J. D. E. T. Wilton-Ely, *New J. Chem.* **2019**, *43*, 3199-3207; e) L. Mognon, S. Richardson, G. Agonigi, T. Bond, F. Marchetti, J. D. E. T. Wilton-Ely, *J. Organomet. Chem.* **2019**, *886*, 9-12.

15. a) J. D. E. T. Wilton-Ely, D. Solanki, G. Hogarth, *Eur. J. Inorg. Chem.* **2005**, 4027–4030; b) E. R. Knight, D. Solanki, G. Hogarth, K. B. Holt, A. L. Thompson, J. D. E. T. Wilton-Ely, *Inorg. Chem.* **2008**, *47*, 9642–9653; c) E. R. Knight, A. R. Cowley, G. Hogarth, J. D. E. T. Wilton-Ely, *Dalton Trans.* **2009**, 607–609; d) E. R. Knight, N. H. Leung, Y. H. Lin, A. R. Cowley, D. J. Watkin, A. L. Thompson, G. Hogarth, J. D. E. T. Wilton-Ely, *Dalton Trans.* **2009**, 3688–3697; e) E. R. Knight, N. H. Leung, A. L. Thompson, G. Hogarth, J. D. E. T. Wilton-Ely, *Inorg. Chem.* **2009**, *48*, 3866–3874; f) K. Oliver, A. J. P. White, G. Hogarth, J. D. E. T. Wilton-Ely, *Dalton Trans.* **2011**, *40*, 5852–5864; g) G. Hogarth, E.-J. C.-R. C. R. Rainford-Brent, S. E. Kabir, I. Richards, J. D. E. T. Wilton-Ely, Q. Zhang, *Inorg. Chim. Acta* **2009**, *362*, 2020–2026; h) V. L. Hurtubise, J. M. McArdle, S. Naeem, A. Toscani, A. J. P. White, N. J. Long, J. D. E. T. Wilton-Ely, *Inorg. Chem.* **2014**, *53*, 11740–11748; i) R. Sherwood, F. González de Rivera, J. H. Wan, Q. Zhang, A. J. P. White, O. Rossell, G. Hogarth, J. D. E. T. Wilton-Ely, *Inorg. Chem.* **2015**, *54*, 4222–4230; j) J. A. Robson, F. González de Rivera, K. Anuar Jantan, M. N. Wenzel, A. J. P. White, O. Rossell, J. D. E. T. Wilton-Ely, *Inorg. Chem.* **2016**, *55*, 12982–12996; k) S. Naeem, S. A. Serapian, A. Toscani, A. J. P. White, G. Hogarth, J. D. E. T. Wilton-Ely, *Inorg. Chem.*, **2014**, *53*, 2404–2416.
16. a) N. W. Alcock, A. F. Hill, R. P. Melling, *Organometallics* **1991**, *10*, 3898–3903; b) A. F. Hill, A. J. P. White, D. J. Williams, J. D. E. T. Wilton-Ely, *Organometallics* **1998**, *17*, 4249–4258; c) J. C. Cannadine, A. F. Hill, A. J. P. White, D. J. Williams, J. D. E. T. Wilton-Ely, *Organometallics* **1996**, *15*, 5409–5415; d) J. C. Green, A. L. Hector, A. F. Hill, S. Lin, J. D. E. T. Wilton-Ely, *Organometallics* **2008**, *27*, 5548–5558.
17. For an overview of vinyl chemistry of ruthenium(II), see: a) M. K. Whittlesey, in *Comprehensive Organometallic Chemistry III*; R. H. Crabtree, D. M. P. Mingos, M. I. Bruce, Eds.; Elsevier: Oxford, U.K., 2006; Vol. 6; b) A. F. Hill, in *Comprehensive Organometallic Chemistry II*; E. W. Abel, F. G. A. Stone, G. Wilkinson.; Eds.; Pergamon Press: Oxford, U.K., 1995, Vol. 7.
18. a) S. Kaloyanova, Y. Zagranyarski, S. Ritz, M. Hanulová, K. Koynov, A. Vonderheit, K. Müllen, K. Peneva, *J. Am. Chem. Soc.* **2016**, *138*, 2881–2884; b) U. Lewandowska, W. Zajaczkowski, L. Chen, F. Bouillière, D. Wang, K. Koynov, W. Pisula, K. Müllen, H. Wennemers, *Angew. Chem. Int. Ed.* **2014**, *53*, 12537–12541; c) A. Bolag, N. Sakai, S. Matile, *Chem. Eur. J.* **2016**, *22*, 9006–9014; d) J. A. Hutchison, H. Uji-i, A. Deres, T. Vosch, S. Rocha, S. Müller, A. A. Bastian, J. Enderlein, H. Nourouzi, C. Li, A. Herrmann, K. Müllen, F. De Schryver, J. Hofkens, *Nature Nanotech.* **2014**, *9*, 131–136; e) U. Lewandowska, W. Zajaczkowski, W.

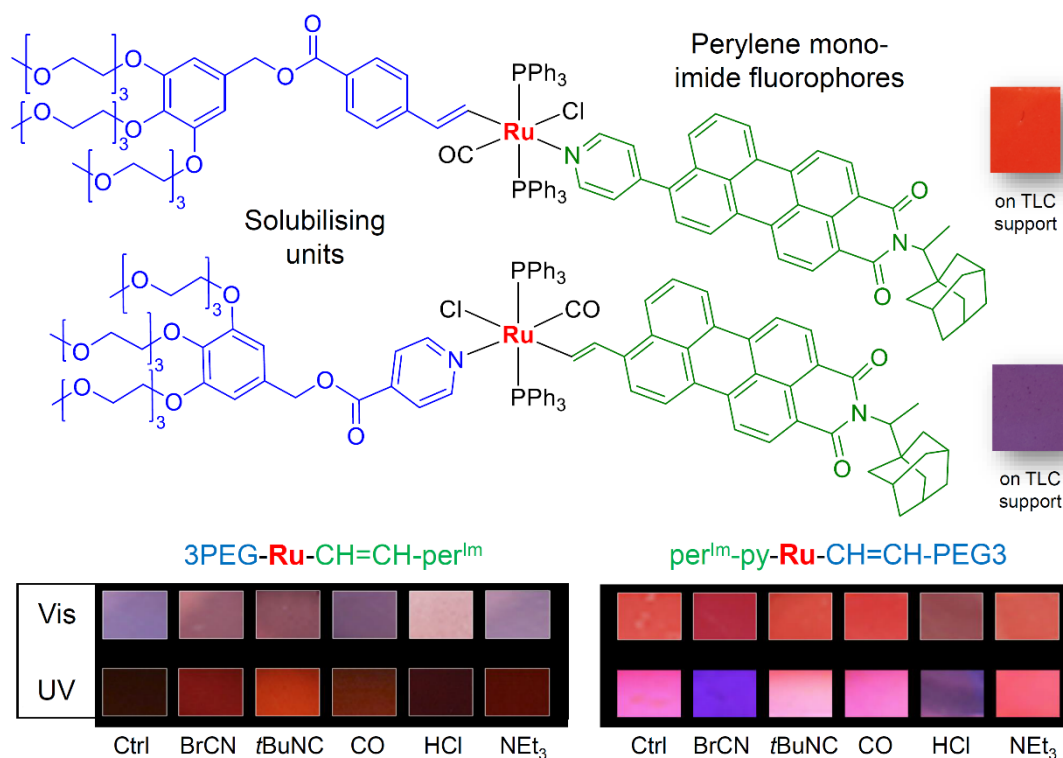
- Pisula, Y. Ma, C. Li, K. Müllen, H. Wennemers, *Chem. Eur. J.* **2016**, *22*, 3804–3809.
19. a) B. Díaz de Greñu, D. Moreno, T. Torroba, A. Berg, J. Gunnars, T. Nilsson, R. Nyman, M. Persson, J. Pettersson, I. Eklind, P. Wästerby, *J. Am. Chem. Soc.* **2014**, *136*, 4125–4128; b) B. Díaz de Greñu, J. García-Calvo, J. Cuevas, G. García-Herbosa, B. García, N. Busto, S. Ibeas, T. Torroba, B. Torroba, A. Herrera, S. Pons, *Chem. Sci.* **2015**, *6*, 3757–3764; c) P. Calvo-Gredilla, J. García-Calvo, J. V. Cuevas, T. Torroba, J.-L. Pablos, F. C. García, J.-M. García, N. Zink-Lorre, E. Font-Sanchis, A. Sastre-Santos, F. Fernández-Lázaro, *Chem. Eur. J.* **2017**, *23*, 13973–13979; d) J. García-Calvo, S. Ibeas, E.-C. Antón-García, T. Torroba, G. González-Aguilar, W. Antunes, E. González-Lavado, M. L. Fanarraga, *ChemistryOpen* **2017**, *6*, 562–570. e) J. García-Calvo, P. Calvo-Gredilla, M. Ibáñez-Llorente, D. C. Romero, J. V. Cuevas, G. García-Herbosa, M. Avella, T. Torroba, *J. Mater. Chem. A* **2018**, *6*, 4416–4423; f) C. Mari, H. Huang, R. Rubbiani, M. Schulze, F. Würthner, H. Chao, G. Gasser, *Eur. J. Inorg. Chem.* **2017**, 1745–1752.
20. a) A. W. Varnes, R. B. Dodson, E. L. Wehry, *J. Am. Chem. Soc.* **1972**, *94*, 946–950; b) C. Wu, J.-L. Zhao, X.-K. Jiang, C.-Z. Wang, X.-L. Ni, X. Zeng, C. Redshaw, T. Yamato, *Dalton Trans.* **2016**, *45*, 14948–14953.
21. a) J. Wu, B. Kwon, W. Liu, E. V. Anslyn, P. Wang, J. S. Kim, *Chem. Rev.* **2015**, *115*, 7893–7943; b) Z. Yang, J. Cao, Y. He, J. H. Yang, T. Kim, X. Peng, J. S. Kim, *Chem. Soc. Rev.* **2014**, *43*, 4563–4601; c) Z. Köstereli, R. Scopelliti, K. Severin, *Chem. Sci.* **2014**, *5*, 2456–2460; d) F. Hof, *Chem. Commun.* **2016**, *52*, 10093–10108; e) D. Wu, A. C. Sedgwick, T. Gunnlaugsson, E. U. Akkaya, J. Yoon, T. D. James, *Chem. Soc. Rev.* **2017**, *46*, 7105–7123.
22. a) B. E. Cavit, K. R. Grundy, W. R. Roper, *J. Chem. Soc., Chem. Commun.* **1972**, 60–61; b) A. F. Hill, D. A. Tocher, A. J. P. White, D. J. Williams, J. D. E. T. Wilton-Ely, *Organometallics* **2005**, *24*, 5342–5355.
23. C. Marín-Hernández, A. Toscani, F. Sancenón, J. D. E. T. Wilton-Ely, R. Martínez-Mañez, *Chem. Commun.* **2016**, *52*, 5902 – 5911.
24. The calculation was performed using the software “R” v2.7 and following the procedure described in reference 19b. A least square regression was carried out before the LODs were calculated by taking into account 5% or less probability of false positives/negatives. The number was always within the range of the performed measurements without considering the value at 0:
25. WHO data - https://www.who.int/water_sanitation_health/dwq/cyanide.pdf (accessed on 6.02.2019)

26. M. E. Moragues Pons, R. Montes Robles, J. V. Ros-Lis, M. Alcañiz Fillol, F. J. Ibáñez Civera, M. T. Pardo Vicente, R. Martínez Mañez, *Sens. Act. B.* **2014**, *191*, 257-263.
27. C. Mari, H. Huang, R. Rubbiani, M. Schulze, F. Würthner, H. Chao, G. Gasser, *Eur. J. Inorg. Chem.* **2017**, 1745–1752.

For Table of Contents use:

Synthesis and application of ruthenium(II) alkenyl complexes with perylene fluorophores for the detection of toxic vapours, gases

José García-Calvo, Jonathan A. Robson, Tomás Torroba*
and James D. E. T. Wilton-Ely*



The first reported examples of ruthenium(II) vinyl complexes bearing perylenemonoimide units are able to detect carbon monoxide, isonitriles or cyanide through fluorescence changes.

Text [22 words]

Supporting Information

Synthesis and application of ruthenium(II) alkenyl complexes with perylene fluorophores for the detection of toxic vapours and gases

José García-Calvo, Jonathan A. Robson, Tomás Torroba* and James D. E. T. Wilton-Ely*

S1 Materials and methods	page 2
S2 Synthesis procedures and characterisation	page 3
S3 Summary of synthesised compounds	page 32
S4 Interpretation of absorption and fluorescence data	page 33
S4.1 Selection and influence of the solvents	page 33
S4.2 Carbon monoxide detection	page 36
S4.3 Effect of CO and Glutathione	page 38
S4.4 Behaviour with cations and anions	page 41
S4.5 Titrations with different analytes	page 44
S4.6 Measurements of immobilised probes	page 52
S5 References	page 62

S1 Materials and methods

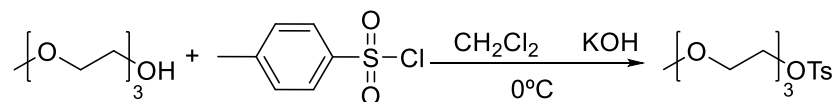
Unless otherwise stated, solvents and reagents were obtained from commercial sources and used as received. *N*-(2-adamantyl-ethylamine)-9-bromo-3,4-perylenemonoimide,^{S1} triethyleneglycol monomethylether monotosylate,^{S2} methyl(3,4,5-monoethyltriethyleneglycol)benzoate,^{S2, S3} (3,4,5-monoethyltetraethyleneglycol)phenylmethanol,^{S3} [RuHCl(CO)(PPh₃)₃]^{S5} and [RuH(CO)(NCMe)₂(PPh₃)₂]^{S6} were prepared as described previously. Column chromatography: SiO₂ (40-63 μm). TLC plates coated with SiO₂ 60F254 were visualized by UV light. Aluminium sheet plates (TLC Silica gel 60, Merck) with no dye were used for modification. NMR spectra were recorded at 25 °C using a Varian Mercury 300 MHz and Varian Unity Inova 400 MHz. Ultraviolet–visible (UV-Vis) and fluorescence spectra were recorded using a Hitachi U-3900 and F-7000 Hitachi Fluorescence spectrophotometers, respectively. IR spectra were recorded with a Nicolet Impact 400D spectrophotometer. FTIR spectra were recorded with a JASCO FT/IR-4200 fitted with a JASCO “ATR PRO ONE” ATR. High resolution Mass spectra were obtained from a Bruker Autoflex matrix-assisted laser desorption/ionization time of flight (MALDI-TOF) using dithranol (DIT) or *trans*-2-[3-(4-tert-butylphenyl)-2-methyl-2-propenylidene]malononitrile (DCTB) as matrix. Time of Flight Mass Spectrometry (MS-TOF) was performed on a Bruker Maxis Impact coupled to an ultra-performance liquid chromatography device Waters Acquity (UPLC-MS-TOF).

Fluorescence decay lifetimes (τ) were measured using a time-correlated single photon counting instrument (FLS980 Series, Edinburgh instruments) with a 510 nm pulsed LED (Edinburgh instruments, EPL-510) light source having a 177.4 ps adjusted by a deconvolution method after measuring the instrumental response (IRF). Fluorescence quantum yields (Φ) were calculated by using the same fluorimeter but provided with an integration sphere for calculating the absolute value of this parameter.

S2 Synthesis procedures and characterisation

Polyethyleneglycol derivatives

Synthesis of triethyleneglycol monomethylether monotosylate



Triethyleneglycol monomethyl ether (20.0 g, 121.8 mmol) and dichloromethane (145 mL) were added to a 500 mL round bottom flask equipped with magnetic stirrer. The homogeneous mixture was stirred at 0 °C. Freshly powdered NaOH (19.5 g, 487.2 mmol) was added in small portions with vigorous stirring at 0-5 °C for 1 h. *Para*-toluenesulfonyl chloride (27.9 g, 146.2 mmol) was dissolved in dichloromethane (36 mL) and added followed by stirring at 0 °C for a further 3 h. The mixture was then filtered under vacuum and extracted with dichloromethane (3 × 200 mL) and the combined organic extracts were dried over anhydrous Na₂SO₄. A pale yellow oil was obtained after filtration and evaporation of the solvent. This oil was subjected to flash chromatography on silica, using CH₂Cl₂/MeOH (25:1) as eluent, to give tetraethylene glycol monomethyl ether *p*-toluene sulfonate (20.55 g, 53% yield) as a colourless oil. ¹H NMR (400 MHz, CDCl₃) δ (ppm): 7.82 (d, *J* = 8.3 Hz, 2H, H_{Ar}), 7.41 – 7.31 (m, 2H, H_{Ar}), 4.22 – 4.15 (m, 2H, S-O-CH₂), 3.74 – 3.66 (m, 2H, CH₂-O), 3.66 – 3.49 (m, 8H, CH₂-O), 3.39 (s, 3H, CH₃-O), 2.47 (s, 3H, C_{Ar}-CH₃). Spectroscopic data obtained agreed well with those reported previously.^{S2, S3}

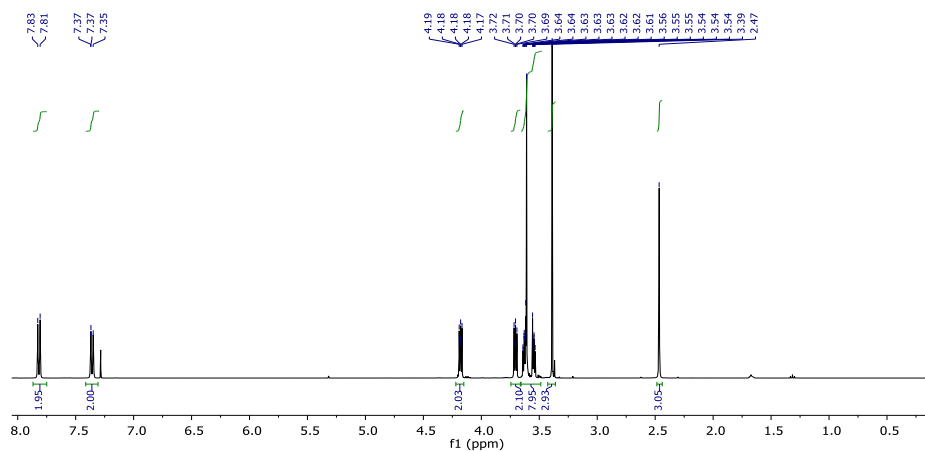
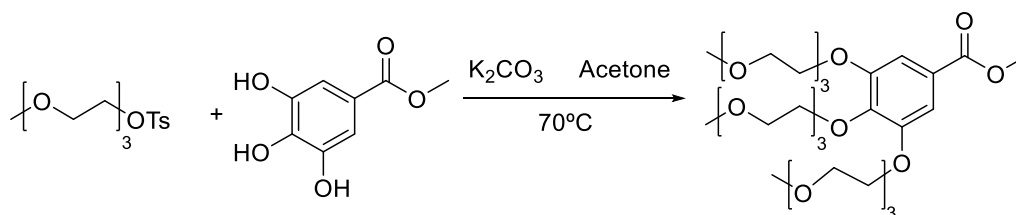


Fig. S2.1 ¹H NMR spectrum (CDCl₃, 400 MHz) of triethyleneglycol monomethylether monotosylate

Synthesis of methyl(3,4,5-monoethyltriethyleneglycol)benzoate



Methyl-3,4,5-trihydroxybenzoate (1.74 g, 9.4 mmol) and triethyleneglycol monomethyl ether *p*-toluene sulfonate (12.0 g, 37.7 mmol) were added to a suspension of K_2CO_3 (6.5 g, 47.1 mmol) in acetone (55 mL) and stirred at 70 °C for 48 h. The solids were removed by filtration through Celite. After removal of the acetone under vacuum, the residue was extracted with $CHCl_3/H_2O$ (4 x 120 mL). The organic layer was washed with 1N HCl aq. and brine, successively. The organic layer was dried over anhydrous Na_2SO_4 . After filtration, the filtrate was evaporated under vacuum and finally the oil was purified by column chromatography, $CH_2Cl_2:MeOH$ (50:3), to give methyl 3,4,5-tris(2-methoxyethoxy)benzoate as a pale yellow oil. Yield 5.5 g (94%). 1H NMR (400 MHz, $CDCl_3$) δ (ppm): 7.31 (s, 2H, H_{Ar}), 4.26 – 4.18 (m, 6H, CH_2-O-C_{Ar}), 3.91 – 3.86 (m, 7H, $CH_3-O-C=O$ + $-CH_2-CH_2-$), 3.83 – 3.78 (m, 2H, $-CH_2-CH_2-$), 3.77 – 3.63 (m, 19H, $-CH_2-CH_2-$), 3.58 – 3.54 (m, 6H, $-CH_2-CH_2-$), 3.39 (d, $J = 1.1$ Hz, 9H, CH_2-O-CH_3). Spectroscopic data obtained agreed well with those reported previously.^{S3}

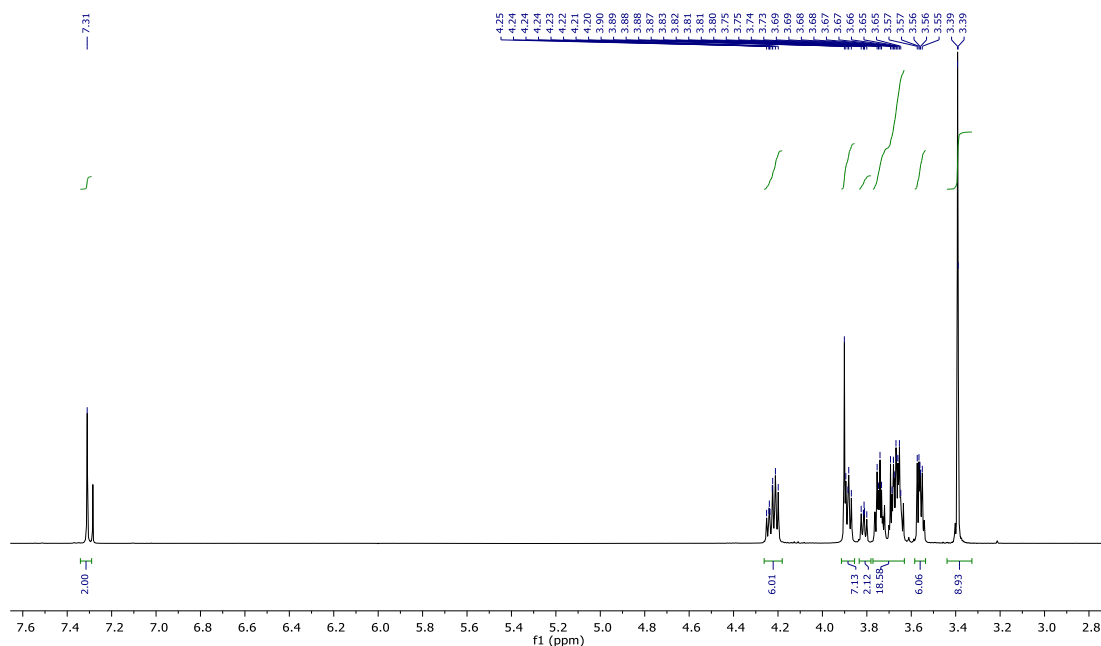
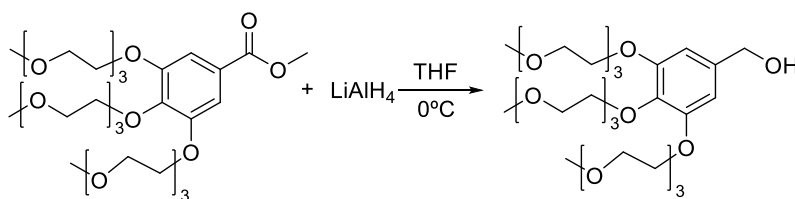


Fig. S2.2 1H NMR spectrum ($CDCl_3$, 400 MHz) of methyl(3,4,5-monoethyltriethyleneglycol)benzoate

Synthesis of (3,4,5-Monoethyltetraethyleneglycol)phenylmethanol



A suspension of LiAlH₄ (1M, 2.3 mL, 2.3 mmol) in THF was slowly added to a solution of methyl-3,4,5-tris(2-methoxyethoxy)benzoate (5.5g, 8.83 mmol) in anhydrous THF (30 mL) under a nitrogen atmosphere at 0 °C. The resulting suspension was stirred at room temperature for 2 h and then at 70 °C overnight. Unreacted metal hydride was neutralized with ethyl acetate (1 mL), ethanol (1 mL) and water (10 mL), the mixture was filtered through Celite and extracted with CH₂Cl₂ (4 x 75 mL). The organic layer was dried over anhydrous Na₂SO₄. After filtration, the liquid phase was evaporated under vacuum giving the product as a pale yellow oil. Yield: 4.78 (91%). ¹H NMR (400 MHz, CDCl₃) δ(ppm): 6.63 (s, 2H, H_{Ar}), 4.57 (d, *J* = 6.0 Hz, 2H, CH₂-OH), 4.18-4.11 (m, 6H, CH₂-O-C_{Ar}), 3.85-3.52 (m, 43H, -CH₂-CH₂-), 3.37 (s, 9H, CH₃). Spectroscopic data obtained agreed well with those reported previously.^{S3}

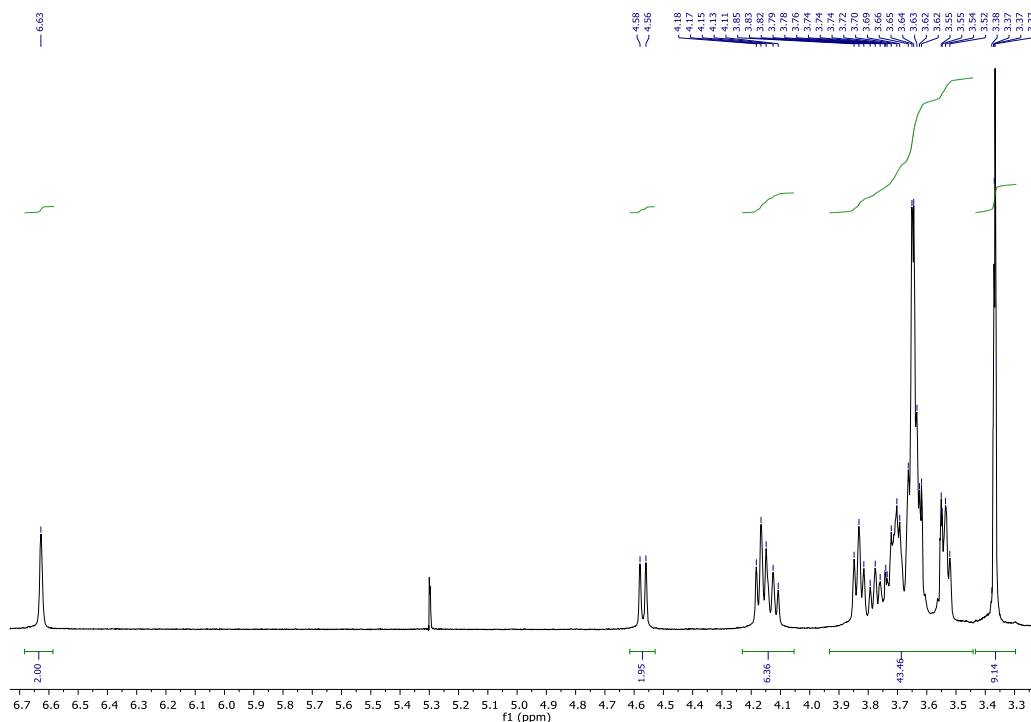
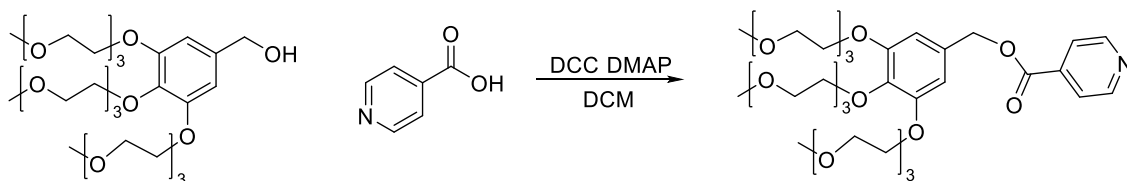


Fig. S2.3 ¹H NMR spectrum (CDCl₃, 400 MHz) of (3,4,5-monoethyltetraethyleneglycol)phenylmethanol

Synthesis of 3,4,5-tris(2-(2-(2-methoxyethoxy)ethoxy)ethoxy)benzyl-4-ethynylbenzoate (py-PEG3)



DCC (*N,N*-dicyclohexylcarbodiimide) (381.3 mg, 1.85 mmol) was added to a stirred solution of (3,4,5-monoethyltetraethyleneglycol)phenylmethanol (1.0 g, 1.68 mmol), isonicotinic acid (207 mg, 1.68 mmol), and 4-(dimethylamino)pyridine [DMAP] (10.3 mg, 0.08 mmol) in CH_2Cl_2 (6 mL) at 0 °C. The resulting suspension was warmed to room temperature and stirred for 2 h. The suspension was filtered and concentrated. Purification by flash column chromatography (with a gradient from neat DCM to DCM:MeOH 3%) afforded a colourless liquid product (0.6 g, 51%). **IR** (ATR, cm^{-1}): 3066, 2866 (C-H), 1728 (C=O), 1594, 1494, 1492, 1352, 1235, 1109, 942, 842, 741. **$^1\text{H NMR}$** (400 MHz, CDCl_3) δ (ppm): 8.79 (dd, $J = 4.2, 2.0$ Hz, 2H, H_{Ar}), 7.91 – 7.81 (m, 2H, H_{Ar}), 6.68 (s, 2H, H_{Ar}), 5.27 (s, 2H, $\text{C}_{\text{Ar}}\text{-CH}_2$), 4.20 – 4.13 (m, 6H, $\text{C}_{\text{Ar}}\text{-O-CH}_2$), 3.88 – 3.84 (m, 4H, O- CH_2), 3.79 (s, 2H, O- CH_2), 3.75 – 3.71 (m, 6H, O- CH_2), 3.65 (ddd, $J = 9.5, 6.0, 2.0$ Hz, 12H, O- CH_2), 3.57 – 3.52 (m, 6H, O- CH_2), 3.37 (t, $J = 1.9$ Hz, 9H, O- CH_3). **$^{13}\text{C NMR}$** (101 MHz, CDCl_3) δ (ppm): 164.9 (C=O), 152.8 (C_{Ar}), 150.6 ($\text{C}_{\text{Ar}}\text{H}$), 138.8 (C_{Ar}), 137.3 (C_{Ar}), 130.5 (C_{Ar}), 122.9 ($\text{C}_{\text{Ar}}\text{H}$), 108.5 ($\text{C}_{\text{Ar}}\text{H}$), 72.3 ($\text{CH}_2\text{-O}$), 71.9 ($\text{CH}_2\text{-O}$), 70.8 ($\text{CH}_2\text{-O}$), 70.7 ($\text{CH}_2\text{-O}$), 70.6 ($\text{CH}_2\text{-O}$), 70.5 ($\text{CH}_2\text{-O}$), 69.7 ($\text{CH}_2\text{-O}$), 69.0 ($\text{CH}_2\text{-O}$), 67.6 ($\text{CH}_2\text{-O}$), 59.0 ($\text{CH}_3\text{-O}$). **HRMS** (ESI+): m/z calcd. for $\text{C}_{37}\text{H}_{54}\text{O}_{14}$: 700.3539; found: 700.3563 (20, $\text{M}+\text{H}^+$). m/z calcd for $\text{C}_{37}\text{H}_{53}\text{NaO}_{14}$: 722.3358; found: 722.3430 (40, $\text{M}+\text{Na}^+$).

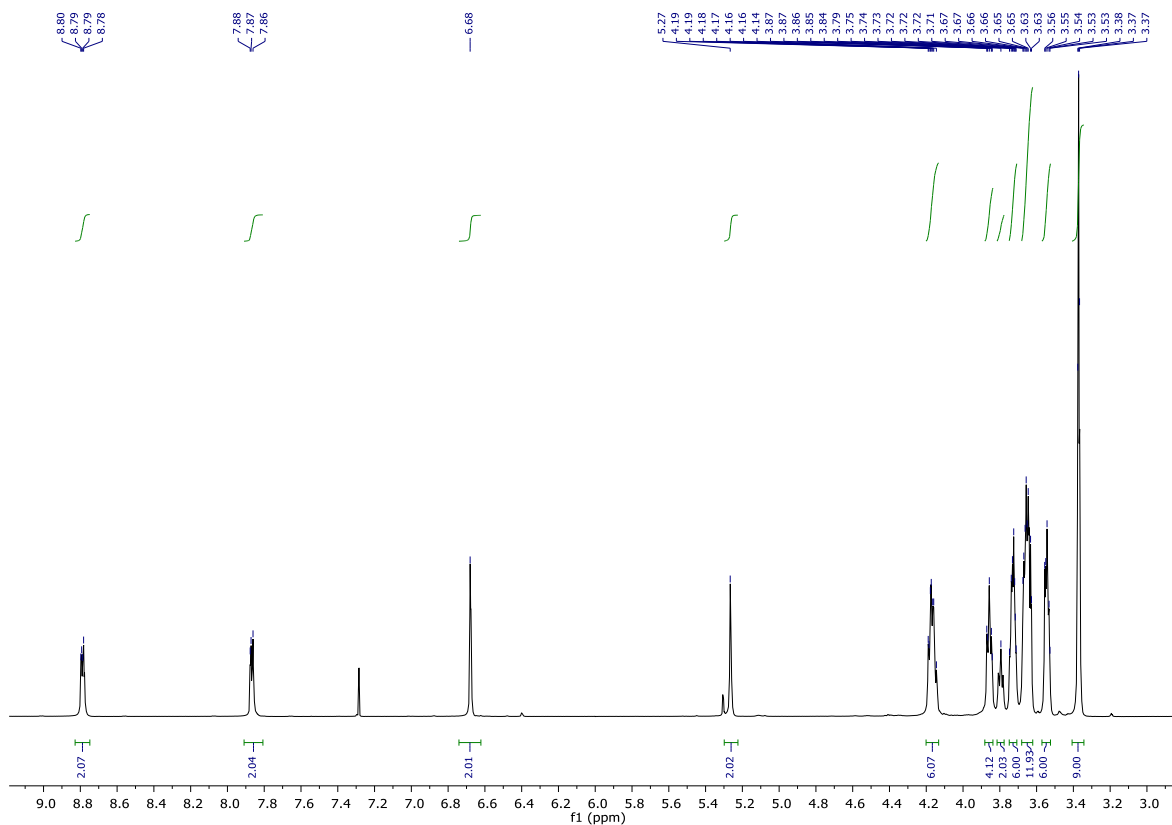


Fig. S2.4 ^1H NMR spectrum (CDCl_3 , 400 MHz) of 3,4,5-tris(2-(2-(2-methoxyethoxy)ethoxy)ethoxy)benzyl-4-ethynylbenzoate (**py-PEG3**)

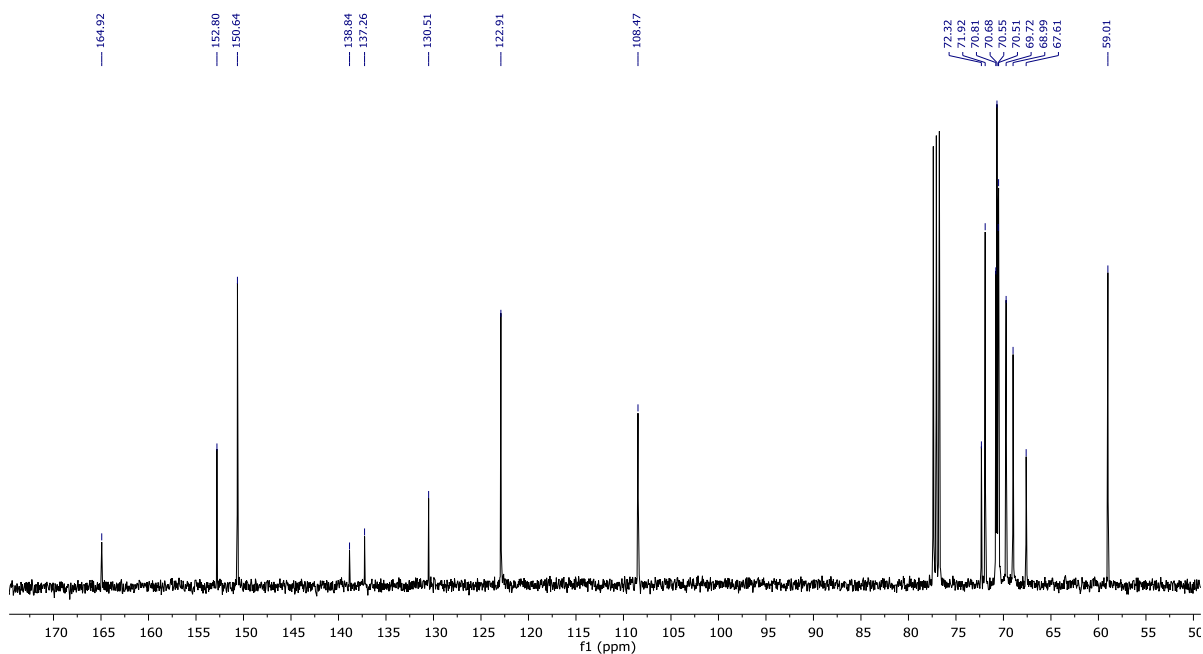


Fig. S2.5 $^{13}\text{C}\{^1\text{H}\}$ NMR spectrum (CDCl_3 , 101 MHz) of 3,4,5-tris(2-(2-(2-methoxyethoxy)ethoxy)ethoxy)benzyl-4-ethynylbenzoate (**py-PEG3**)

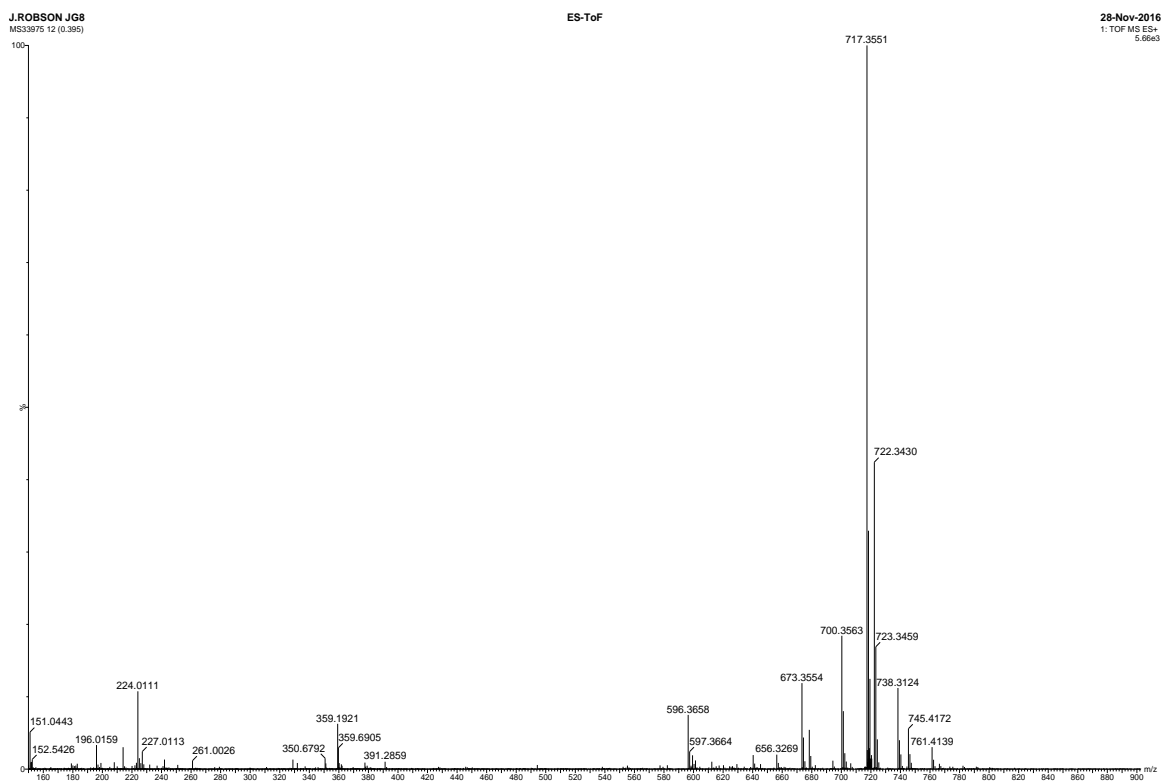


Fig. S2.6 High resolution mass spectrum (ESI+) of 3,4,5-tris(2-(2-(2-methoxyethoxy)ethoxy)ethoxy)benzyl-4-ethynylbenzoate (**py-PEG3**)

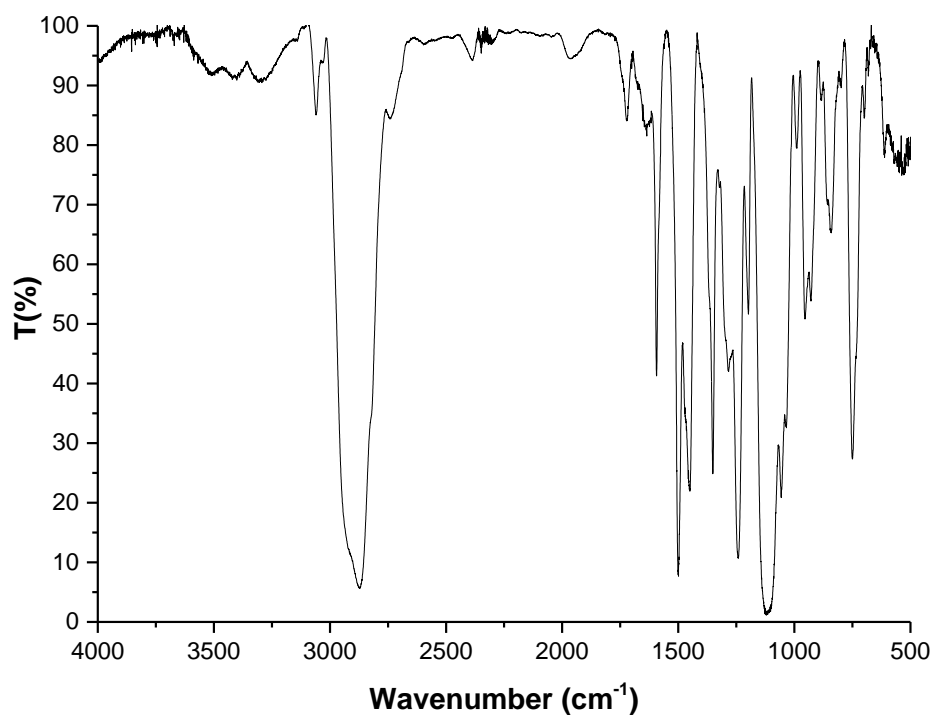
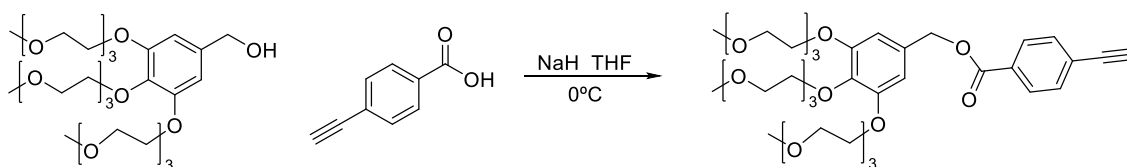


Fig. S2.6 Infrared spectrum (ATR) of 3,4,5-tris(2-(2-(2-methoxyethoxy)ethoxy)ethoxy)benzyl-4-ethynylbenzoate (**py-PEG3**).

Synthesis of 3,4,5-tris(2-(2-(2-methoxyethoxy)ethoxy)ethoxy)benzyl isonicotinate (HC≡C-PEG3)



N,N-dicyclohexylcarbodiimide (DCC) (381.3 mg, 1.85 mmol) was added to a stirred solution of (3,4,5-monoethyltetraethyleneglycol)phenylmethanol (1.0 g, 1.68 mmol), 4-ethynylbenzoic acid (245.5 mg, 1.68 mmol), and 4-(dimethylamino)pyridine (DMPA) (10.3 mg, 0.08 mmol) in CH₂Cl₂ (6 mL) at 0 °C. The resulting suspension was warmed to room temperature and stirred for 2 h. The suspension was filtered and concentrated. Purification by flash column chromatography (gradient from neat DCM to DCM:MeOH 3%) afforded a pale yellow liquid product (0.65 g, 53%). **IR (ATR, cm⁻¹):** 3245 (≡CH), 2879 (C-H), 1718 (C=O), 1592, 1439, 1268, 1100, 858. **¹H NMR** (400 MHz, CDCl₃) δ (ppm): 8.03 (d, *J* = 8.4 Hz, 2H, H_{Ar}), 7.57 (d, *J* = 8.4 Hz, 2H, H_{Ar}), 6.69 (s, 2H), 5.25 (s, 2H, C_{Ar}-CH₂), 4.18 (ddd, *J* = 8.0, 5.8, 4.4 Hz, 6H, C_{Ar}-O-CH₂), 3.87 (dd, *J* = 5.7, 4.4 Hz, 4H, O-CH₂), 3.83-3.79 (m, 2H, O-CH₂), 3.75 (td, *J* = 5.1, 4.7, 1.5 Hz, 6H, O-CH₂), 3.70-3.64 (m, 12H, O-CH₂), 3.58-3.54 (m, 6H, O-CH₂), 3.39 (d, *J* = 1.7 Hz, 9H, O-CH₃), 3.26 (s, 1H, C≡CH). **¹³C NMR** (101 MHz, CDCl₃) δ (ppm): 165.7 (C=O), 152.7 (C_{Ar}), 138.6 (C_{Ar}), 132.1 (C_{Ar}H), 131.1 (C_{Ar}), 129.6 (C_{Ar}H), 126.9 (C_{Ar}), 108.2 (C_{Ar}), 82.8 (C≡CH), 80.2 (C≡CH), 72.3 (CH₂-O), 71.9 (CH₂-O), 70.8 (CH₂-O), 70.7 (CH₂-O), 70.5 (CH₂-O), 70.5 (CH₂-O), 69.7 (CH₂-O), 68.9 (CH₂-O), 67.0 (CH₂-O), 59.0 (CH₃-O). **HRMS** (ESI⁺): *m/z* calcd. for C₃₇H₅₄NaO₁₄: 745.3406; found: 745.3411 (30, M+Na⁺).

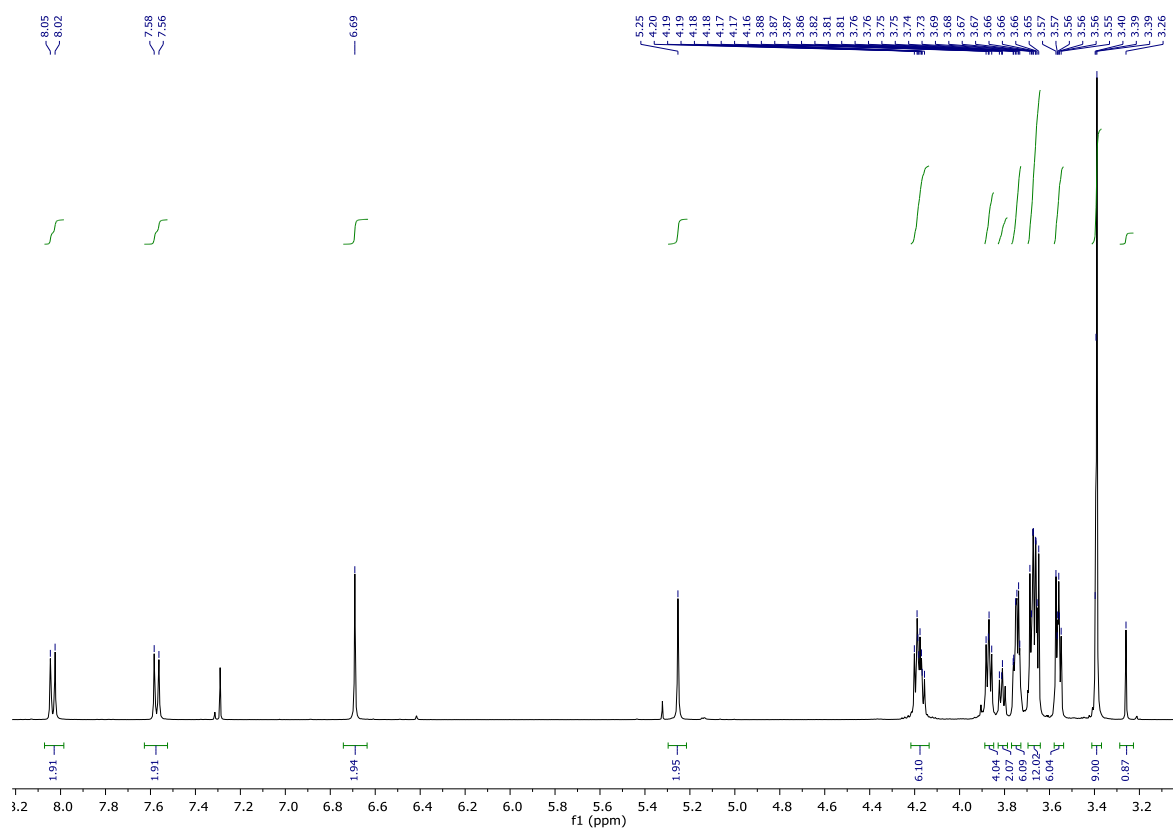


Fig. S2.7 ^1H NMR spectrum (CDCl_3 , 400 MHz) of 3,4,5-tris(2-(2-(2-methoxyethoxy)ethoxy)ethoxy)benzyl isonicotinate (**HC≡C-PEG3**)

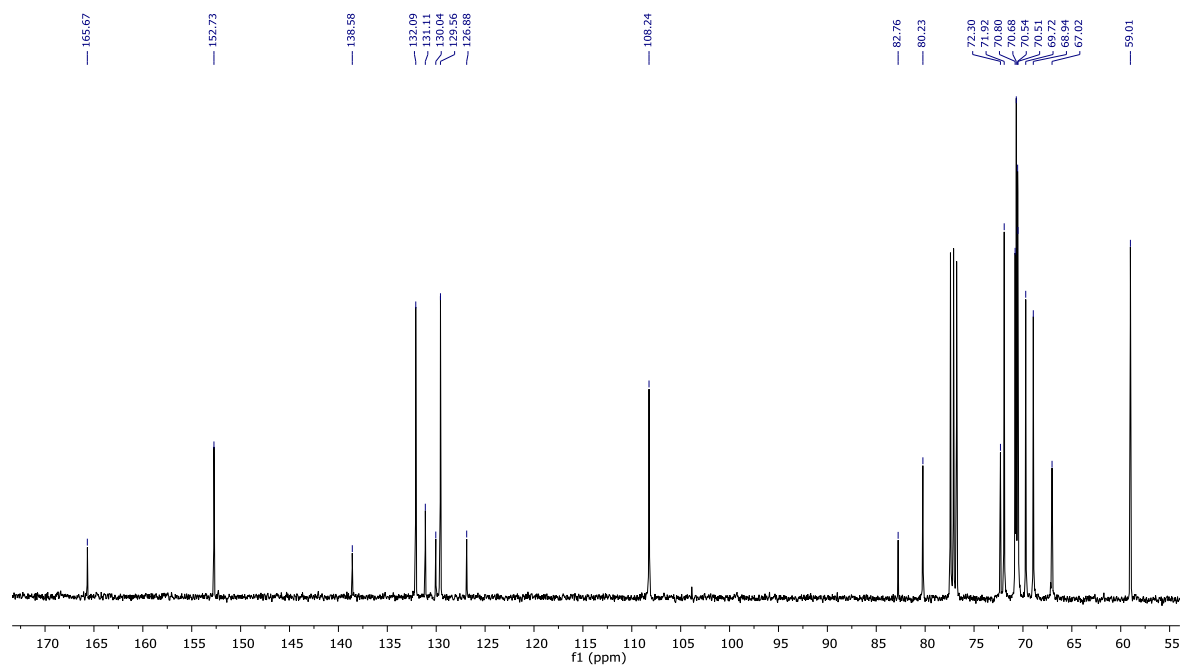


Fig. S2.8 $^{13}\text{C}\{^1\text{H}\}$ NMR (CDCl_3 , 101 MHz) of 3,4,5-tris(2-(2-(2-methoxyethoxy)ethoxy)ethoxy)benzyl isonicotinate (**HC≡C-PEG3**)

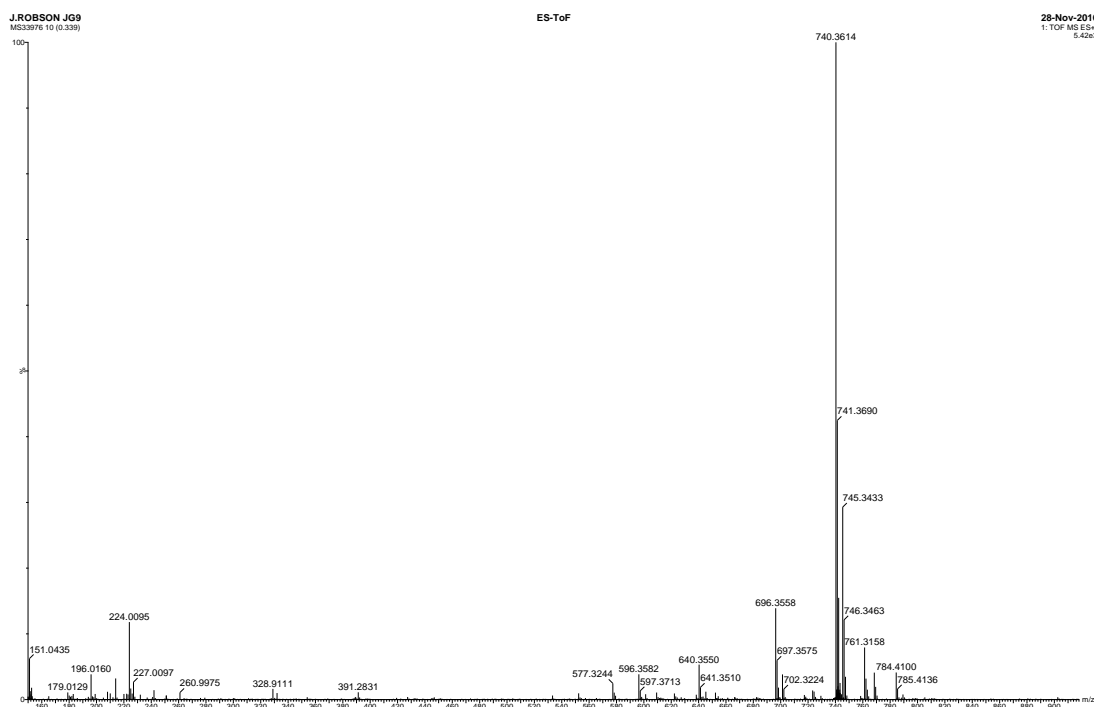


Fig. S2.9 High resolution mass spectrum (ESI+) of 3,4,5-tris(2-(2-(2-methoxyethoxy)ethoxy)ethoxy)benzyl isonicotinate (**HC≡C-PEG3**).

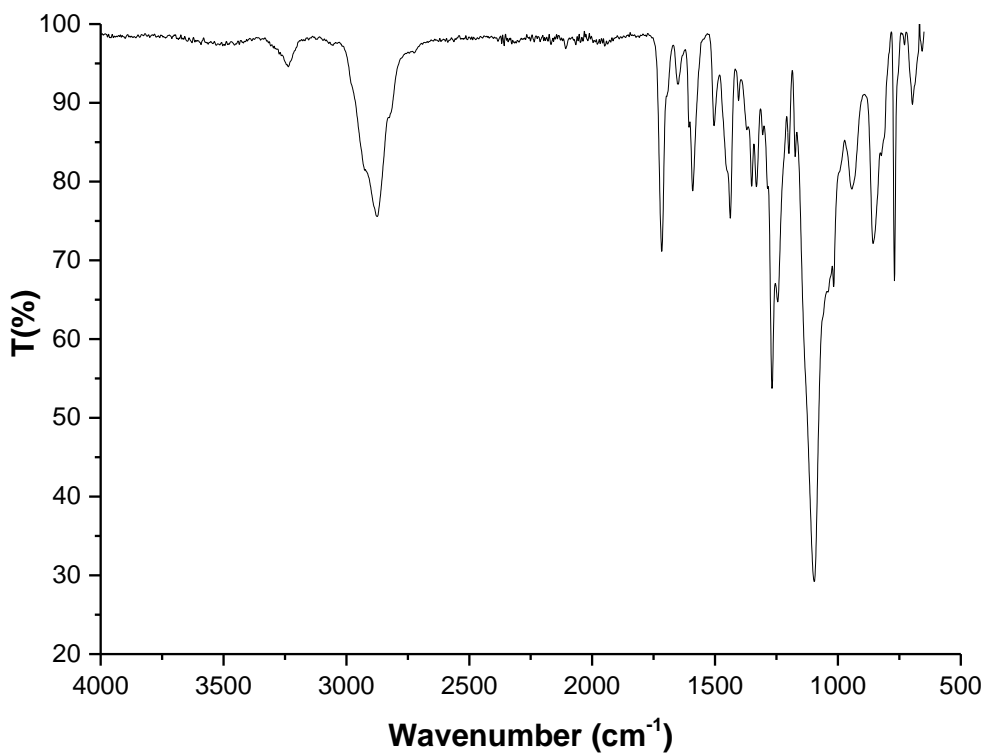
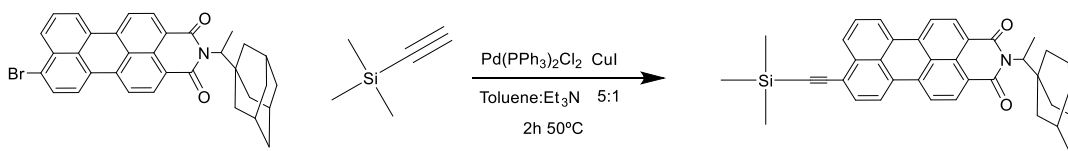


Fig. S2.10 Infrared spectrum (ATR) of 3,4,5-tris(2-(2-(2-methoxyethoxy)ethoxy)ethoxy)benzyl isonicotinate (**HC≡C-PEG3**)

Perylene derivatives

Synthesis of *N*-(2-adamantyl-ethylamine)-9-trimethylsilylethynyl-3,4-perylenemonoimide



Under a nitrogen atmosphere, *N*-(2-adamantyl-ethylamine)-9-bromo-3,4-perylenemonoimide^{S1} (200 mg, 0.36 mmol), copper iodide (2 mg, 0.005 mmol) and dichlorobis(triphenylphosphine)palladium(II) (17.6 mg, 0.025 mmol) were dissolved in a 5:1 mixture of toluene and triethylamine (50:10 mL). The mixture was sealed with a septum and stirred. Trimethylsilylacetylene (90 μ L, 0.6 mmol) was added using a syringe and the reaction mixture was stirred at 50 °C. After 2 hours, the mixture was filtered through celite and evaporated to dryness. The residue was purified by column chromatography using silica gel and a 1:2 mixture of hexane and DCM as eluent. The product was obtained as a bright red-purple solid and analysed by ¹H NMR spectroscopy before deprotection (below). **¹H NMR** (400 MHz, CDCl₃) δ (ppm): 8.44 (dt, J = 13.4, 7.9 Hz, 2H, **H_{Ar}**), 8.30 (d, J = 8.2 Hz, 1H, **H_{Ar}**), 8.23 (dd, J = 6.7, 2.5 Hz, 1H, **H_{Ar}**), 8.19 (d, J = 8.1 Hz, 1H, **H_{Ar}**), 8.14 (d, J = 8.1 Hz, 1H, **H_{Ar}**), 8.11 (dd, J = 8.1, 2.5 Hz, 1H, **H_{Ar}**), 7.69 (dd, J = 7.9, 1.9 Hz, 1H, **H_{Ar}**), 7.63 – 7.56 (m, 1H, **H_{Ar}**), 5.13 (q, J = 7.2 Hz, 1H, **CH**), 2.01 (s, 3H, 3**×CH**), 1.86-1.66 (m, 15H, 6**×CH**₂ + **CH**₃), 0.42 (s, 9H, 3**×CH**₃).

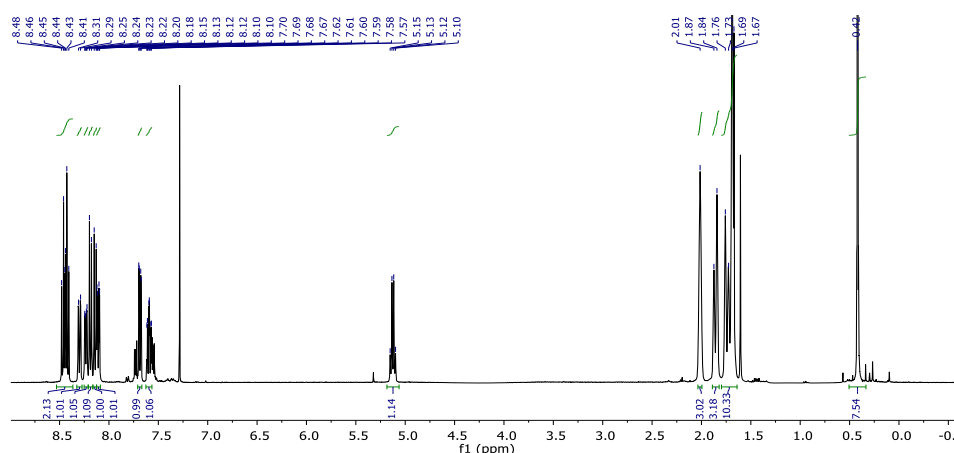
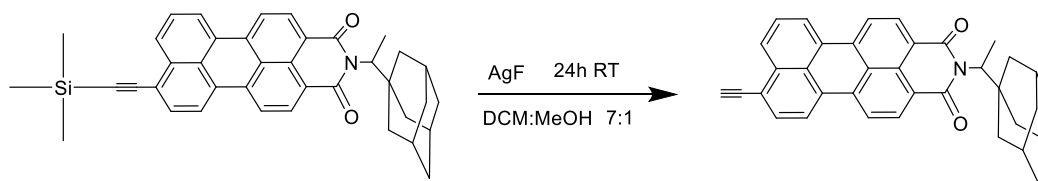


Fig. S2.11 ¹H NMR spectrum (CDCl₃, 400 MHz) of *N*-(2-adamantyl-ethylamine)-9-trimethylsilylethynyl-3,4-perylenemonoimide

Synthesis of *N*-(2-adamantyl-ethylamine)-9-ethynyl-3,4-perylene-dicarboxylic acid monoimide (HC≡C-per^{Im})



N-(2-adamantyl-ethylamine)-9-trimethylsilylethynyl-3,4-perylenemonoimide^{S1} (200 mg, 0.34 mmol) was dissolved in DCM:MeOH (14:2 mL). Then AgF (0.1 g, 0.78 mmol) was added to the solution. After stirring overnight at room temperature, 15 mL of aqueous HCl (17%), was added to the mixture to form a precipitate. This mixture was filtered under vacuum and the organic phase was washed twice with HCl (17%) aqueous solution and once with water. The combined organic extracts were dried using sodium sulfate, concentrated under reduced pressure and the residue was purified by column chromatography using silica gel and DCM:Hexane as eluent (8:2). The product was obtained as a red solid (127 mg, 74%). **IR** (ATR, cm^{-1}): 3245 ($\equiv\text{CH}$), 2879 (C-H), 1718 (C=O), 1592, 1439, 1268, 1100, 858. **¹H NMR** (400 MHz, CDCl_3) δ (ppm): 8.42 – 8.27 (m, 2H, H_{Ar}), 8.16 (d, $J = 8.2$ Hz, 1H, H_{Ar}), 8.05 – 7.83 (m, 4H, H_{Ar}), 7.56 (dd, $J = 7.8$, 2.1 Hz, 1H, H_{Ar}), 7.45 (td, $J = 7.9$, 2.2 Hz, 1H, H_{Ar}), 5.12 (q, $J = 7.2$ Hz, 1H, N-CH), 3.65 (s, 1H, C \equiv CH), 2.12 – 1.97 (m, 3H, 3 \times CH), 1.96-1.63 (m, 15H, CH₂+CH₃). **¹³C{¹H} NMR** (101 MHz, CDCl_3) δ (ppm): 165.3 (C=O), 164.6 (C=O), [136.0, 135.5, 134.2, 131.6, 131.5, 131.0, 130.8, 129.6, 129.3, 129.1, 128.4, 127.4, 125.9, 123.5, 122.2, 122.0, 121.1, 120.5, 120.2] (CH_{Ar} + C_{Ar}), 84.8 (C \equiv CH), 81.3 (C \equiv CH), 58.1 (CH), 40.3 (CH₂), 38.0 (C_q), 37.0 (CH₂), 28.8 (CH), 13.2 (CH₃). **HRMS** (ESI⁺): m/z calcd for C₃₆H₃₀NO₂: 508.2271; found: 508.2277 (22, M+H⁺). **UV-Vis** (CHCl_3): λ_{max} (ϵ) = 440 nm (16300 M⁻¹ cm⁻¹); 470 nm (39000 M⁻¹ cm⁻¹); 500 nm (48900 M⁻¹ cm⁻¹); $\Phi = 90.2 \pm 2$ %, calculated in CH₂Cl₂; τ (CH₂Cl₂, $\lambda_{\text{exc}} = 510$ nm) = 4.62 ns, $\chi^2 = 1.085$.

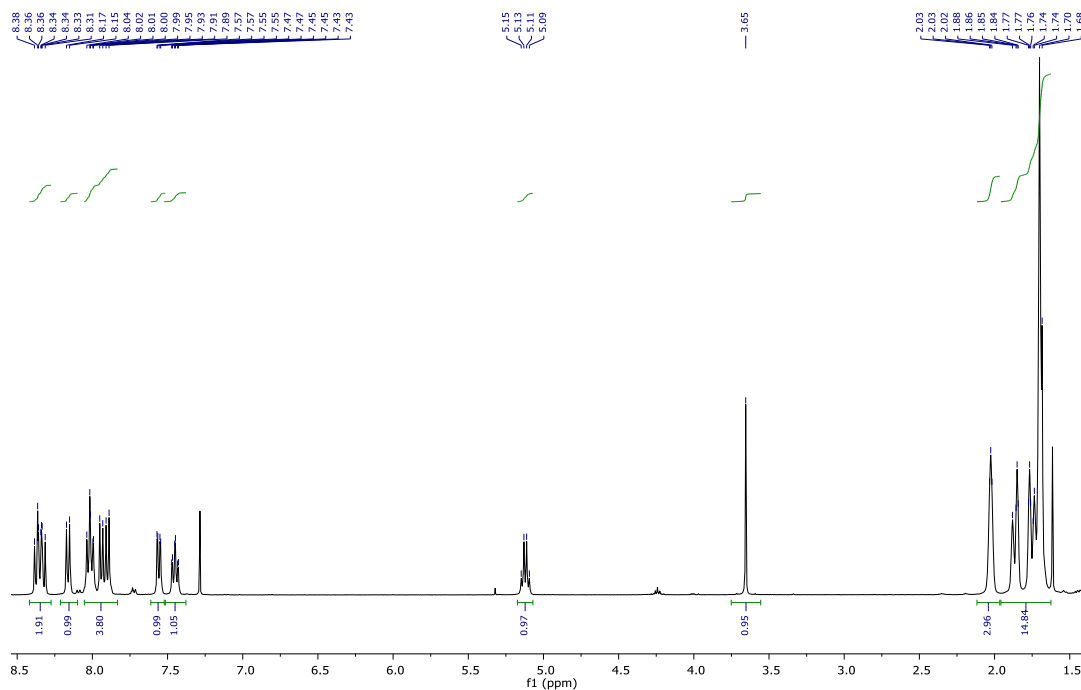


Fig. S2.12 ^1H NMR spectrum (CDCl_3 , 400 MHz) of *N*-(2-adamantyl-ethylamine)-9-ethynyl-3,4-perylene-dicarboxylic acid monoimide (**HC≡C-per^{Im}**).

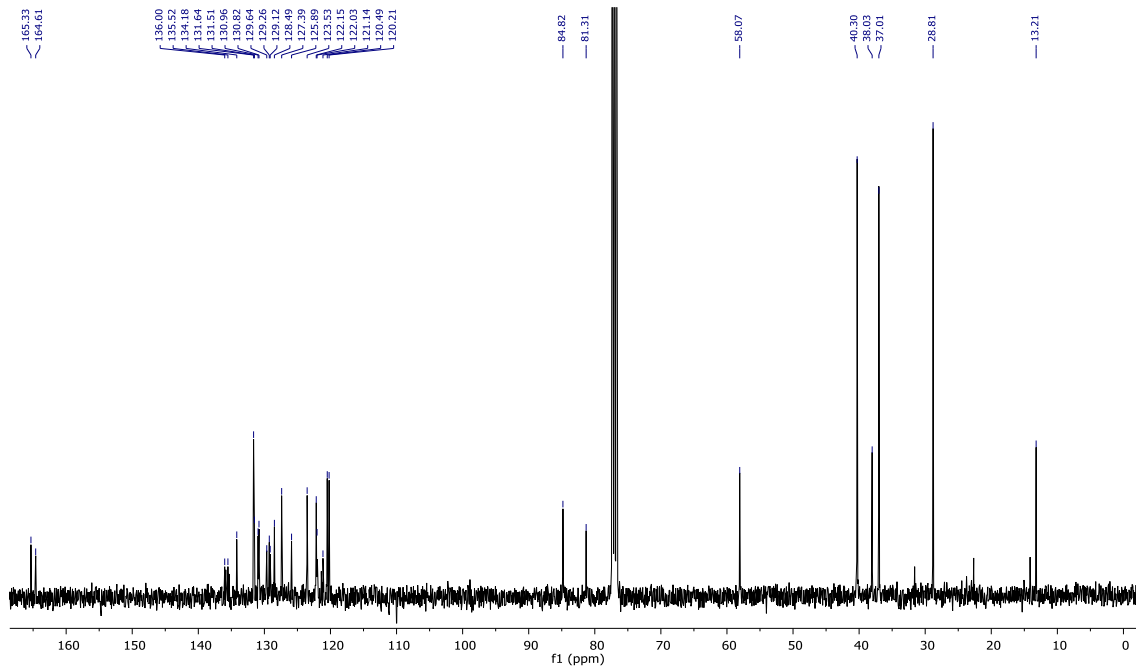


Fig. S2.13 $^{13}\text{C}\{^1\text{H}\}$ NMR (CDCl_3 , 101 MHz) of *N*-(2-adamantyl-ethylamine)-9-ethynyl-3,4-perylene-dicarboxylic acid monoimide (**HC≡C-per^{Im}**).

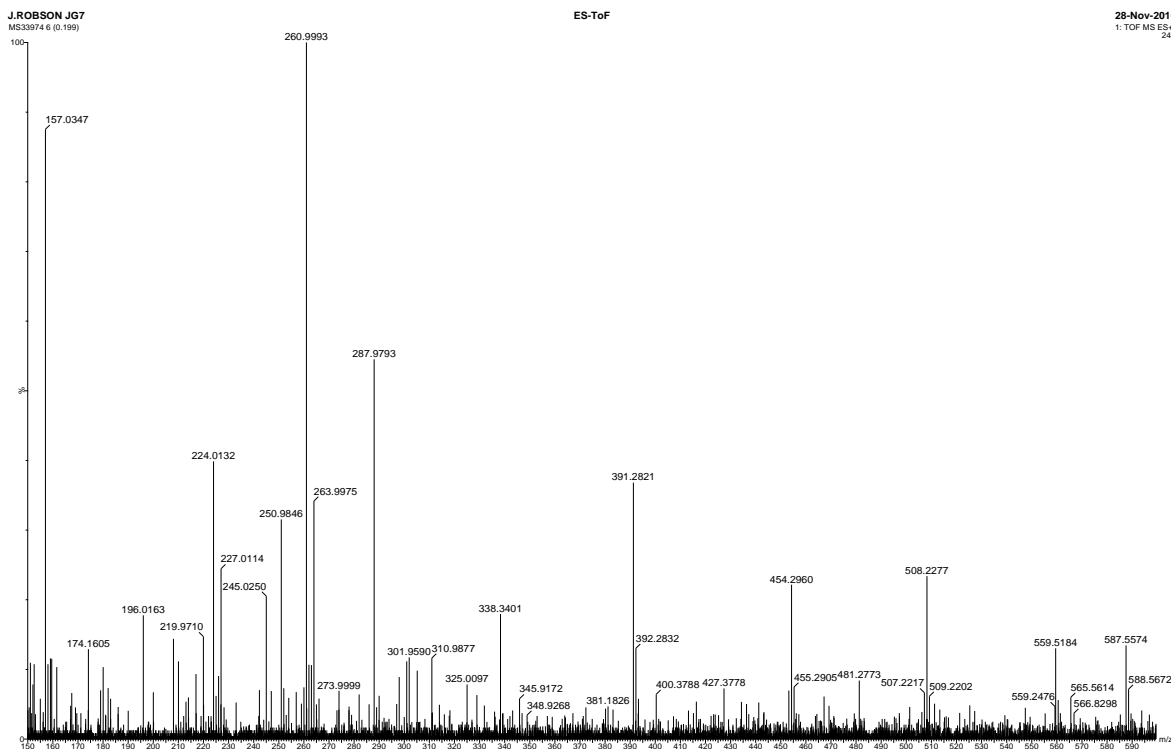


Fig. S2.14 High resolution mass spectrum (ESI+) of *N*-(2-adamantyl-ethylamine)-9-ethynyl-3,4-perylene-dicarboxylic acid monoimide (**HC≡C-per^{Im}**).

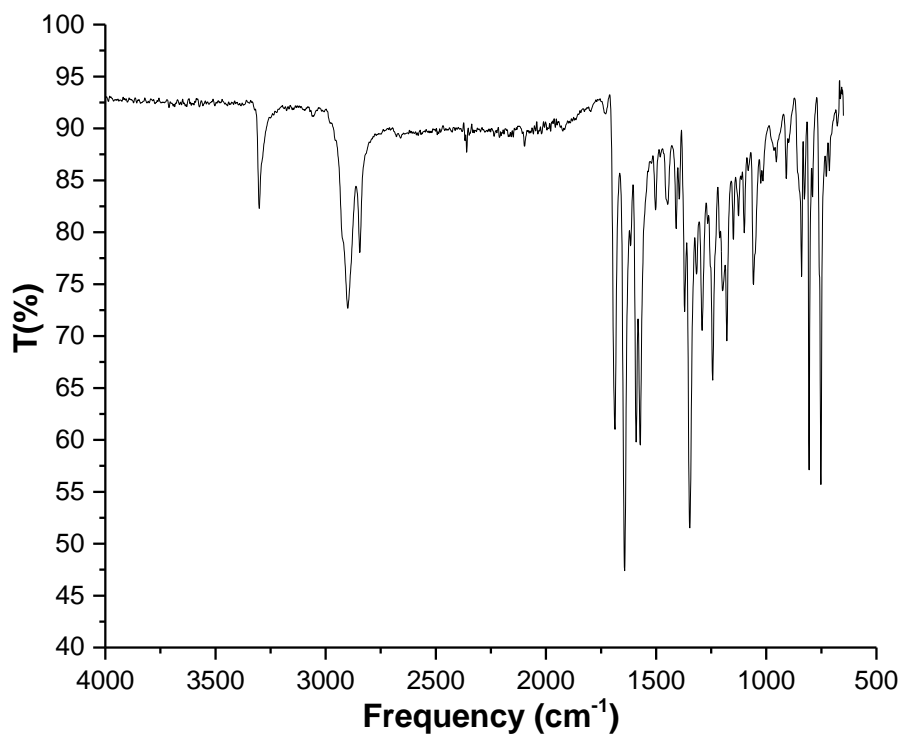


Fig. S2.15 Infrared spectrum (ATR) of *N*-(2-adamantyl-ethylamine)-9-ethynyl-3,4-perylene-dicarboxylic acid monoimide (**HC≡C-per^{Im}**).

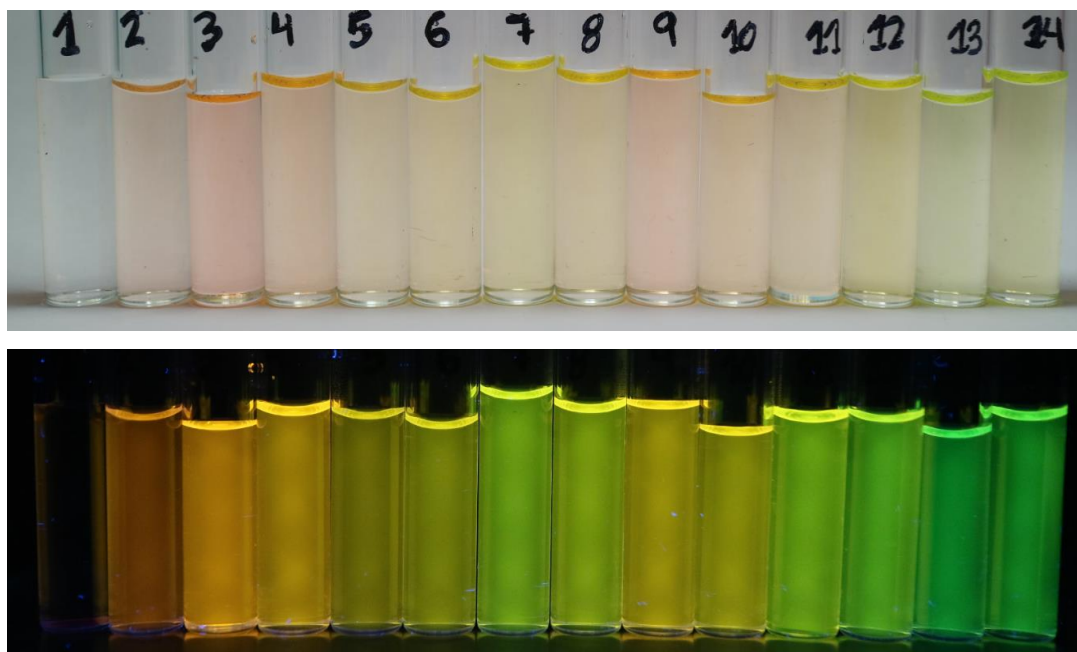
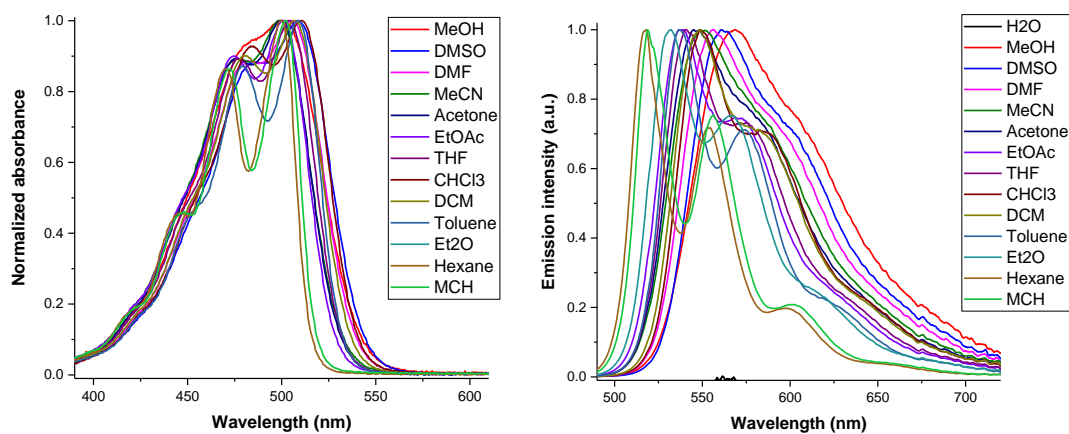
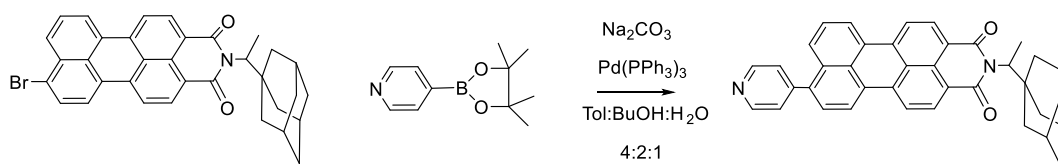


Fig. S2.16 Solvatochromism of *N*-(2-adamantyl-ethylamine)-9-ethynyl-3,4-perylene-dicarboxylic acid monoimide (**HC≡C-per^{lm}**) investigated in 14 solvents (water, methanol, DMSO, DMF, MeCN, acetone, EtOAc, THF, chloroform, dichloromethane, toluene, diethylether, hexane and methylcyclohexane) of decreasing polarity (probe concentration 10 μ M) in visible light (middle) and under UV light (bottom).

Synthesis of *N*-(2-adamantyl-ethylamine)-9-(5-pyridine)-3,4-perylenemonoimide (py-per^{Im})



In a 100 mL Schlenk tube under an atmosphere of nitrogen, *N*-(2-adamantyl-ethylamine)-9-bromo-3,4-perylenemonoimide^{S1} (100 mg, 0.18 mmol) was dissolved in a mixture of toluene:*n*BuOH (12:5 mL). $\text{Pd}(\text{PPh}_3)_3$ (8.2 mg, 5 mol%) was added under nitrogen followed by 4-pyridylboronic ester (36.5 mg, 0.18 mmol) dissolved in a mixture of toluene:*n*BuOH (4:2 mL). Finally, Na_2CO_3 (151 mg, 1.42 mmol) was added, dissolved in water (3.5 mL). The reaction was stirred for 18 hours and the product was then extracted DCM:Water (100:50 mL, 3 × 100 mL DCM). Purification by column chromatography in DCM provided a red solid (62.3 mg, 62%). **IR** (ATR, cm^{-1}): 2902-2849 (C-H), 1693 (C=O), 1650, 1592, 1350, 1245, 1060, 809, 753. **¹H NMR** (400 MHz, CDCl_3) δ (ppm): 8.86 (s, 2H, H_{Ar}), 8.50 – 8.40 (m, 2H, H_{Ar}), 8.36 – 8.18 (m, 4H, H_{Ar}), 7.85 (d, $J = 8.4$ Hz, 1H, H_{Ar}), 7.61 – 7.46 (m, 4H, H_{Ar}), 5.16 – 5.06 (m, 1H, N-CH), 2.00 (s, 3H, 3×CH), 1.86-1.66 (m, 15H, 6×CH₂+CH₃). **¹³C{¹H} NMR** (101 MHz, CDCl_3) δ (ppm): 165.4 (C=O), 164.7 (C=O), 149.8 ($\text{C}_{\text{Ar}}-\text{N}_{\text{Ar}}$), [148.2, 139.6, 139.5, 136.4, 136.2, 136.0, 135.8, 131.7, 131.7, 131.1, 131.0, 129.7, 129.6, 129.5, 129.4, 128.2, 127.9, 127.9, 127.4, 126.2, 125.0, 123.6, 122.8, 122.7, 122.2, 122.1, 121.3, 121.2, 120.4, 120.3] (CH_{Ar} + C_{Ar}), 58.1 (CH), 40.3 (CH₂), 38.0 (C_{q}), 37.0 (CH₂), 28.8 (CH), 13.2 (CH₃). **HRMS** (ESI⁺): m/z calcd for $\text{C}_{39}\text{H}_{33}\text{N}_2\text{O}_2$: 561.2537; found: 561.2542 (43, $\text{M}+\text{H}^+$). **UV-Vis** (CHCl_3): λ_{max} (ϵ) = 440 nm (13400 $\text{M}^{-1} \text{cm}^{-1}$); 470 nm (29800 $\text{M}^{-1} \text{cm}^{-1}$); 500 nm (34200 $\text{M}^{-1} \text{cm}^{-1}$); $\Phi = 91.2 \pm 2$ %, calculated in CH_2Cl_2 ; τ (CH_2Cl_2 , $\lambda_{\text{exc}} = 510$ nm) = 4.45 ns, $\chi^2 = 1.116$.

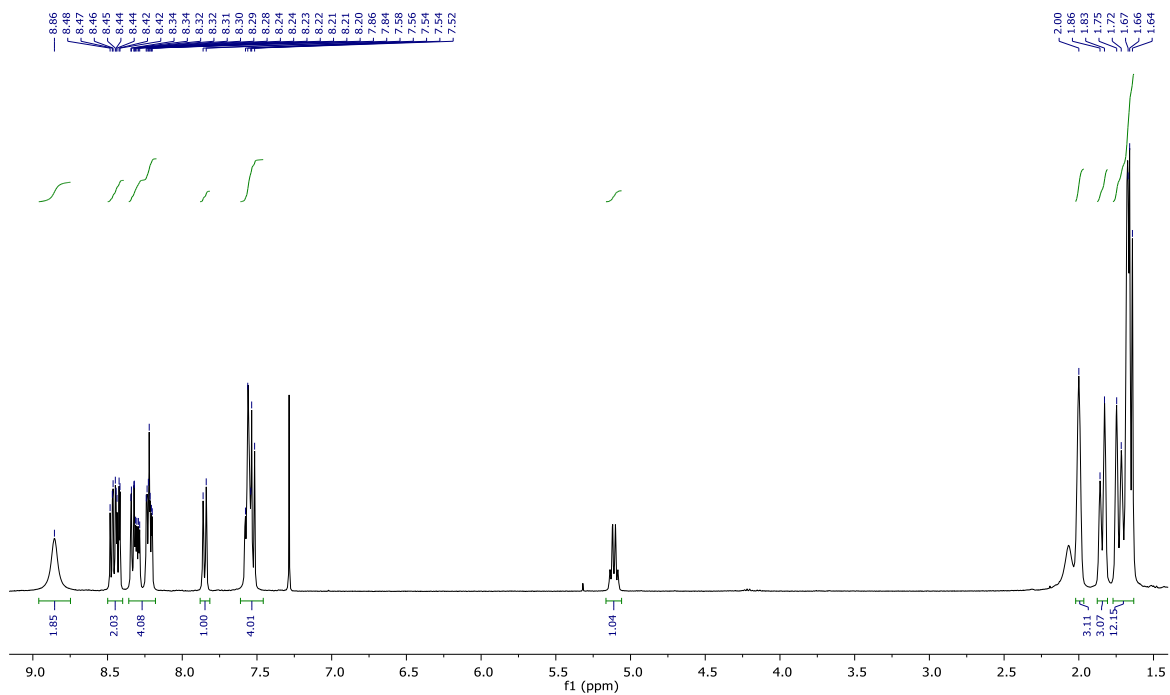


Fig. S2-17 ^1H NMR spectrum (CDCl_3 , 400 MHz) of *N*-(2-adamantyl-ethylamine)-9-(5-pyridine)-3,4-perylenemonoimide (**py-per^{Im}**).

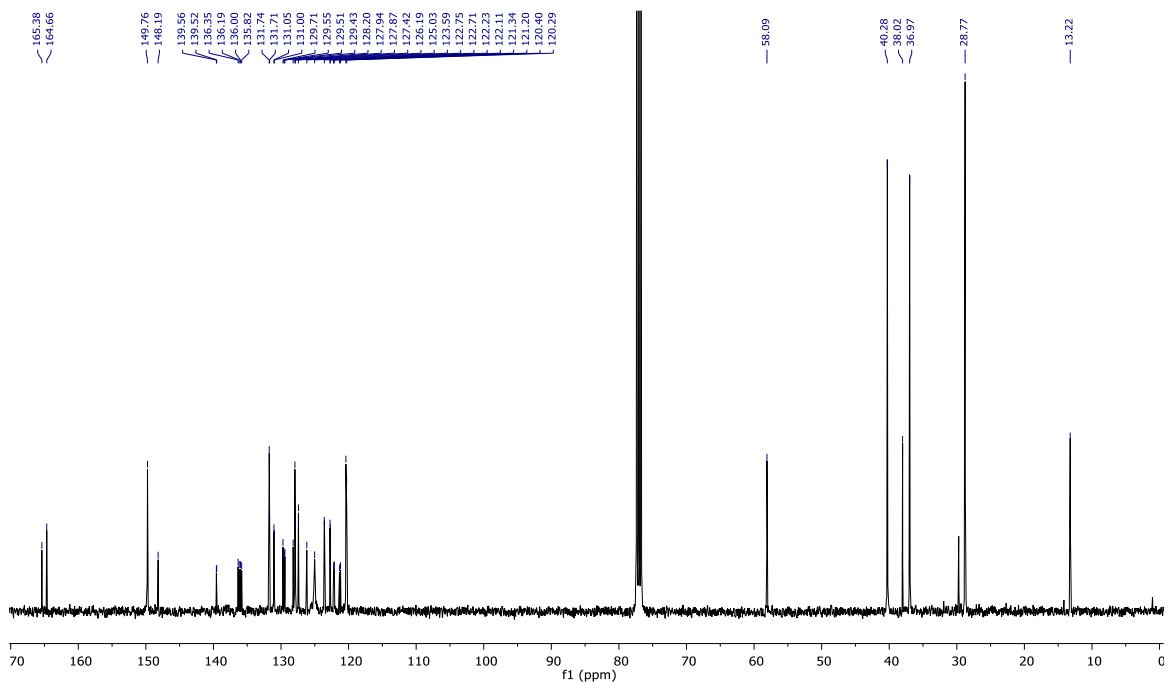


Fig. S2-18 $^{13}\text{C}\{^1\text{H}\}$ NMR (CDCl_3 , 101 MHz) of *N*-(2-adamantyl-ethylamine)-9-(5-pyridine)-3,4-perylenemonoimide (**py-per^{Im}**).

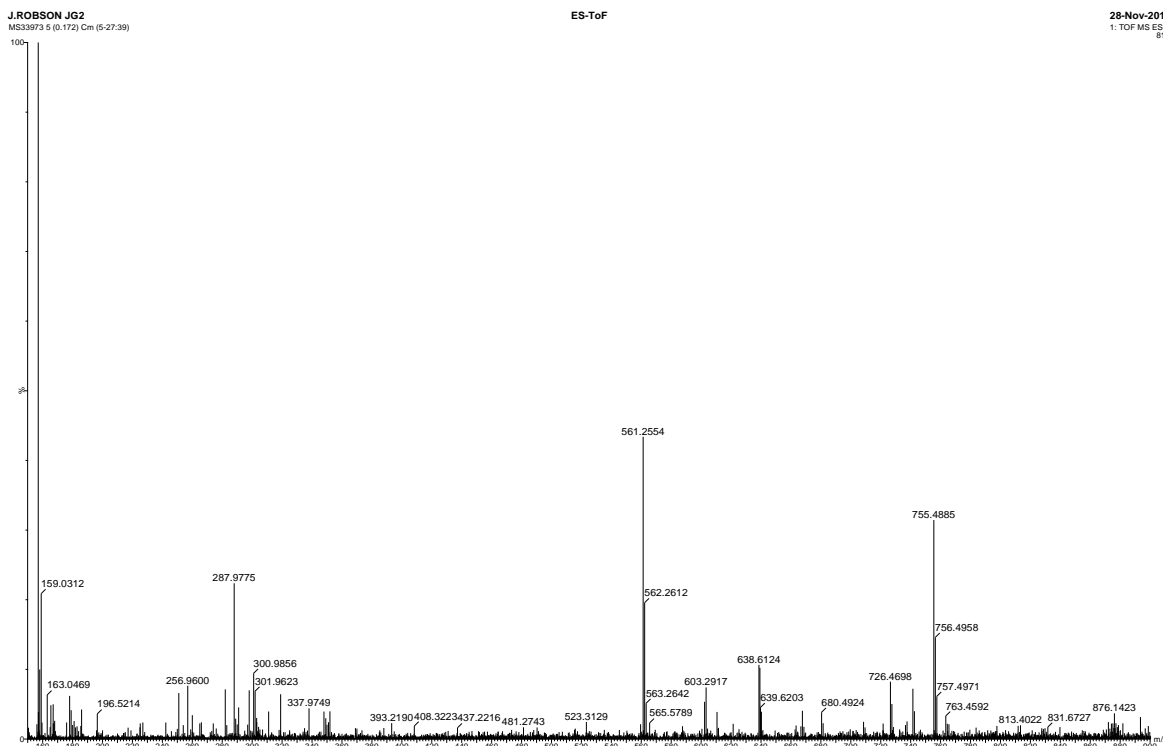


Fig. S2.19 High resolution mass spectrum (ESI+) of *N*-(2-adamantyl-ethylamine)-9-(5-pyridine)-3,4-perylenemonoimide (**py-per^{Im}**).

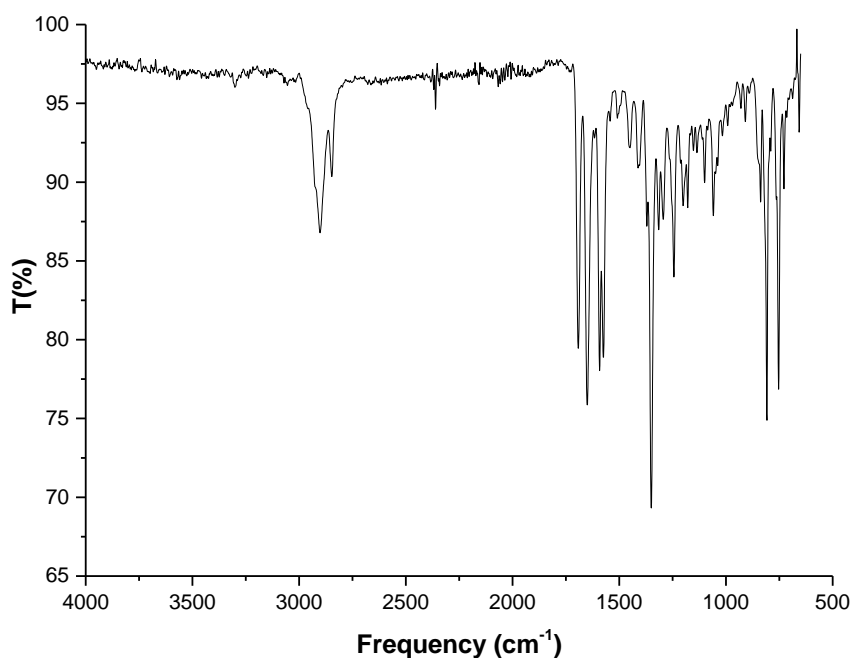


Fig. S2.20 Infrared (ATR) spectrum of *N*-(2-adamantyl-ethylamine)-9-(5-pyridine)-3,4-perylenemonoimide (**py-per^{Im}**).

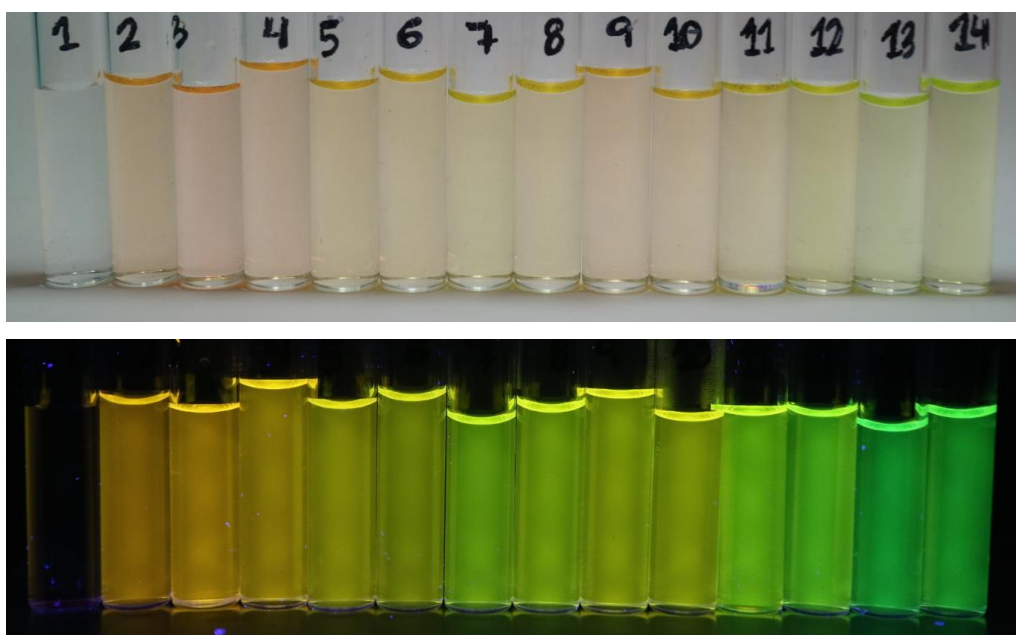
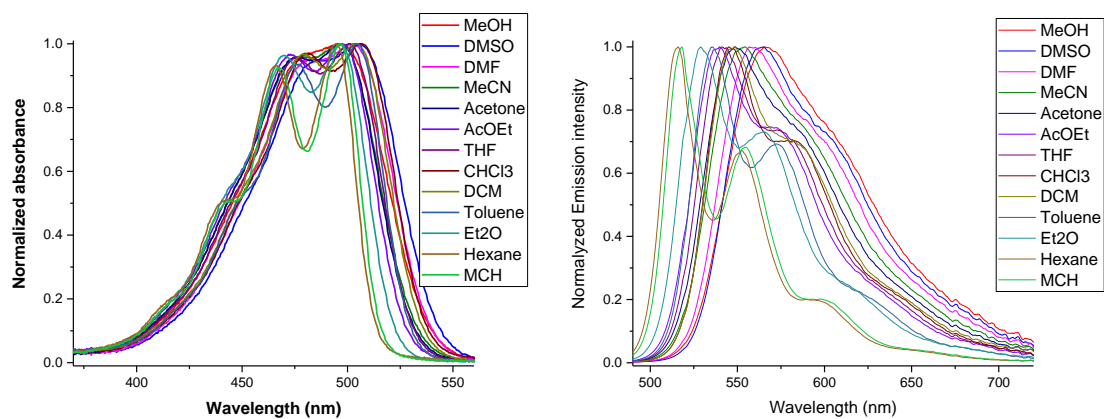
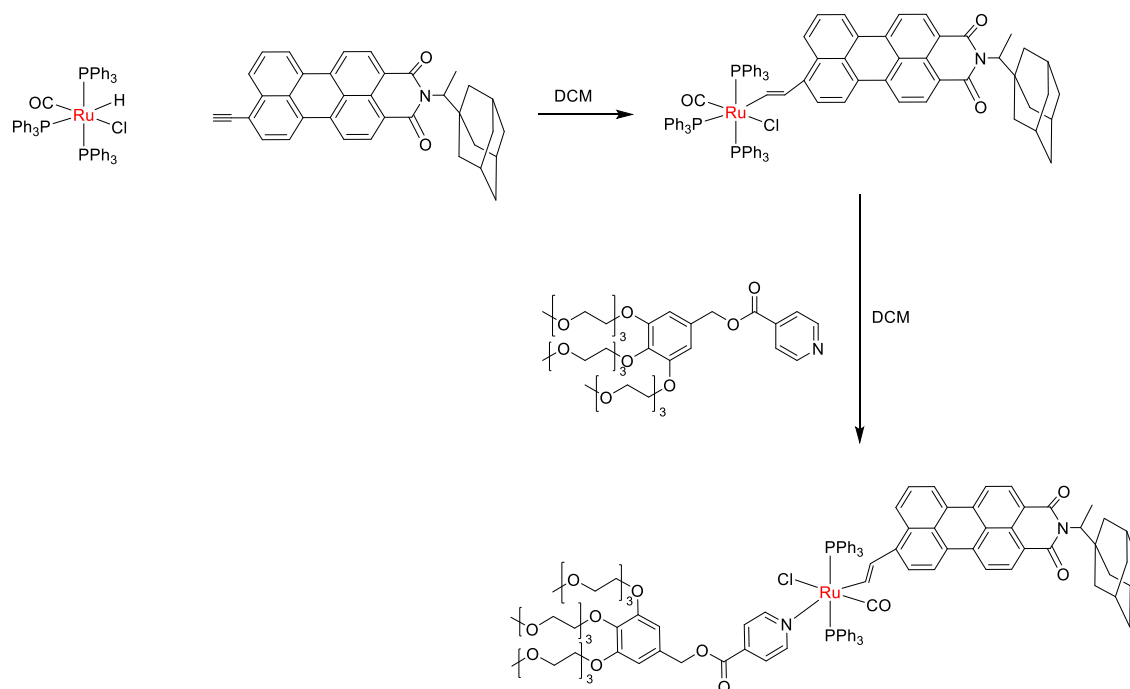


Fig. S2.21 Solvatochromism of *N*-(2-adamantyl-ethylamine)-9-(5-pyridine)-3,4-pyrenemonoimide (**py-per^{lm}**) in 14 solvents (water, methanol, DMSO, DMF, MeCN, acetone, EtOAc, THF, chloroform, dichloromethane, toluene, diethylether, hexane and methylcyclohexane) in order of decreasing polarity (probe concentration 10 μ M) in visible light (middle) and UV light (bottom).

Synthesis of ruthenium complexes

Synthesis of $[\text{Ru}(\text{CH}=\text{CH-per}^{\text{Im}})\text{Cl}(\text{CO})(\text{py-PEG3})(\text{PPh}_3)_2]$ (**3PEG-Ru-CH=CH-per^{Im}**)



In a 50 mL flask, $[\text{RuHCl}(\text{CO})(\text{PPh}_3)_3]^{\text{S5}}$ (50 mg, 0.053 mmol) was dissolved in dichloromethane (10 mL) and treated with *N*-(2-adamantyl-ethylamine)-9-ethynyl-3,4-perylene-dicarboxylic acid monoimide (**HC≡C-per^{Im}**) (26.7 mg, 0.053 mmol). The solution became dark blue instantly. After 30 mins, 3,4,5-tris(2-(2-(2-methoxyethoxy)ethoxy)ethoxy)benzyl-4-ethynylbenzoate (**py-PEG3**) (36.7 mg, 0.053 mmol) was added to the solution. After stirring for one hour, the reaction was concentrated under vacuum and hexane added. This formed a solid precipitate, which was filtered and washed with hexane several times to give a dark blue product (84 mg, 84%). **IR** (ATR, cm^{-1}): 3066 (=C-H), 2864 (C-H), 1926 ($\text{C}\equiv\text{O}$), 1734 (C=O), 1687, 1647, 1589, 1567, 1435, 1280, 1095, 1051, 849, 814, 747, 690. **¹H NMR** (400 MHz, CD_2Cl_2) δ (ppm): 9.59 (d, $J = 16.3$ Hz, 1H, **H_{Ar}**), 8.74 (s, 2H, **H_{Ar}**), 8.39 (dd, $J = 15.1, 8.1$ Hz, 1H, **H_{Ar}**), 8.29 (dd, $J = 17.7, 8.1$ Hz, 1H, **H_{Ar}**), 8.20 (dd, $J = 20.8, 7.9$ Hz, 2H, **H_{Ar}**), 8.10 (dd, $J = 8.3, 6.4$ Hz, 1H, **H_{Ar}**), 8.02 (dd, $J = 8.3, 6.5$ Hz, 1H, **H_{Ar}**), 7.66 (d, $J = 8.5$ Hz, 1H, **H_{Ar}**), 7.58 – 7.53 (m, 12H, **H_{Ar}**), 7.37 – 7.32 (m, 2H, **H_{Ar}**), 7.29 (d, $J = 7.4$ Hz, 6H, **H_{Ar}**), 7.21 (t, $J = 7.3$

Hz, 12H), 6.96 (d, $J = 16.3$ Hz, 1H, \mathbf{H}_{Ar}), 6.72 (s, 2H, \mathbf{H}_{Ar}), 5.28 (s, 2H, $\mathbf{CH=CH}$), 5.09 (q, $J = 7.3$ Hz, 1H, \mathbf{CH}), 4.19 (ddd, $J = 18.8, 5.8, 4.1$ Hz, 6H, \mathbf{CH}_2), 3.89 (dd, $J = 5.7, 4.0$ Hz, 4H, \mathbf{CH}_2), 3.82 – 3.77 (m, 2H, \mathbf{CH}_2), 3.73 – 3.58 (m, 18H, \mathbf{CH}_2), 3.54 – 3.48 (m, 6H, \mathbf{CH}_2), 3.34 (d, $J = 6.4$ Hz, 9H, \mathbf{CH}_3), 1.98 (s, 3H, $3\times\mathbf{CH}$), 1.87–1.63 (m, 15H, $6\times\mathbf{CH}_2+\mathbf{CH}_3$). $^{13}\mathbf{C}\{\mathbf{^1H}\}$ NMR (101 MHz, CD_2Cl_2) δ (ppm): 203.6 ($\mathbf{C}\equiv\mathbf{O}$), 166.0 ($\mathbf{C}=\mathbf{O}$), 165.9 ($\mathbf{C}=\mathbf{O}$), 165.3 ($\mathbf{C}=\mathbf{O}$), 165.2 ($\mathbf{C}=\mathbf{O}$), 164.6 ($\mathbf{C}=\mathbf{O}$), 155.3, 153.4, 140.4, 139.2, 138.2, 138.0, 137.8, 137.3, 134.9, 134.8, 134.8, 134.5, 133.0, 132.8, 132.6, 132.2, 131.9, 131.5, 131.3, 131.2, 130.4, 130.2, 129.3, 128.8, 128.4, 128.3, 128.3, 127.9, 126.7, 126.1, 125.0, 123.8, 123.6, 123.1, 121.9, 121.0, 120.8, 119.9, 119.0, 108.4 ($\mathbf{CH=CH}$), 73.0, 72.5, 71.4, 71.1, 71.1, 71.0, 70.3, 69.6, 68.2, 59.2 (\mathbf{CH}_3), 58.1 ($\mathbf{CH-Adam}$), 58.1, 40.9, 38.5, 37.6, 32.1, 29.6, 23.2, 14.4, 13.5 (\mathbf{CH}_3). $^{31}\mathbf{P}\{\mathbf{^1H}\}$ NMR (162 MHz, CD_2Cl_2) δ (ppm): 26.2. **UV-Vis** (CD_2Cl_2): λ_{max} (ϵ) = 520 nm ($37840 \text{ M}^{-1} \text{ cm}^{-1}$); 575 nm ($46445 \text{ M}^{-1} \text{ cm}^{-1}$); $\Phi = 37.5 \pm 2 \%$, calculated in CH_2Cl_2 ; τ (CH_2Cl_2 , $\lambda_{\text{exc}} = 510 \text{ nm}$) = 4.74 ns, $\chi^2 = 1.078$. **Elemental Analysis:** Calculated for $\text{C}_{107}\text{H}_{113}\text{ClN}_2\text{O}_{17}\text{P}_2\text{Ru} \cdot 0.5\text{CH}_2\text{Cl}_2$: C 66.6%, H 5.9%, N 1.4%. Found C 66.9%, H 6.0%, N 1.7%.

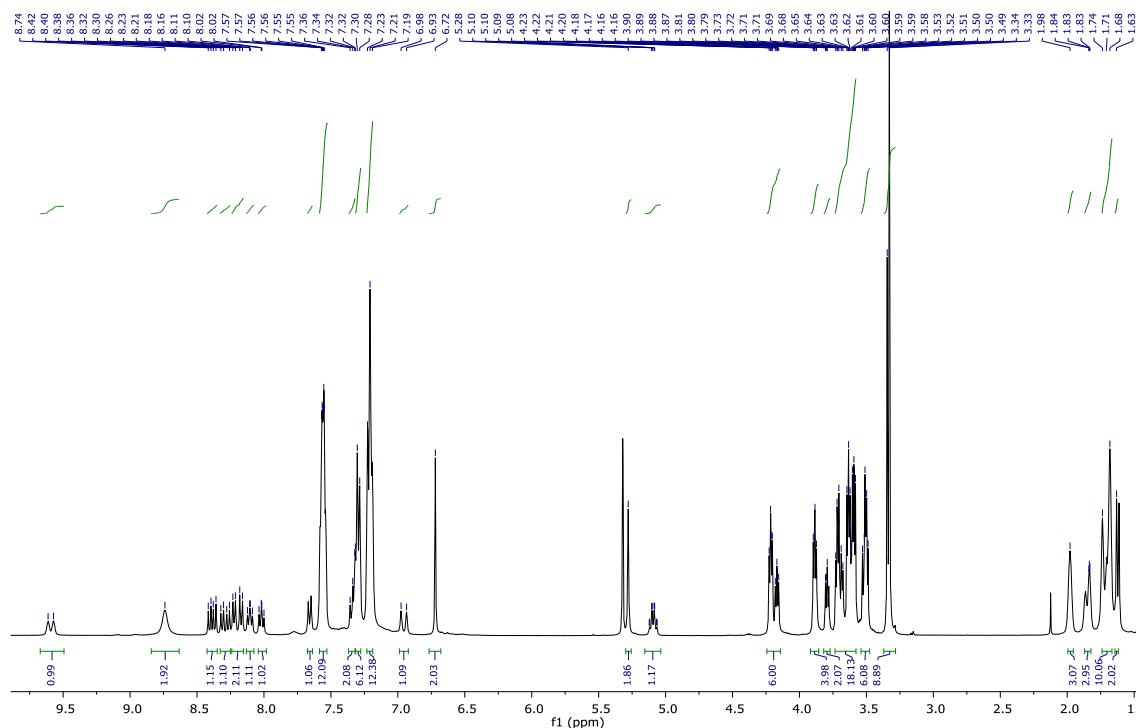


Fig. S2.22 ^1H NMR spectrum (CD_2Cl_2 , 400 MHz) of $[\text{Ru}(\text{CH}=\text{CH}\text{-per}^{\text{Im}})\text{Cl}(\text{CO})(\text{py-PEG3})(\text{PPh}_3)_2]$ (**3PEG-Ru-CH=CH-per^{Im}**).

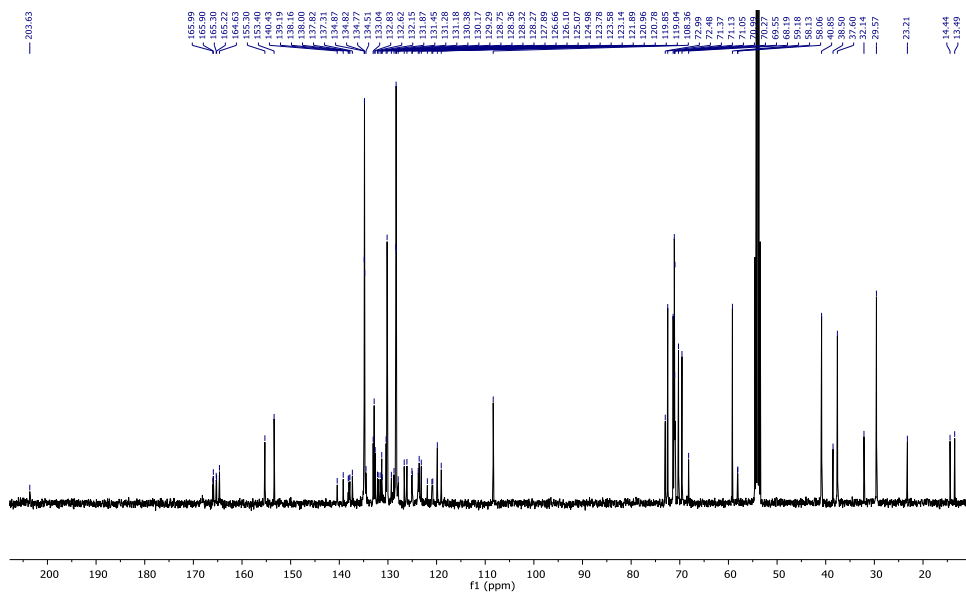


Fig. S2.23 $^{13}\text{C}\{^1\text{H}\}$ NMR (CD_2Cl_2 , 101 MHz) of $[\text{Ru}(\text{CH}=\text{CH}\text{-per}^{\text{Im}})\text{Cl}(\text{CO})(\text{py}\text{-PEG3})(\text{PPh}_3)_2]$ (**3PEG-Ru-CH=CH-per^{Im}**).

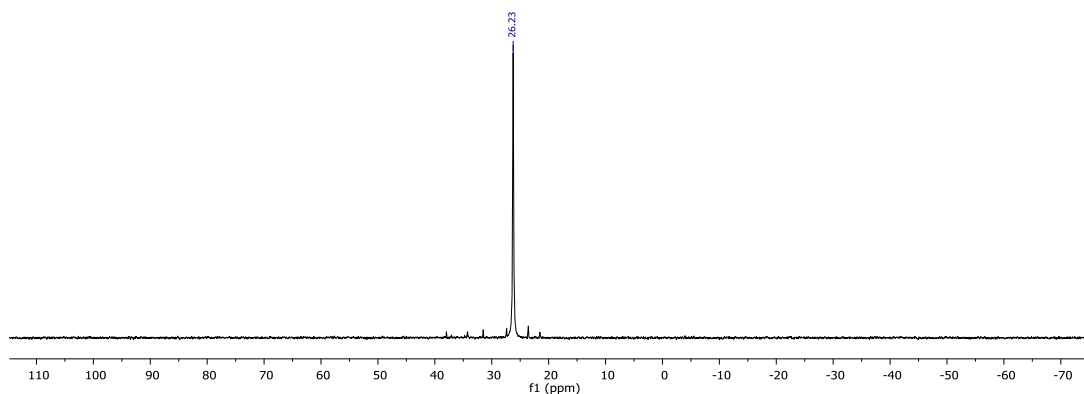


Fig. S2.24 $^{31}\text{P}\{^1\text{H}\}$ NMR (CD_2Cl_2 , 162 MHz) of $[\text{Ru}(\text{CH}=\text{CH}\text{-per}^{\text{Im}})\text{Cl}(\text{CO})(\text{py}\text{-PEG3})(\text{PPh}_3)_2]$ (**3PEG-Ru-CH=CH-per^{Im}**).

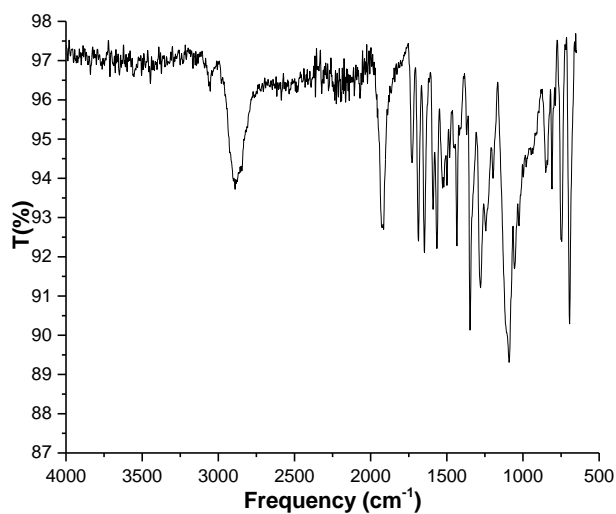


Fig. S2.25 Infrared spectrum (ATR) of $[\text{Ru}(\text{CH}=\text{CH}\text{-per}^{\text{Im}})\text{Cl}(\text{CO})(\text{py}\text{-PEG3})(\text{PPh}_3)_2]$ (**3PEG-Ru-CH=CH-per^{Im}**).

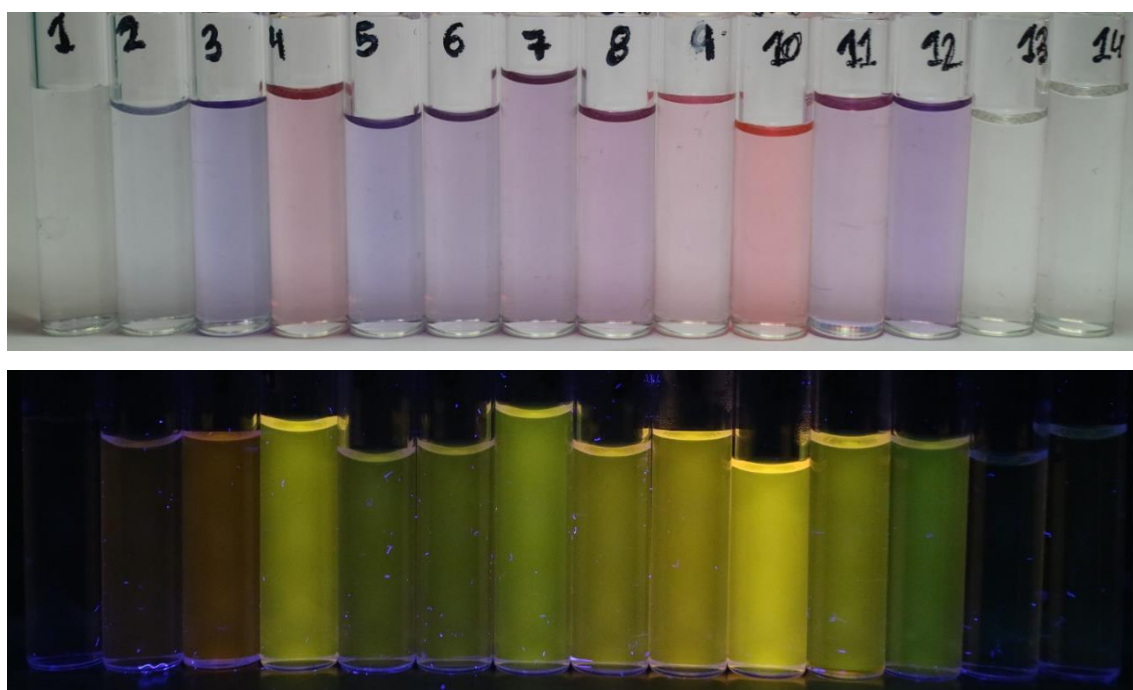
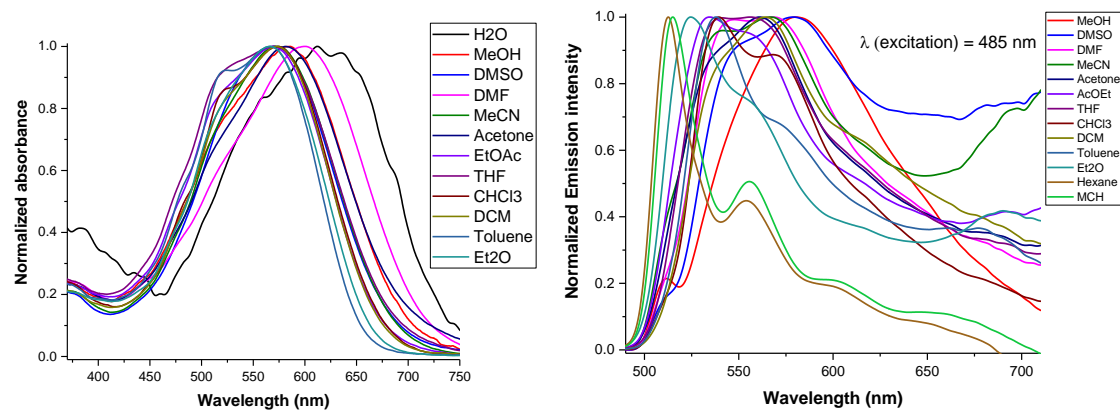
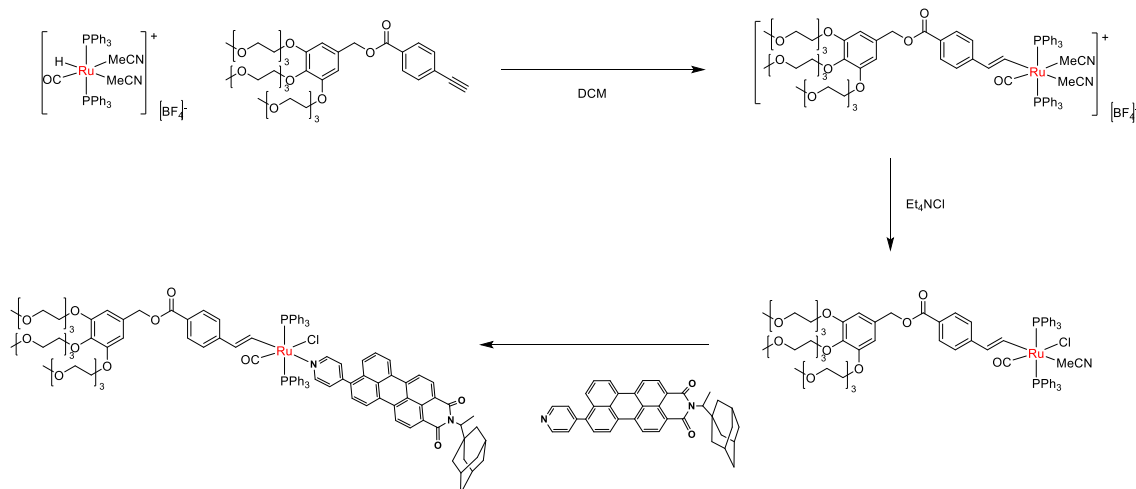


Fig. S2.26 Solvatochromism of $[\text{Ru}(\text{CH}=\text{CH}\text{-per}^{\text{Im}})\text{Cl}(\text{CO})(\text{py}\text{-PEG3})(\text{PPh}_3)_2]$ (**3PEG-Ru-CH=CH-per^{Im}**) measured in 14 solvents (probe concentration 10 μM) of decreasing polarity (water, methanol, DMSO, DMF, MeCN, acetone, EtOAc, THF, chloroform, dichloromethane, toluene, diethylether, hexane and methylcyclohexane) in visible light (middle) and UV light (below).

Synthesis of $[\text{Ru}(\text{CH}=\text{CH}\text{-PEG}_3)\text{Cl}(\text{CO})(\text{py}\text{-per}^{\text{Im}})(\text{PPh}_3)_2]$ (**3PEG-Ru-py-per^{Im}**)



In a 50 mL flask, the $[\text{RuH}(\text{CO})(\text{NCMe})_2(\text{PPh}_3)_2]\text{BF}_4^{\text{S6}}$ (45 mg, 0.055 mmol) was dissolved in DCM (8 mL) and 3,4,5-tris(2-(2-(2-methoxyethoxy)ethoxy)ethoxy)benzyl isonicotinate (**HC≡C-PEG3**) (46 mg, 0.066 mmol) added. After stirring for 30 mins, tetraethylammonium chloride was added to the solution. After one hour, *N*-(2-adamantyl-ethylamine)-9-(5-pyridine)-3,4-perylenemonoimide (**py-per^{Im}**) (33.8 mg, 0.061 mmol) was added to the solution. The reaction was stirred for one hour and then the solvent volume was concentrated under vacuum and diethylether added to the solution to precipitate a solid. The precipitate was filtered and washed with diethylether (10 times) and with hexane (twice) to provide a red, non-fluorescent product (70 mg, 65%). **IR** (ATR, cm^{-1}): 3055 (=C-H), 2895 (C-H), 1926 ($\text{C}\equiv\text{O}$), 1703 (C=O), 1660, 1585, 1436, 1351, 1266, 1244, 1085, 808, 734, 691. **¹H NMR** (400 MHz, CD_2Cl_2) δ (ppm): 9.35 (d, $J = 16.8$ Hz, 1H, H_{Ar}), 8.76 (s, 2H, H_{Ar}), 8.39 – 8.28 (m, 4H, H_{Ar}), 8.18 – 8.12 (m, 2H, H_{Ar}), 7.85 (d, $J = 8.3$ Hz, 2H, H_{Ar}), 7.61 (dtd, $J = 8.3, 4.6, 2.2$ Hz, 12H, H_{Ar}), 7.37 (t, $J = 7.4$ Hz, 6H, H_{Ar}), 7.29 – 7.24 (m, 12H, H_{Ar}), 6.99 (d, $J = 8.2$ Hz, 2H, H_{Ar}), 6.94 – 6.88 (m, 2H, H_{Ar}), 6.73 (s, 2H, H_{Ar}), 6.00 (d, $J = 16.8$ Hz, 1H, H_{Ar}), 5.22 (s, 2H, $\text{CH}=\text{CH}$), 5.10 (d, $J = 7.1$ Hz, 1H, CH), 4.21-4.14 (m, 6H, CH_2), 3.89-3.85 (m, 4H, CH_2), 3.81-3.77 (m, 2H, CH_2), 3.73-3.67 (m, 6H, CH_2), 3.66-3.58 (m, 12H, CH_2), 3.54 – 3.49 (m, 6H, CH_2), 3.35 (s, 3H, CH_3), 3.34 (s, 6H, CH_3), 1.98 (s, 3H, $3\times\text{CH}$), 1.84-1.65 (m, 15H, $6\times\text{CH}_2+\text{CH}_3$). **¹³C{¹H} NMR**

(101 MHz, CD₂Cl₂) δ (ppm): 203.6 (C≡O), 167.1 (C=O), 165.6 (C=O), 164.9 (C=O), 154.6, 153.2, 145.2, 138.6, 136.5, 136.4, 136.2, 136.0, 135.0, 135.0, 134.9, 133.3, 133.1, 132.9, 132.6, 131.9, 131.3, 130.4, 130.3, 130.0, 129.9, 128.6, 128.3, 128.2, 128.2, 128.1, 127.7, 126.6, 125.7, 125.4, 124.2, 123.2, 121.0, 120.8, 108.1 (CH=CH), 72.9, 72.5, 71.3, 71.1, 71.0, 70.3, 69.4, 66.8, 59.2 (CH₃), 58.4 (CH), 40.8, 38.5, 37.5, 29.5, 23.2, 14.4, 13.6 (CH₃). ³¹P{¹H} NMR (162 MHz, CD₂Cl₂) δ (ppm): 26.68. UV-Vis (CH₂Cl₂): λ_{max} (ε) = 475 nm (44142 M⁻¹ cm⁻¹); 500 nm (45056 M⁻¹ cm⁻¹); Φ = 29.5 ± 2 %, calculated in CH₂Cl₂; τ (CH₂Cl₂, λ_{exc} = 510 nm) = 4.57 ns, χ² = 1.098. Elemental Analysis: Calculated for C₁₁₃H₁₁₇ClN₂O₁₇P₂Ru 0.25CH₂Cl₂: C 68.2%, H 5.9%, N 1.4%. Found C 67.9%, H 6.3%, N 1.7%.

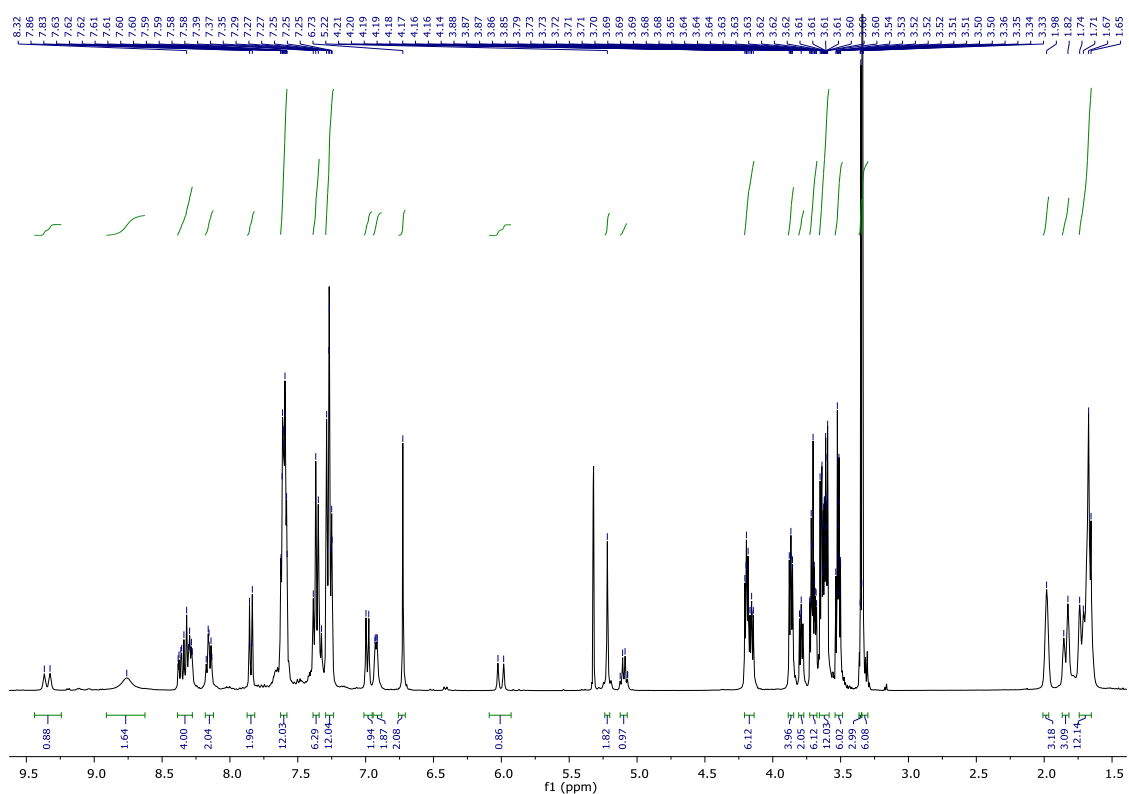


Fig. S2.27 ¹H NMR spectrum (CD₂Cl₂, 400 MHz) of [Ru(CH=CH-PEG3)Cl(CO)(py-per^{Im})(PPh₃)₂] (**3PEG-Ru-py-per^{Im}**).

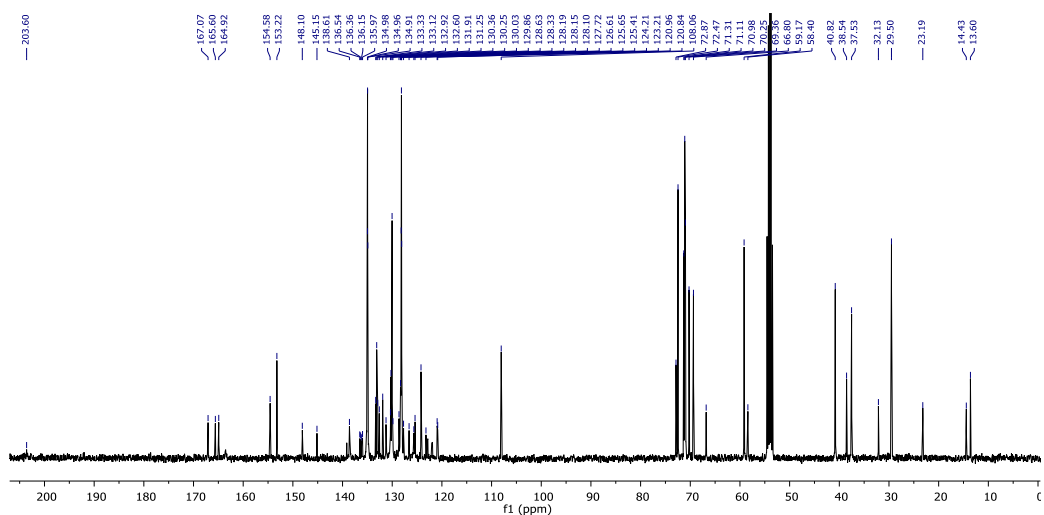


Fig. S2.28 $^{13}\text{C}\{^1\text{H}\}$ NMR (CD_2Cl_2 , 101 MHz) of $[\text{Ru}(\text{CH}=\text{CH}\text{-PEG}_3)\text{Cl}(\text{CO})(\text{py}\text{-per}^{\text{Im}})(\text{PPh}_3)_2]$ (**3PEG-Ru-py-per^{Im}**).

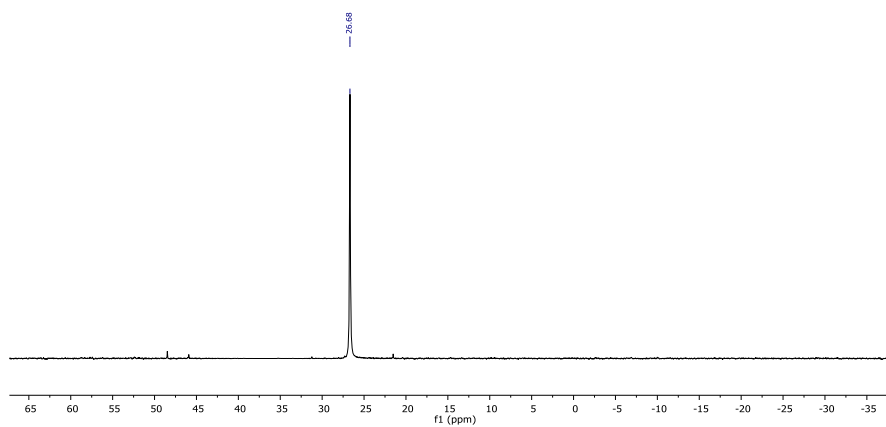


Fig. S2.29 $^{31}\text{P}\{^1\text{H}\}$ NMR (CD_2Cl_2 , 162 MHz) of $[\text{Ru}(\text{CH}=\text{CH}\text{-PEG}_3)\text{Cl}(\text{CO})(\text{py}\text{-per}^{\text{Im}})(\text{PPh}_3)_2]$ (**3PEG-Ru-py-per^{Im}**).

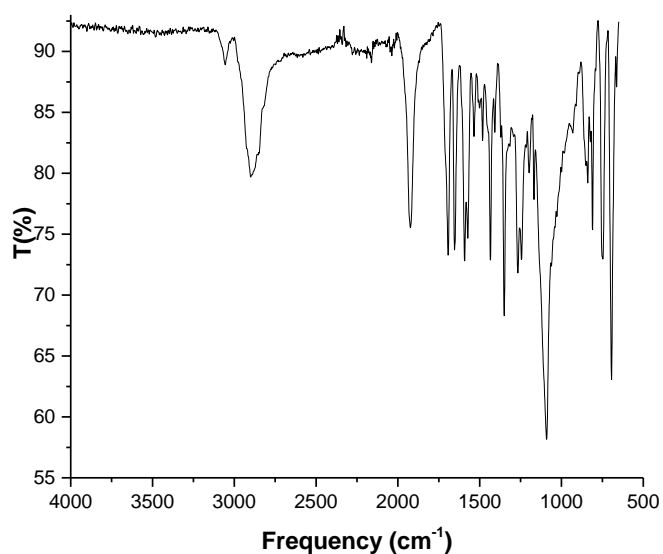


Fig. S2.30 Infrared spectrum (ATR) of $[\text{Ru}(\text{CH}=\text{CH}\text{-PEG}_3)\text{Cl}(\text{CO})(\text{py}\text{-per}^{\text{Im}})(\text{PPh}_3)_2]$ (**3PEG-Ru-py-per^{Im}**).

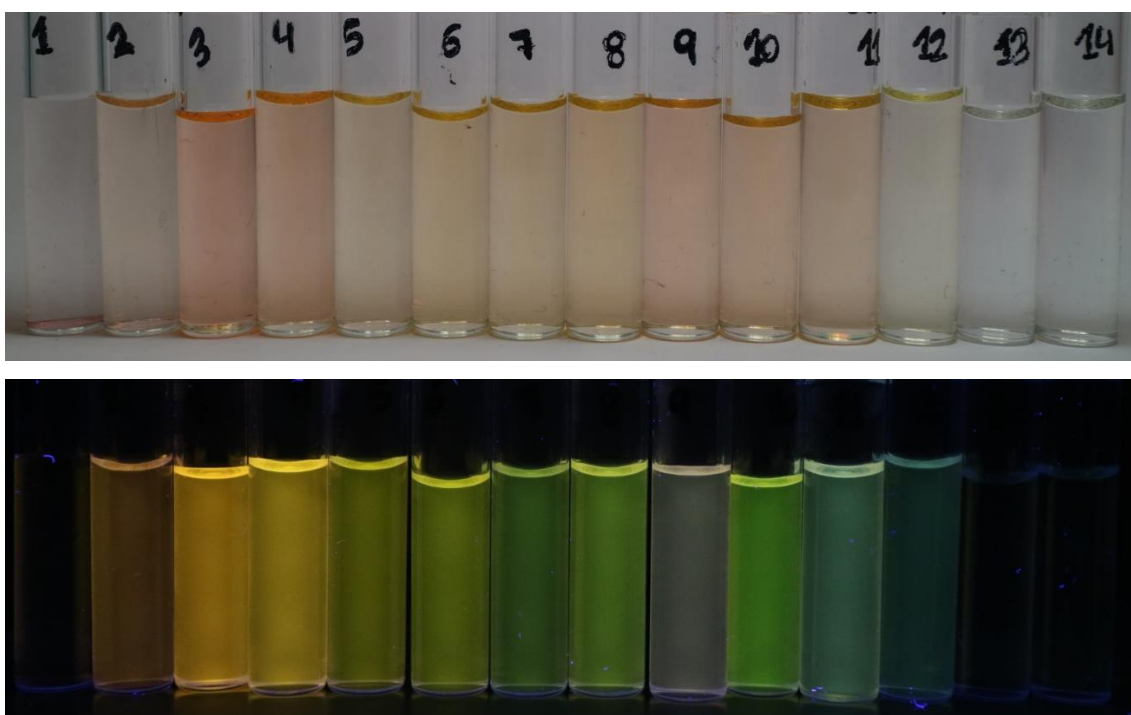
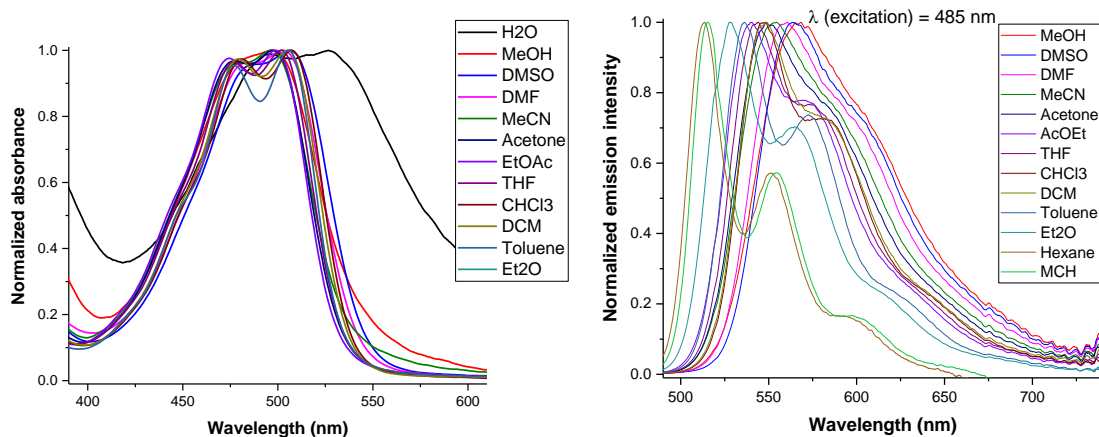
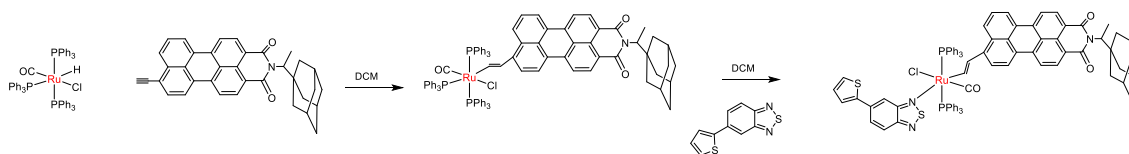


Fig. S2.31 Solvatochromism of $[\text{Ru}(\text{CH}=\text{CH}\text{-PEG3})\text{Cl}(\text{CO})(\text{py}\text{-per}^{\text{Im}})(\text{PPh}_3)_2]$ (**3PEG-Ru-py-per^{Im}**) in 14 solvents (water, methanol, DMSO, DMF, MeCN, acetone, EtOAc, THF, chloroform, dichloromethane, toluene, diethylether, hexane and methylcyclohexane) of decreasing polarity (probe concentration 10 μM) in visible light (middle) and UV light (bottom).

Synthesis of $[\text{Ru}(\text{CH}=\text{CH-per}^{\text{Im}})\text{Cl}(\text{CO})(\text{TBTD})(\text{PPh}_3)_2]$ (TBTD-Ru-CH=CH-per^{Im})



In a 50 mL flask, $[\text{RuHCl}(\text{CO})(\text{PPh}_3)_3]^{\text{S5}}$ (40 mg, 0.042 mmol) was dissolved in DCM (8 mL) and treated with 3,4,5-tris(2-(2-(2-methoxyethoxy)ethoxy)ethoxy)benzyl isonicotinate (**HC≡C-PEG3**) (21.3 mg, 0.042 mmol). The solution became dark blue instantly. After 30 mins, 5-(3-thienyl)-2,1,3-benzothiadiazole (**TBTD**) (9.2 mg, 0.042 mmol) was added to the solution. After one hour, the reaction mixture was concentrated under vacuum and hexane added to precipitate a solid, which was filtered and washed with hexane several times to provide a dark blue powder (42.4 mg, 71%). **IR** (ATR, cm^{-1}): 3046 ($\equiv\text{CH}$), 2902 (C-H), 1926 ($\text{C}\equiv\text{O}$), 1693 (C=O), 1654, 1595, 1435, 1350, 1271, 1093, 811, 754, 692. **$^1\text{H NMR}$** (400 MHz, CD_2Cl_2) δ (ppm): 9.41 (d, $J = 15.5$ Hz, 1H, H_{Ar}), 8.42 (dd, $J = 15.0, 8.1$ Hz, 3H, H_{Ar}), 8.35 – 8.27 (m, 3H, H_{Ar}), 8.18 (dt, $J = 7.9, 3.4$ Hz, 2H, H_{Ar}), 7.86 (s, 1H, H_{Ar}), 7.74 (t, $J = 2.2$ Hz, 1H, H_{Ar}), 7.63 (d, $J = 8.3$ Hz, 1H, H_{Ar}), 7.59 – 7.56 (m, 2H, H_{Ar}), 7.52 (m, 12H, H_{Ar}), 7.40 (t, $J = 8.0$ Hz, 2H, H_{Ar}), 7.30 (t, $J = 7.4$ Hz, 6H, H_{Ar}), 7.25 (d, $J = 7.6$ Hz, 1H, H_{Ar}), 7.18 (t, $J = 7.6$ Hz, 12H, H_{Ar}), 6.94 (d, $J = 15.6$ Hz, 1H, H_{Ar}), 5.08 (q, $J = 7.4$ Hz, 1H, **CH**), 1.97 (s, 3H, $3\times\text{CH}$), 1.83-1.60 (m, 15H, $6\times\text{CH}_2+\text{CH}_3$). **$^{13}\text{C}\{^1\text{H}\}$ NMR** (101 MHz, CD_2Cl_2) δ (ppm): 204.9 ($\text{C}\equiv\text{O}$), 165.9 (**C=O**), 165.3 (**C=O**), 155.4 (**C=N**), 154.4 (**C=N**), 140.9, 140.3, 137.9, 137.8, 137.7, 137.3, 134.6, 134.6, 134.5, 132.6, 132.5, 132.4, 132.2, 132.1, 131.8, 131.4, 131.1, 130.5, 130.4, 130.2, 129.3, 129.1, 129.0, 128.7, 128.3, 128.3, 128.2, 128.0, 127.8, 126.6, 126.2, 125.4, 124.9, 123.7, 123.4, 123.3, 121.9, 121.0, 120.9, 119.9, 119.1, 117.1, 58.1 (**CH-Adam**), 40.9 (**CH₂**), 38.5 (**Cq**), 37.6 (**CH₂**), 32.1, 29.6 (**CH**), 23.2, 14.4, 13.5 (**CH₃**). **$^{31}\text{P}\{^1\text{H}\}$ NMR** (162 MHz, CD_2Cl_2) δ (ppm): 26.78. **Elemental Analysis:** Calculated for $\text{C}_{83}\text{H}_{66}\text{ClN}_3\text{O}_3\text{P}_2\text{RuS}_2 \cdot 2.25\text{CH}_2\text{Cl}_2$: C 63.7%, H 4.4%, N 2.6%. Found C 63.7%, H 4.3%, N 2.8%.

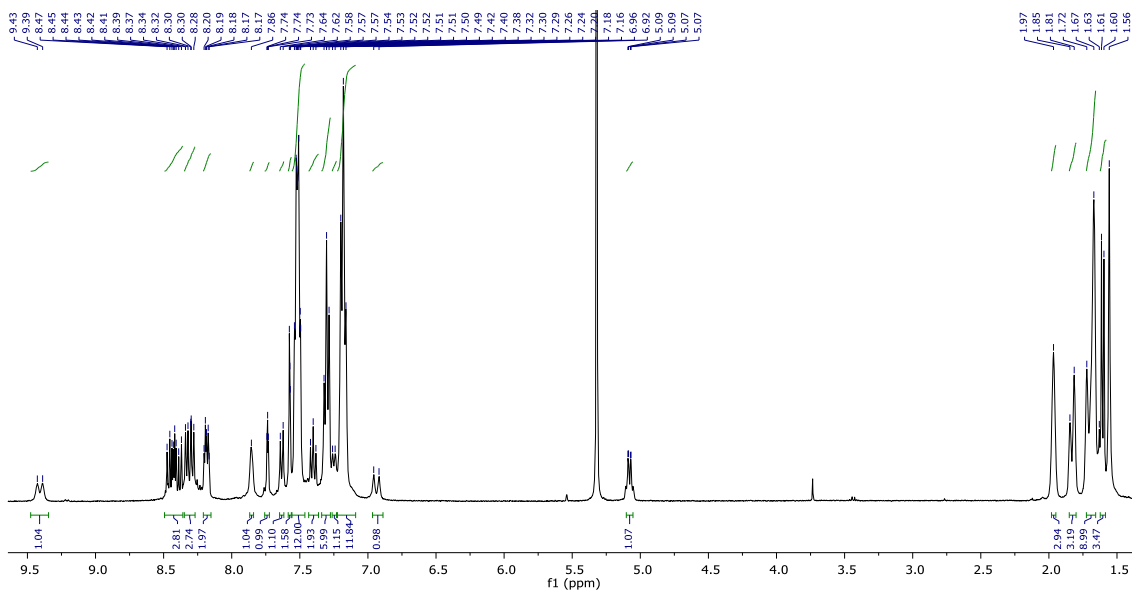


Fig. S2.32 ^1H NMR spectrum (CD_2Cl_2 , 400 MHz) of $[\text{Ru}(\text{CH}=\text{CH}\text{-per}^{\text{lm}})\text{Cl}(\text{CO})(\text{TBTD})(\text{PPh}_3)_2]$ (**TBTD-Ru-CH=CH-per^{lm}**).

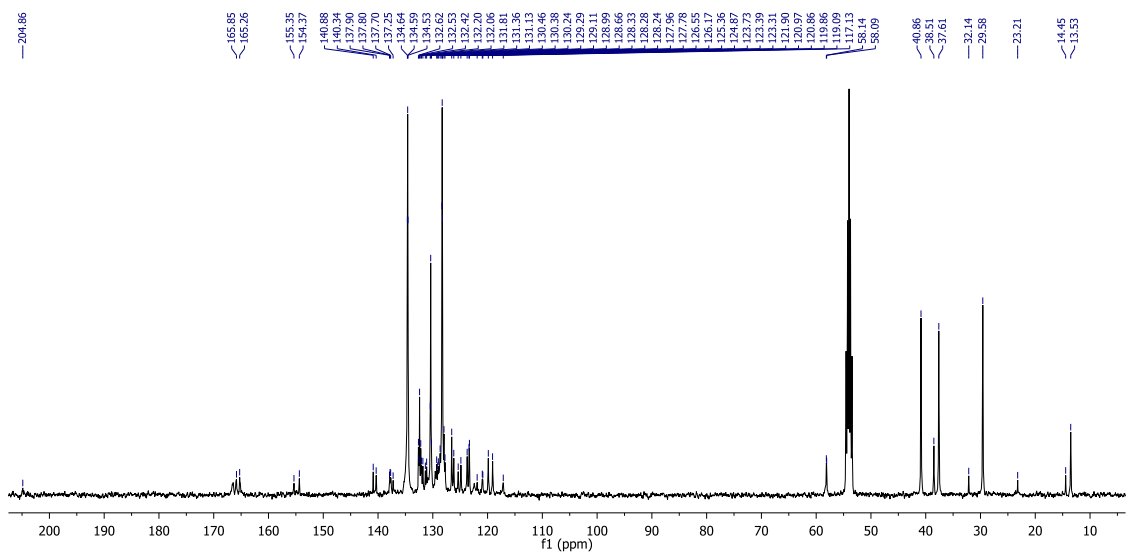


Fig. S2.33 $^{13}\text{C}\{^1\text{H}\}$ NMR spectrum (CD_2Cl_2 , 101 MHz) of $[\text{Ru}(\text{CH}=\text{CH}\text{-per}^{\text{lm}})\text{Cl}(\text{CO})(\text{TBTD})(\text{PPh}_3)_2]$ (**TBTD-Ru-CH=CH-per^{lm}**).

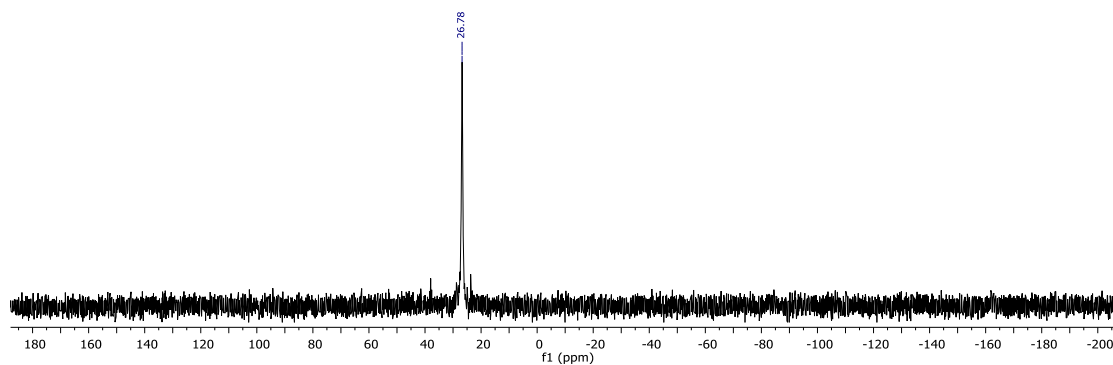


Fig. S2.34 $^{31}\text{P}\{^1\text{H}\}$ NMR spectrum (CD_2Cl_2 , 162 MHz) of $[\text{Ru}(\text{CH}=\text{CH}\text{-per}^{\text{lm}})\text{Cl}(\text{CO})(\text{TBTD})(\text{PPh}_3)_2]$ (**TBTD-Ru-CH=CH-per^{lm}**).

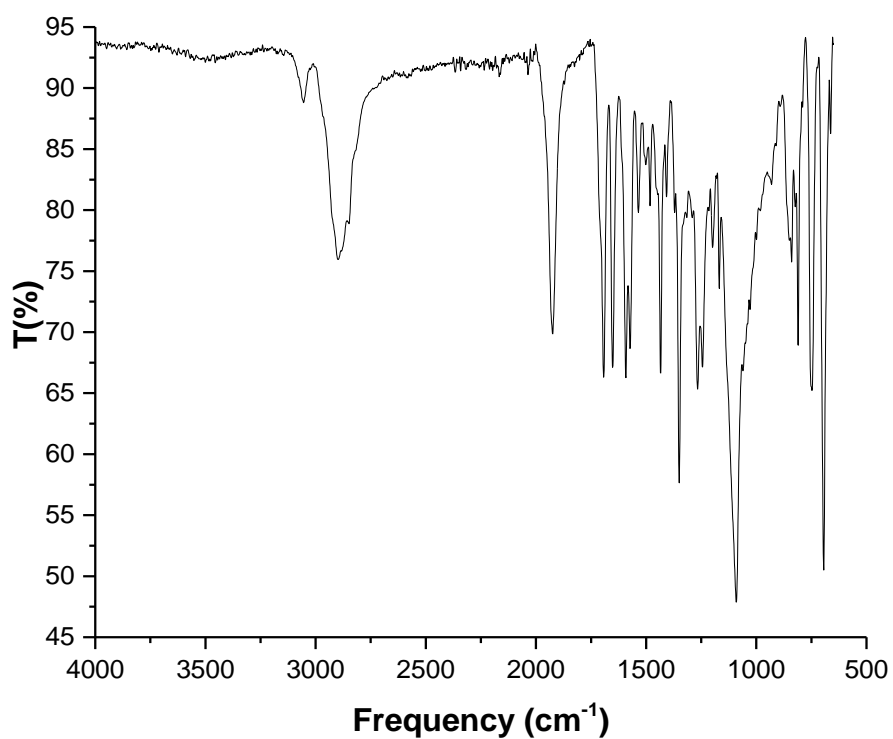
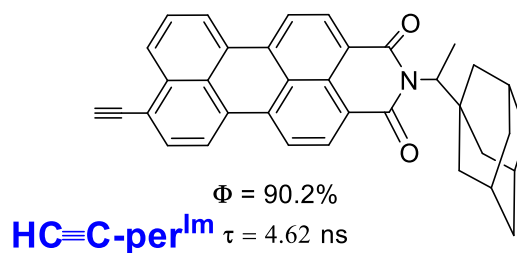
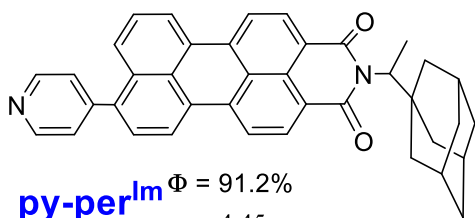


Fig. S2.35 Infrared (ATR) spectrum of $[\text{Ru}(\text{CH}=\text{CH}\text{-per}^{\text{lm}})\text{Cl}(\text{CO})(\text{TBTD})(\text{PPh}_3)_2]$ (**TBTD-Ru-CH=CH-per^{lm}**).

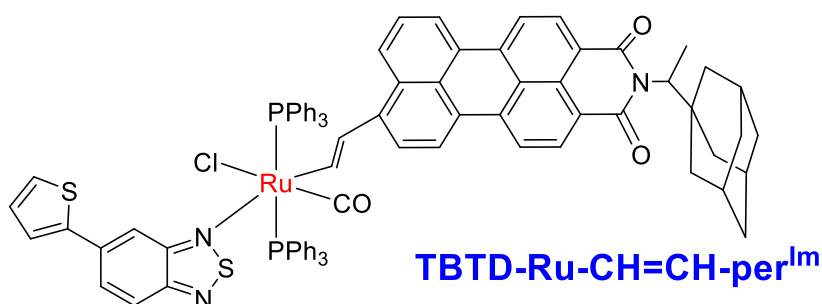
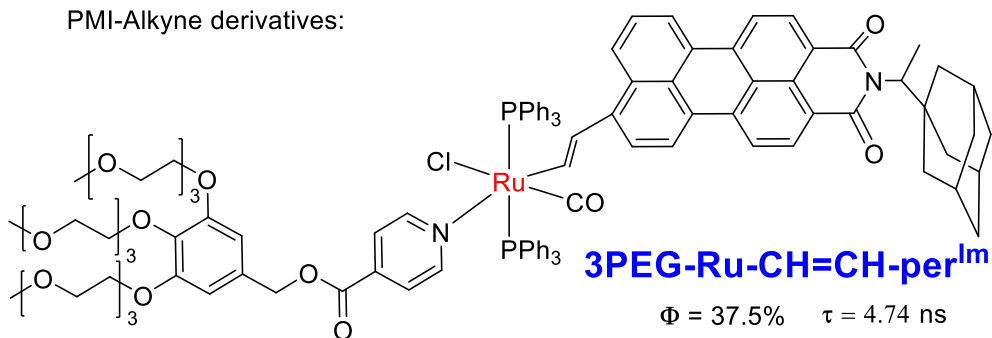
S3 Summary of synthesised compounds

PERYLENEMONOIMIDE DERIVATIVES (DCM):

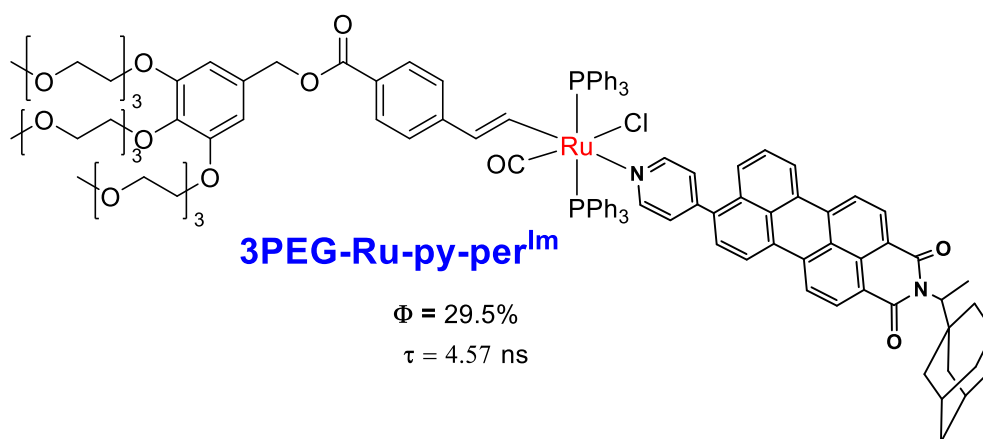


RUTHENIUM COMPLEXES (DCM):

PMI-Alkyne derivatives:



PMI-p-pyridine derivative:



S4 Interpretation of absorption and fluorescence data

S4.1 Selection and influence of the solvents

The response for the complexes $[\text{Ru}(\text{CH}=\text{CH-per}^{\text{Im}})\text{Cl}(\text{CO})(\text{py-PEG3})(\text{PPh}_3)_2]$ (**3PEG-Ru-CH=CH-per^{Im}**) was compared between different solvents of interest:

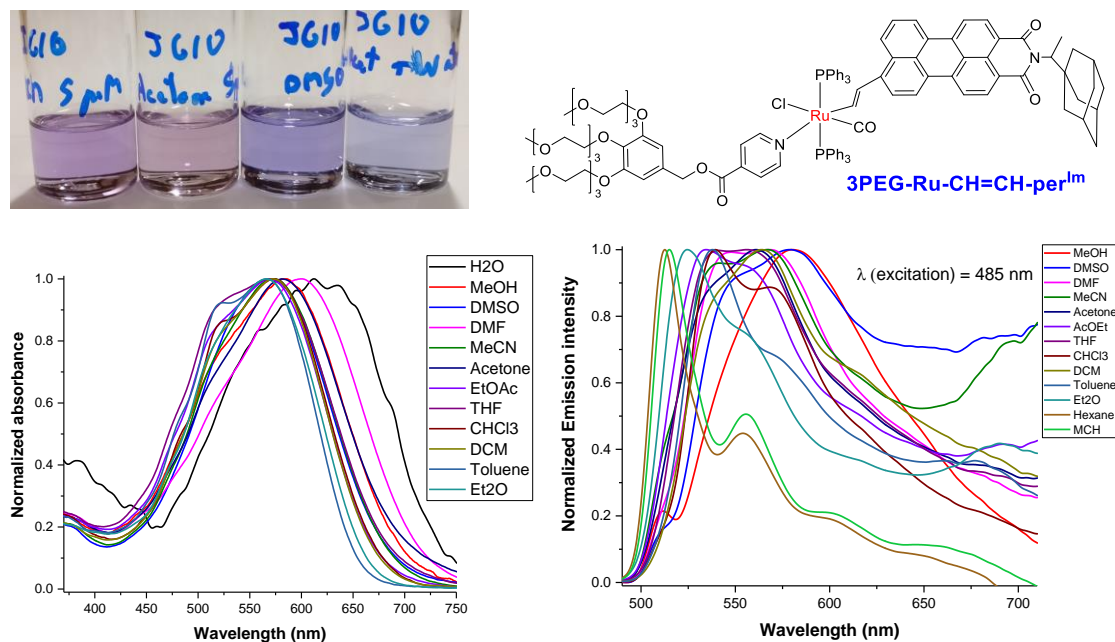


Fig. S4.1 Results from solvatochromic studies showing the visible appearance (above) of 5 μM solutions of **3PEG-Ru-CH=CH-per^{Im}** in different solvents and absorption (bottom left) and fluorescence (bottom right) spectra of **3PEG-Ru-CH=CH-per^{Im}** (10 μM) in different solvents.

From the absorption and fluorescence studies it was concluded that **3PEG-Ru-CH=CH-per^{Im}** has a remarkable bathochromic shift with polarity. In addition, absorption bands were broader than in free perylene monoimides, being partially overlapped with emission bands. It was also observed the presence of a secondary emission at wavelengths above 650 nm. The fluorescence quantum yields compared to **HC \equiv C-per^{Im}** decreased from **90% to 38%** and the fluorescence lifetime decay associated with the perylene core **increased by 0.12 ns**.

Little difference is apparent between **3PEG-Ru-CH=CH-per^{Im}** and **TBTD-Ru-CH=CH-per^{Im}** in absorption nor fluorescence, with the exception of the absorption in the region 300-400 nm, where the absorption of the TBTD group was observed:

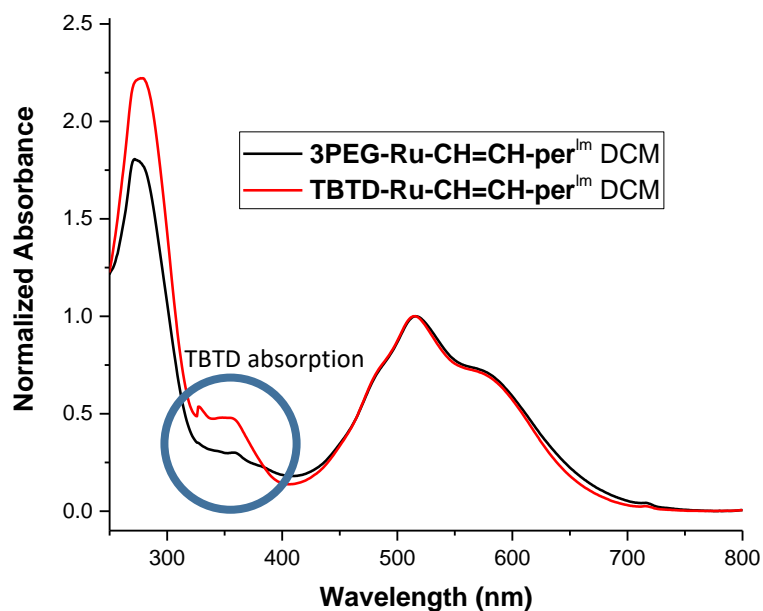


Fig. S4.2 Absorption comparison of **3PEG-Ru-CH=CH-per^{Im}** and **TBTD-Ru-CH=CH-per^{Im}** in DCM.

The lack of difference between **3PEG-Ru-CH=CH-per^{Im}** and **TBTD-Ru-CH=CH-per^{Im}**, led us to focus on **3PEG-Ru-CH=CH-per^{Im}**, which was more soluble in water mixtures, increasing the potential for application.

Similarly to **3PEG-Ru-CH=CH-per^{Im}**, the response for the complex **[Ru(CH=CH-PEG3)Cl(CO)(py-per^{Im})(PPh₃)₂] (3PEG-Ru-py-per^{Im})** was compared between different solvents of interest:

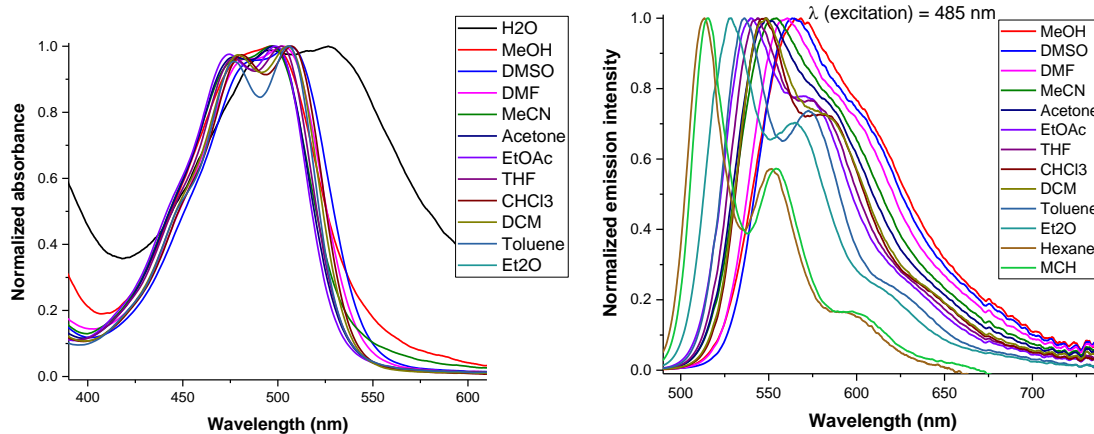
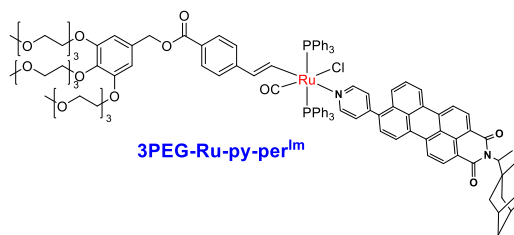


Fig. S4.3 Solvatochromic study of 10 μM solutions of **3PEG-Ru-py-per^{Im}** with appearance in different solvents above and absorption (bottom left) and fluorescence (bottom right) behaviour in different solvents.

The absorption and fluorescence of **3PEG-Ru-py-per^{Im}** depends on the solvent in the same way as its perylene monoimide precursor **py-per^{Im}** but complexation to a metal increased its solubility, rendering it slightly soluble in organic:water mixtures, although the fluorescence was found to be quenched. In addition, the fluorescence quantum yield decreased substantially, from **91% to 30%**, while the fluorescence lifetime decay associated with the perylene core increased by 0.12 ns compared to **HC \equiv C-per^{Im}**.

S4.2 Carbon monoxide detection

The response to bubbling carbon monoxide (CO) through solutions of [Ru(CH=CH-per^{lm})Cl(CO)(py-PEG3)(PPh₃)₂] (**3PEG-Ru-CH=CH-per^{lm}**) in DCM are shown below in Figure S4.4. The substitution reactions observed on addition of CO to similar complexes have already been reported by us.^{S7} Replacing the pyridyl group with a CO molecule led to changes in the properties of the complex; affecting absorption, fluorescence and solubility (Fig. S4.4).

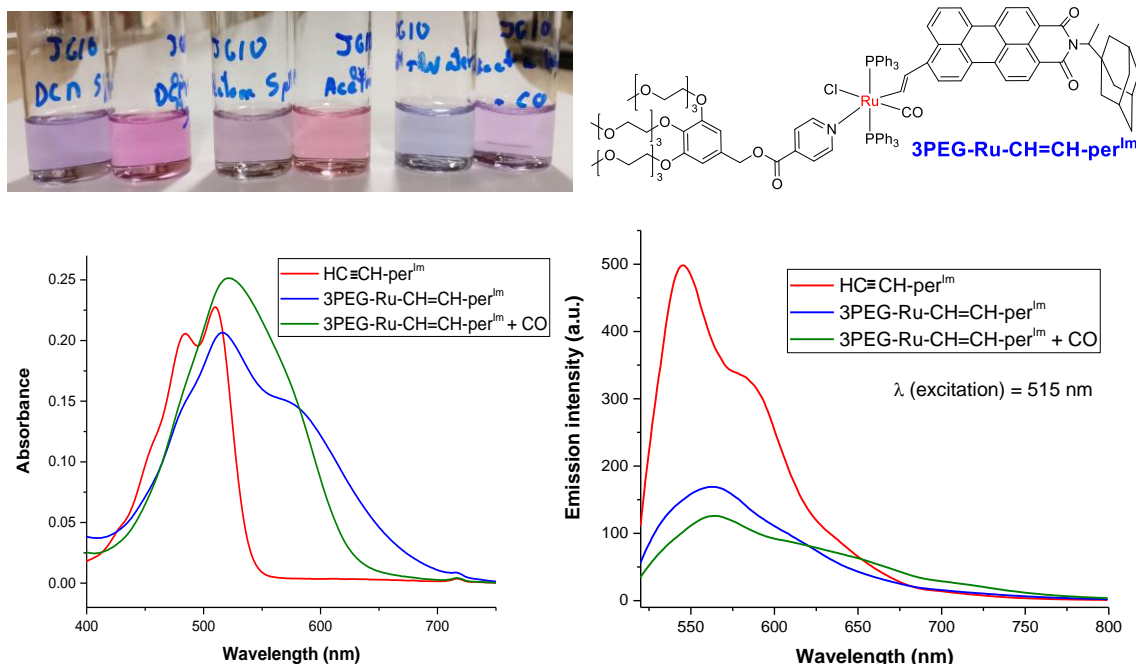


Fig. S4.4 Visible appearance (above) without (left vial) and with (right vial) CO of 5 μ M solutions of **3PEG-Ru-CH=CH-per^{lm}** in DCM, acetone and acetone:water (9:1) and response to CO of the same compound (10 μ M) in terms of absorption (bottom left) and fluorescence (bottom right).

It was concluded that the **emission increased at higher wavelengths** (region of 620 nm) and **decreased at its initial maximum** (570 nm). The **absorption peaks were extended** from the maximum of the initial band.

For $[\text{Ru}(\text{CH}=\text{CH-PEG3})\text{Cl}(\text{CO})(\text{py-per}^{\text{lm}})(\text{PPh}_3)_2]$ (**3PEG-Ru-py-per^{lm}**), the behaviour was found to be substantially different with little visible difference on addition of CO but a substantial change in absorption and fluorescence (Figure S4.5):

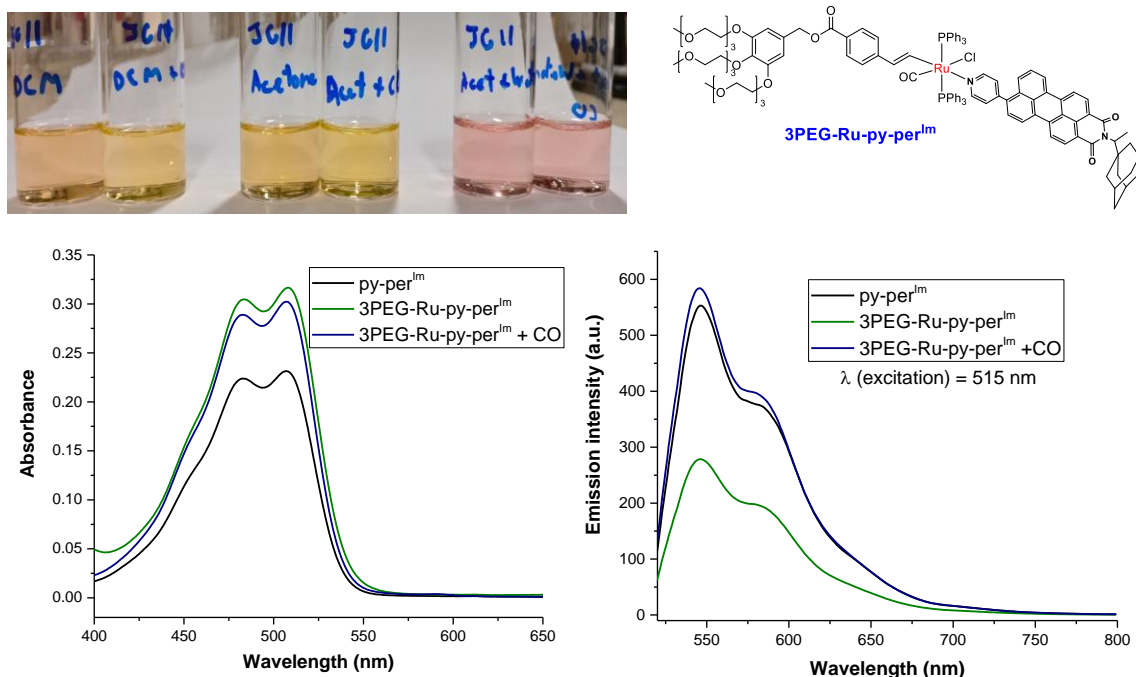
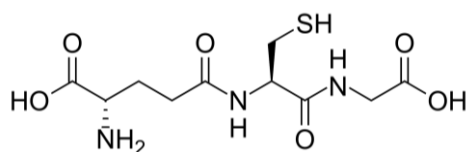


Fig. S4.5 Visible appearance (above) without (left vial) and with (right vial) CO of 5 μM solutions **3PEG-Ru-py-per^{lm}** in DCM, acetone and acetone:water (9:1) and response to CO of the same compound (10 μM) in terms of absorption (bottom left) and fluorescence (bottom right).

The **fluorescence of 3PEG-Ru-py-per^{lm} doubled in the presence of CO**, the absorption increased too, the perylenemonoimide was substituted by CO in the complex, this led to an increase in fluorescence, as it was checked by comparing with **py-per^{lm}** and with the values of the fluorescence quantum yield.

S4.3 Effect of CO and glutathione



Glutathione (Glut) is a tripeptide present in cells (structure above), it possesses a thiol group and acts as an antioxidant. For the purpose of detecting CO within the cellular environment, it is important to evaluate the possible interference of this species. The first compound to be investigated was $[\text{Ru}(\text{CH}=\text{CH}\text{-per}^{\text{Im}})\text{Cl}(\text{CO})(\text{py}\text{-PEG3})(\text{PPh}_3)_2]$ (**3PEG-Ru-CH=CH-per^{Im}**), which showed a modest colour change in response to the presence of CO.

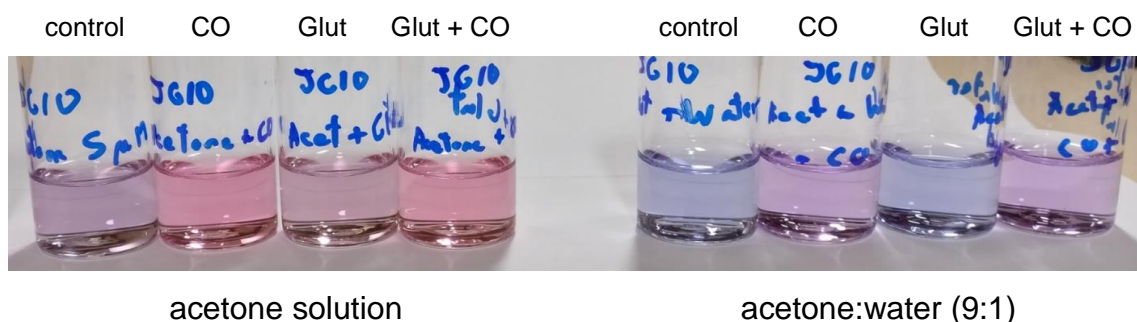


Fig. S4.6 Visible appearance of 5 μM solutions of **3PEG-Ru-CH=CH-per^{Im}** with either no additive (control) or with bubbled CO, 0.1 mM glutathione only or 0.1 mM glutathione + bubbled CO.

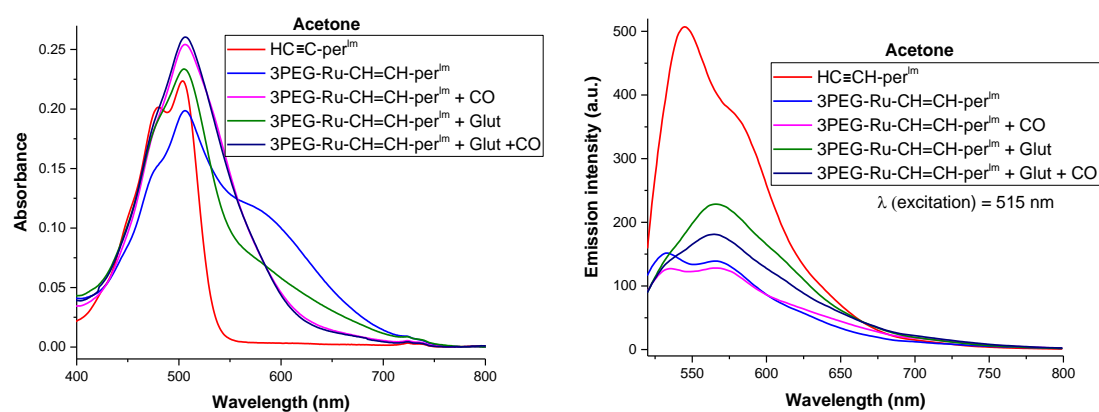


Fig. S4.7 Absorption (left) and fluorescence (right) spectra of 5 μM solutions in acetone of **HC≡C-per^{Im}** alongside **3PEG-Ru-CH=CH-per^{Im}** with either no additive (control) or with bubbled CO, 0.1 mM glutathione only or 0.1 mM glutathione + bubbled CO.

The presence of **CO** increased the fluorescence band at 650 nm slightly. The absorption at 600 nm decreased in the presence of CO. The same experiment was also carried out in acetone;water (9:1) mixtures:

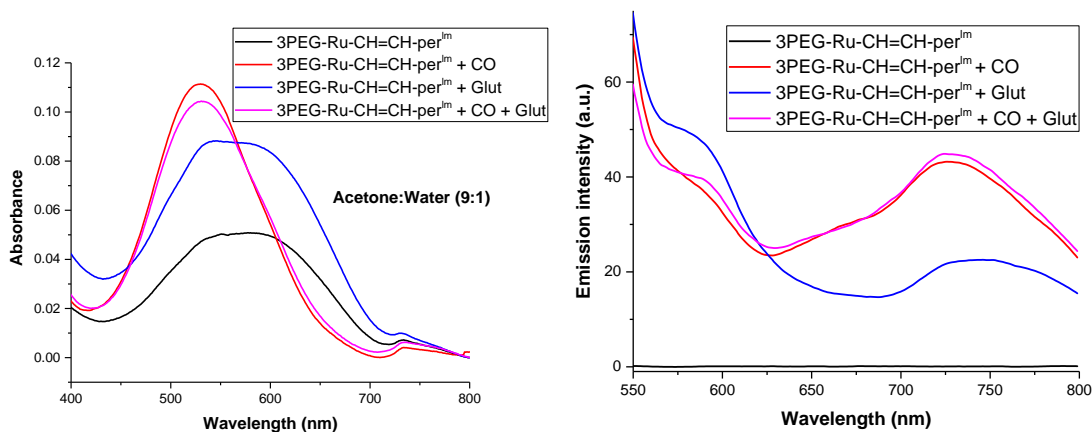


Fig. S4.8 Absorption (left) and fluorescence (right) spectra of 5 μM solutions in water:acetone (9:1) of **3PEG-Ru-CH=CH-per^{Im}** with either no additive (control) or with bubbled CO, 0.1 mM glutathione only or 0.1 mM glutathione + bubbled CO.

The compound was found to precipitate slowly from the mixture water:acetone (9:1). In the presence of CO, the **absorption broadened** and the **fluorescence** shifted to the IR region, the **fluorescence** also increased in the presence of CO.

Data were also collected for $[\text{Ru}(\text{CH}=\text{CH}-\text{PEG}3)\text{Cl}(\text{CO})(\text{py-per}^{\text{Im}})(\text{PPh}_3)_2]$ (**3PEG-Ru-py-per^{Im}**) in the presence of glutathione and CO.

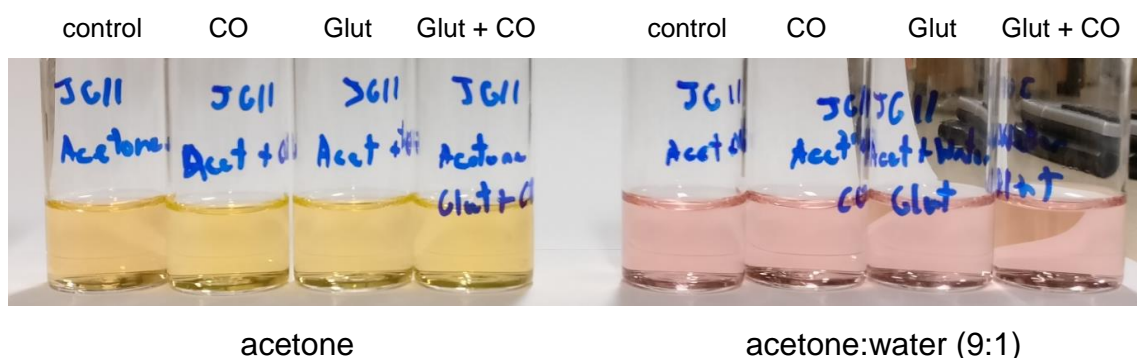


Fig. S4.9 Visible appearance of 5 μM solutions of **3PEG-Ru-py-per^{Im}** with either no additive (control) or with bubbled CO, 0.1 mM glutathione only or 0.1 mM glutathione + bubbled CO.

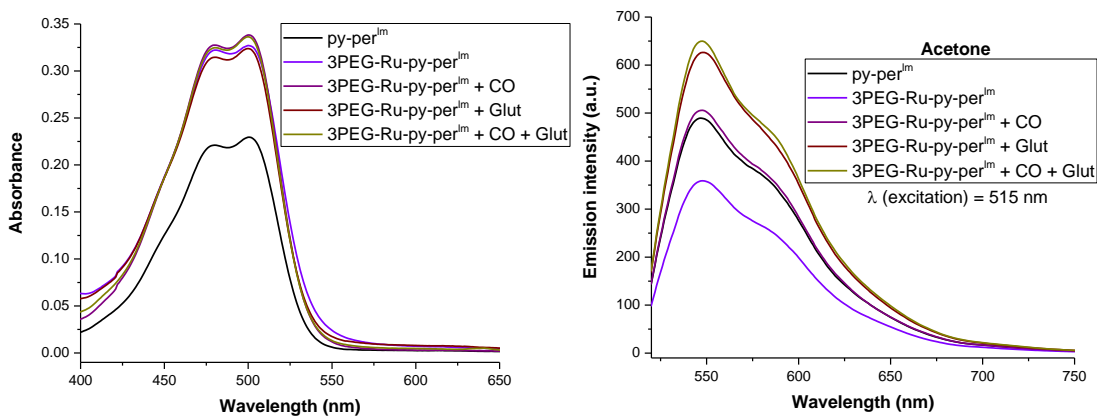


Fig. S4.10 Absorption (left) and fluorescence (right) spectra of 5 μM solutions in acetone of **3PEG-Ru-py-per^{lm}** with either no additive (control) or with bubbled CO, 0.1 mM glutathione only or 0.1 mM glutathione + bubbled CO.

When CO was passed through the solution, **3PEG-Ru-py-per^{lm}** increased its **fluorescence** until it was the same as the free ligand, **py-per^{lm}**. However, the fluorescence increased slightly more when glutathione was also present in the media.

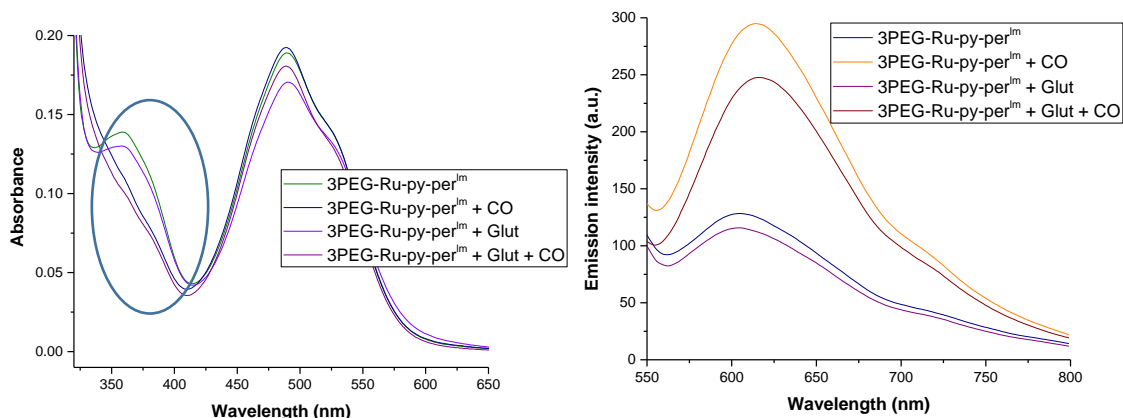


Fig. S4.11 Absorption (left) and fluorescence (right) spectra of 5 μM solutions of **3PEG-Ru-py-per^{lm}** in acetone:water (1:9) with either no additive (control) or with bubbled CO, 0.1 mM glutathione only or 0.1 mM glutathione + bubbled CO.

The compound became red and started to precipitate **except when CO was bubbled** through the solution. The **absorption at 350 nm did not appear in presence of CO** and the fluorescence increased selectively with the presence of CO.

S4.4 Behaviour with cations and anions

Acetone solutions (20 μM) of $[\text{Ru}(\text{CH}=\text{CH-per}^{\text{Im}})\text{Cl}(\text{CO})(\text{py-PEG3})(\text{PPh}_3)_2]$ (**3PEG-Ru-CH=CH-per^{Im}**) and $[\text{Ru}(\text{CH}=\text{CH-PEG3})\text{Cl}(\text{CO})(\text{py-per}^{\text{Im}})(\text{PPh}_3)_2]$ (**3PEG-Ru-py-per^{Im}**) were studied in the presence of different cations and anions. The cations were added in water with non-coordinating counterions such as perchlorate or triflate (except in the case of HAuCl_4 and Pd^{2+}).

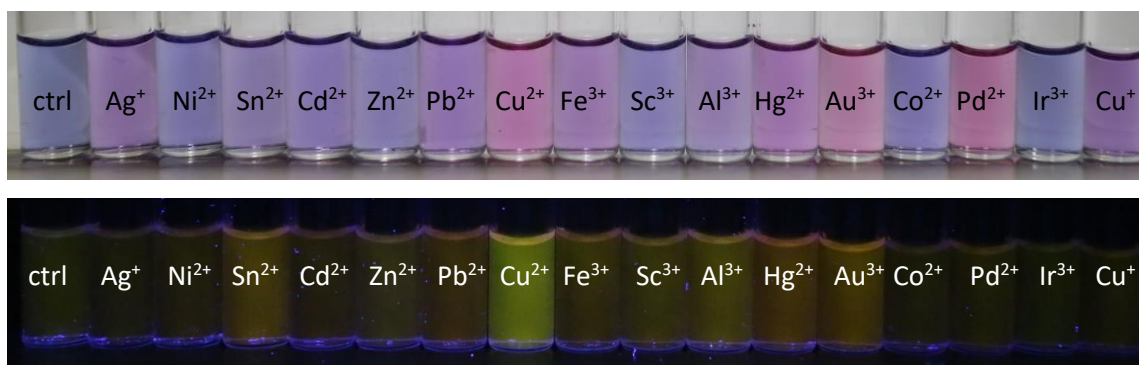


Fig. S4.12 Visible appearance of 20 μM solutions of **3PEG-Ru-CH=CH-per^{Im}** in acetone with different cations (80 μM) under visible light (above) and UV, 366 nm, light (below).

The most remarkable change occurred in the presence of Cu^{2+} , changing the final colour and fluorescence. In addition, there was a slight increase of fluorescence for Lewis acid cations such as Fe^{3+} and Sn^{2+} . This led to the effect of different pH being investigated, which revealed no clear variation until adding water with a pH of 12.3.

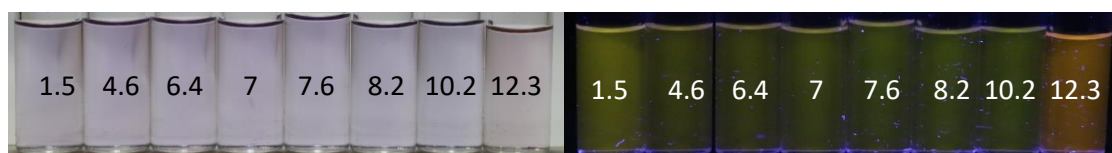


Fig. S4.13 Appearance of 5 μM solutions of **3PEG-Ru-CH=CH-per^{Im}** in acetone:water (95:5) under different pH conditions (PBS 0.1 mM) in visible light (left) and UV light, 366 nm, (right) after 72 hours.

There was no significant change in fluorescence except for Au³⁺ cations, which may be due to its acidic nature.

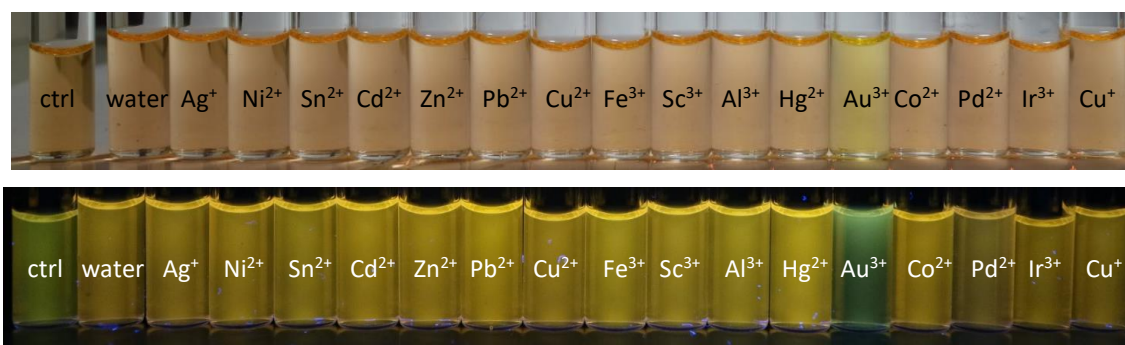


Fig. S4.14 Appearance of 20 μM solutions of **3PEG-Ru-py-per^{lm}** in acetone with various cations (80 μM) under visible light (above) and UV, 366 nm, light (below).

There was no significant change except for **CN⁻**, in which the colour became **pale blue** and the fluorescence reddish. This is attributed to the π-acid cyanide forming a complex with the ruthenium compound.

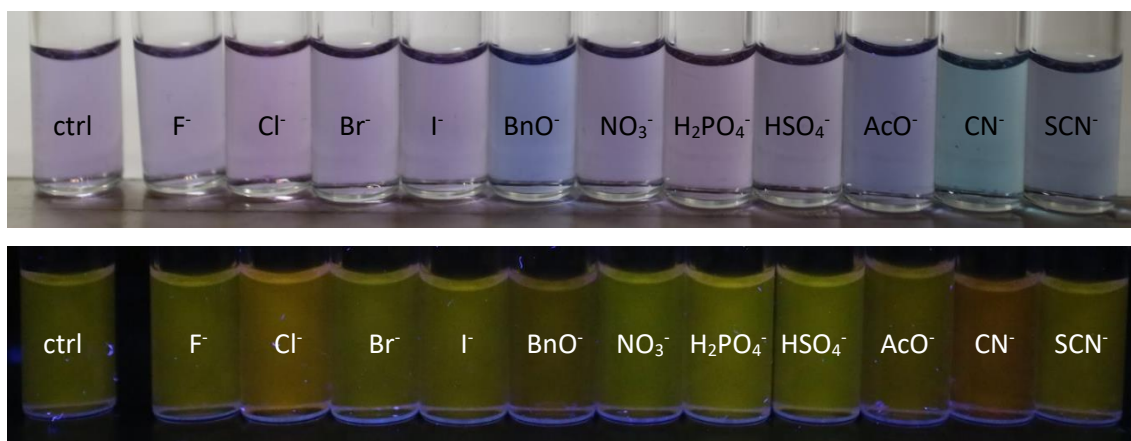


Fig. S4.15 Appearance of 20 μM solutions of **3PEG-Ru-CH=CH-per^{lm}** in acetone with different anions (80 μM) under visible light (above) and UV, 366 nm, light (below).

No significant change was observed for solutions of [Ru(CH=CH-PEG₃)Cl(CO)(py-per^{lm})(PPh₃)₂] (**3PEG-Ru-py-per^{lm}**) but a small increase with cyanide and acids such as H₂PO₄⁻ was noted:

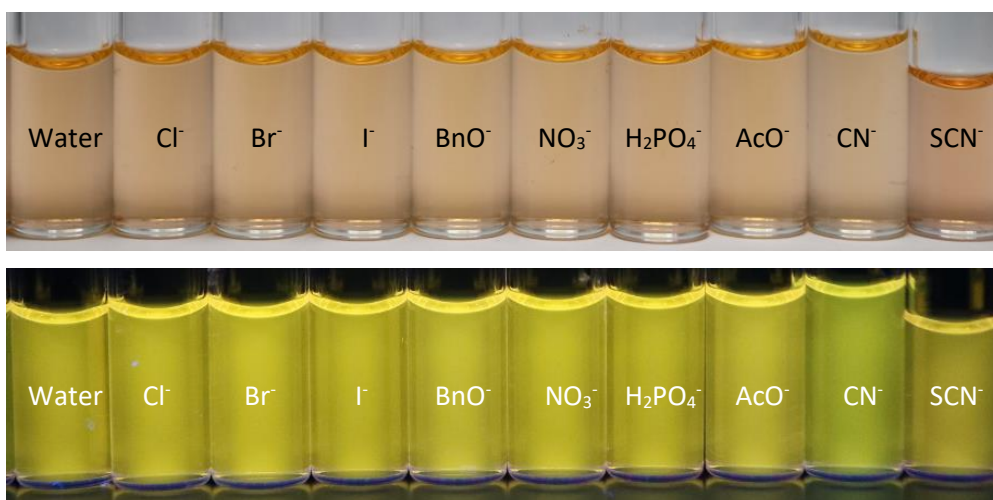


Fig. S4.16 Appearance of 20 μM solutions of **3PEG-Ru-py-per^{lm}** in acetone with different anions (80 μM) under visible light (above) and UV, 366 nm, light (below) after 72 hours.

S4.5 Titrations with different analytes

In addition to CO, several other π -acid analytes were studied to investigate the fluorescence response of the complexes. It was of particular interest to explore the detection of toxic substances found as gases or vapours as the risk of exposure is particularly great. The detection of carbon monoxide (CO), cyanide (CN^-) and a representative isonitrile ($t\text{BuNC}$) was studied. In all cases the mechanism proceeded via substitution of the pyridyl group, but there were also significant differences in the products (Figure S4.17):

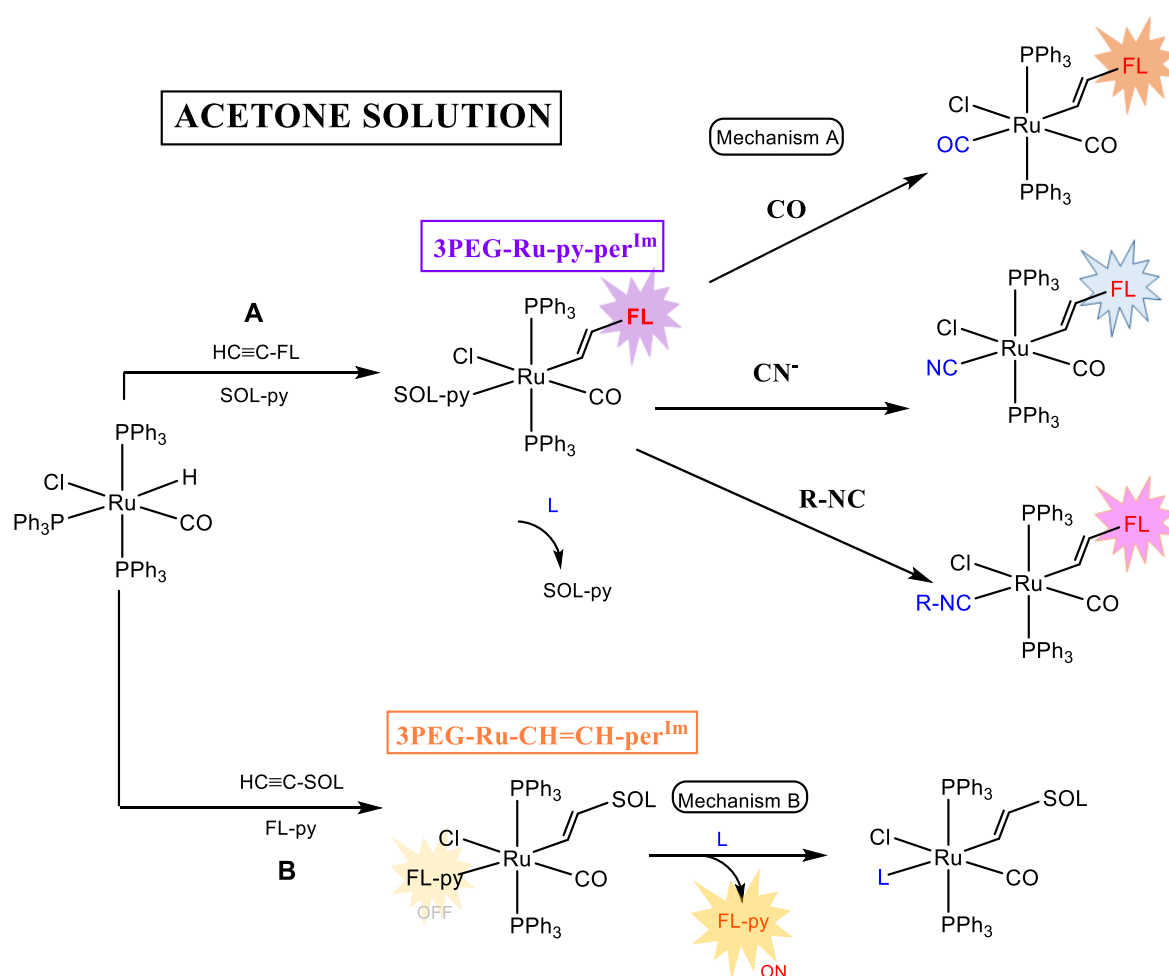


Fig. S4.17 Scheme of the fluorescent response of probes **3PEG-Ru-CH=CH-per^{Im}** and **3PEG-Ru-py-per^{Im}** to various analytes.

Below can be seen a comparison of the changes in fluorescence and colour in the presence of these substances (Figures S4.18 and S4.19).

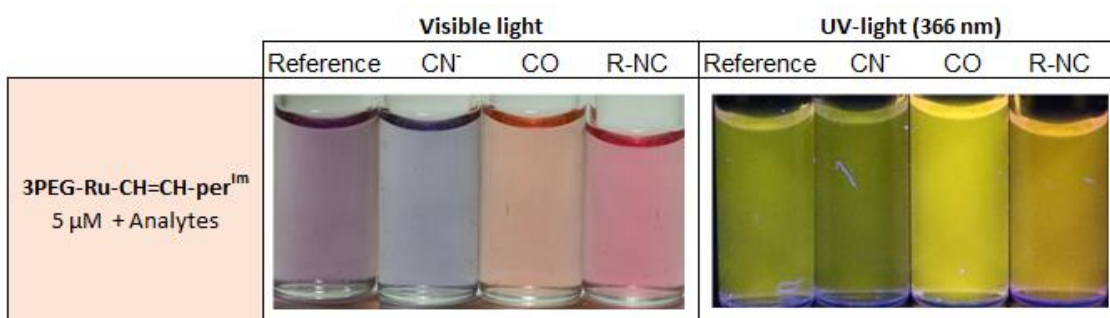


Fig. S4.18 Colour and fluorescence changes for **3PEG-Ru-CH=CH-per^{Im}** with different analytes (20 μM of CN⁻ or *t*BuNC; CO was bubbled for 15 minutes).

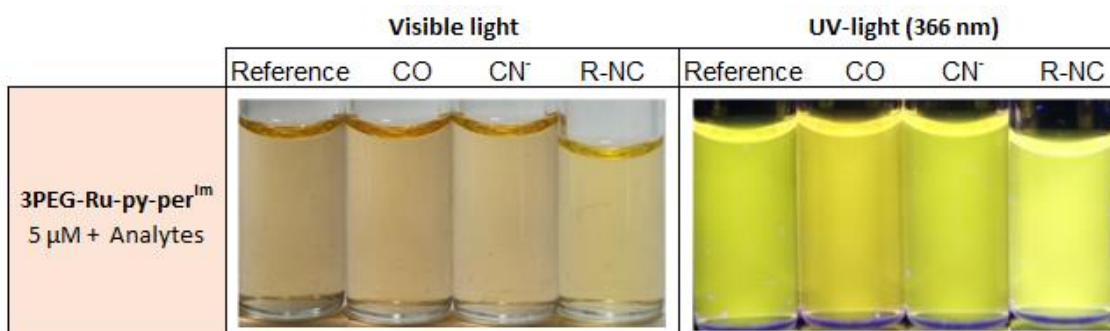


Fig. S4.19 Colour and fluorescence changes for **3PEG-Ru-py-per^{Im}** with different analytes (20 μM of CN⁻ or *t*BuNC; CO was bubbled for 15 minutes).

Several titrations were performed in solution adding a cyanide salt (NBu₄CN) and a dilute isonitrile (*t*BuNC) solution. Absorption and fluorescence spectra were first measured for these compounds (Figure S4.20).

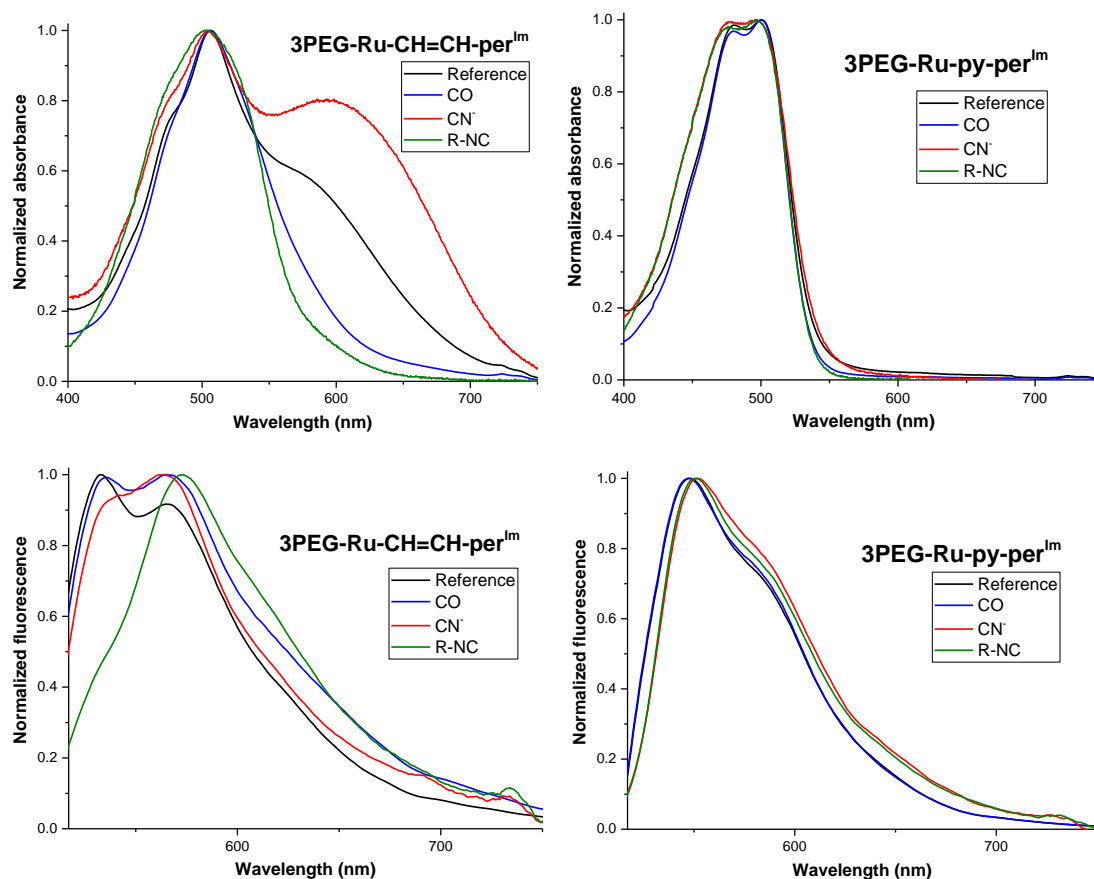


Fig. S4.20 Normalized absorption and fluorescence spectra of **3PEG-Ru-CH=CH-per^{Im}** on the left and **3PEG-Ru-py-per^{Im}** on the right.

In the case of cyanide and *t*BuNC, the response was evaluated by titration adding the compound in solution as a dissolved salt in acetone (NBu₄CN) and as a diluted liquid (*t*BuNC), respectively. This allowed the calculation of an experimental Limit of Detection (LOD).

Titration with cyanide

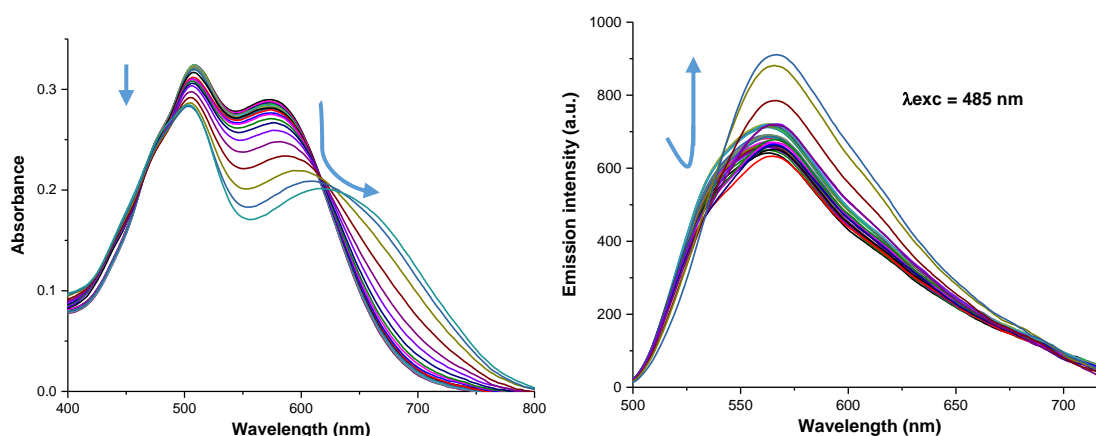


Fig. S4.21 Absorption (left) and fluorescence (right) spectra of **3PEG-Ru-CH=CH-per^{Im}** with an increasing concentration of **CN⁻**.

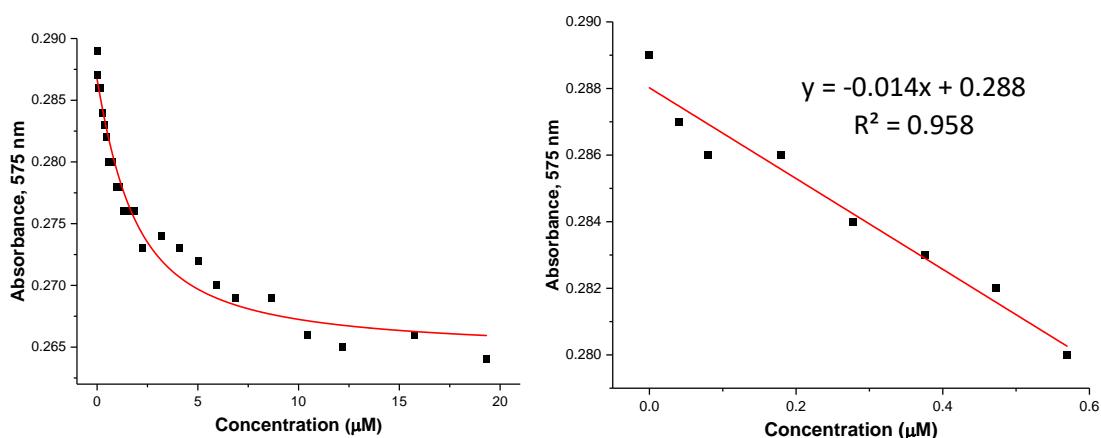


Fig. S4.22 Titration of **3PEG-Ru-CH=CH-per^{Im}** with increasing concentration of **CN⁻**. Absorption fitting for the calculation of the LOD.

The absorption spectra changed with the increasing concentration of cyanide, showing a shift of the band from 575 to 620 nm, with a decrease in the maximum of absorption. The variation in fluorescence was low and associated to the increasing absorption at more than 620 nm, being overlapped emission/absorption. The experimental LOD was found to be **0.29 μM for CN⁻** with a 5% of false positive-negative.^{S4}

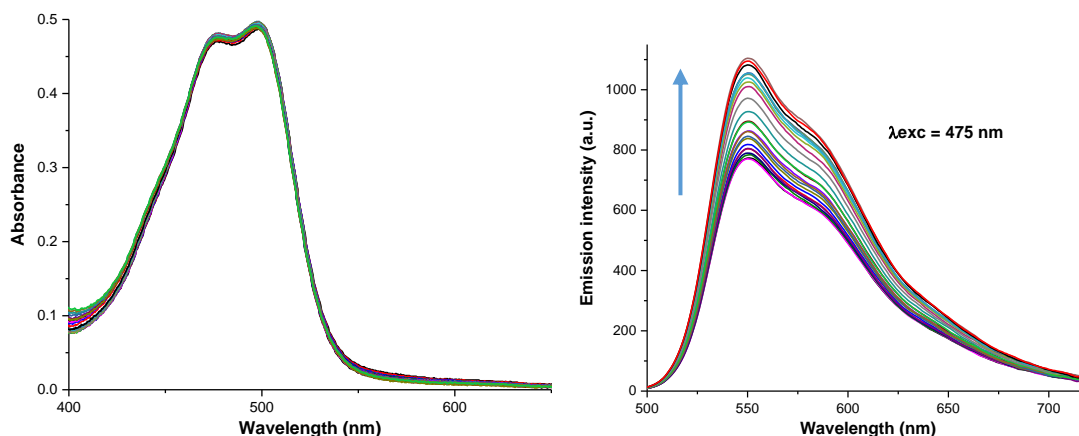


Fig. S4.23 Absorption (left) and fluorescence (right) spectra of **3PEG-Ru-py-per^{Im}** with an increasing concentration of CN⁻.

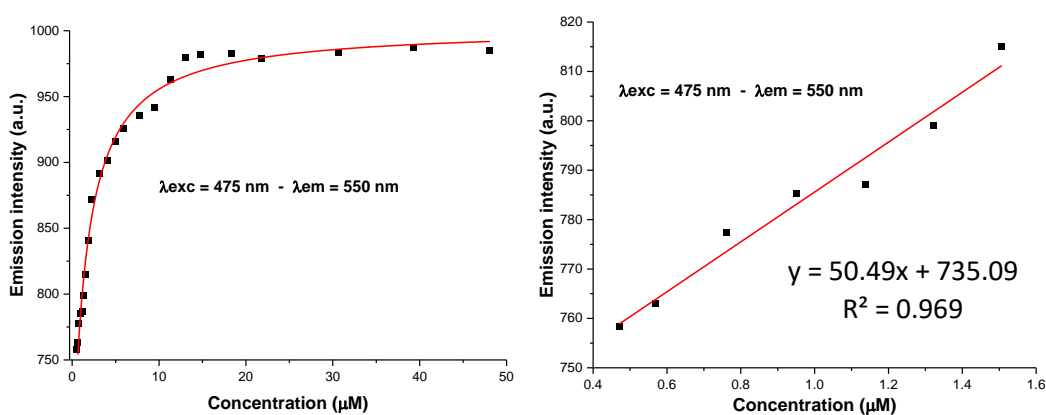


Fig. S4.24 Titration of **3PEG-Ru-py-per^{Im}** with increasing concentration of CN⁻.
Fluorescence fitting for the calculation of the LOD.

The absorption spectra barely changed but the emission increased by 50% from 0 to 10 μM. The experimental LOD was calculated to be **0.41 μM for CN⁻** with a 5% of false positive-negative.^{S4}

Titration with isonitrile

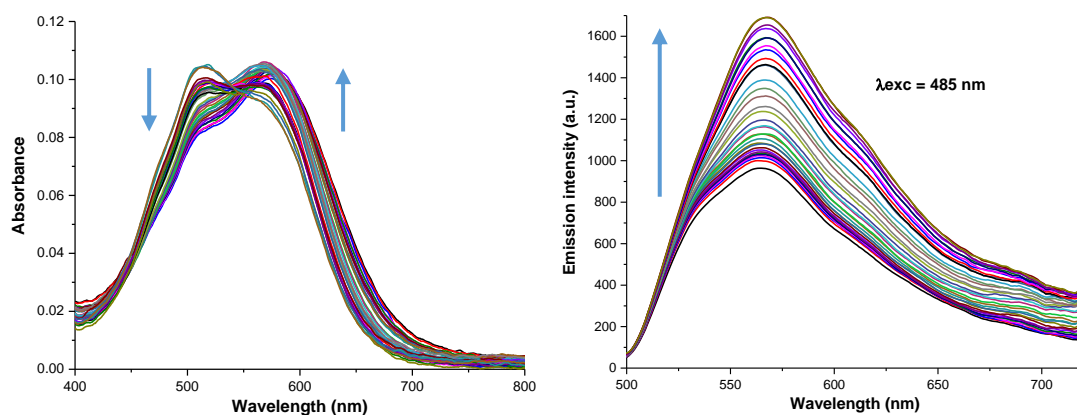


Fig. S4.25 Absorption and fluorescence spectra showing the titration of **3PEG-Ru-CH=CH-per^{Im}** with increasing concentration of *t*BuNC.

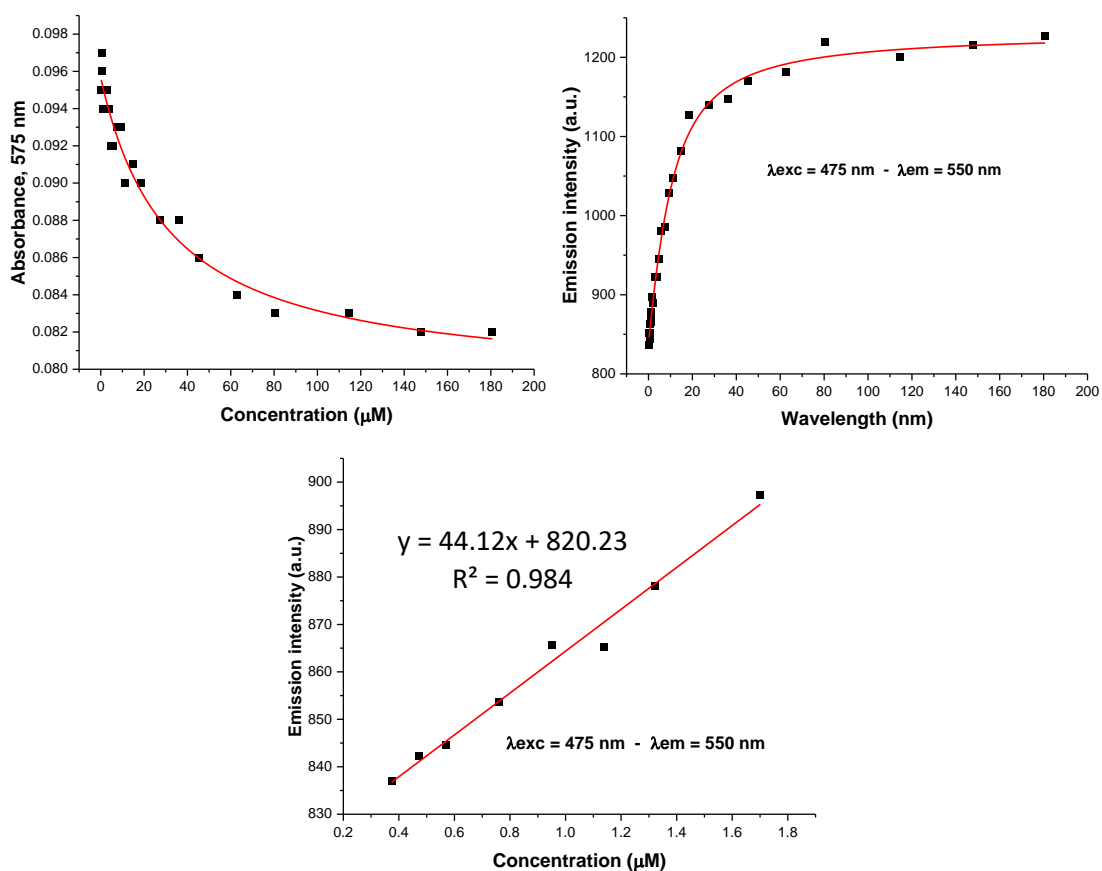


Fig. S4.26 Titration of **3PEG-Ru-CH=CH-per^{Im}** with increasing concentration of *t*BuNC. Fluorescence emission fitting for LOD calculation.

The absorption spectra displayed a band shift and the emission was found to increase by 50% from 0 to 40 μM . The experimental LOD was calculated to be **0.29 μM for *t*BuNC** with a 5% of false positive-negative.^{S4}

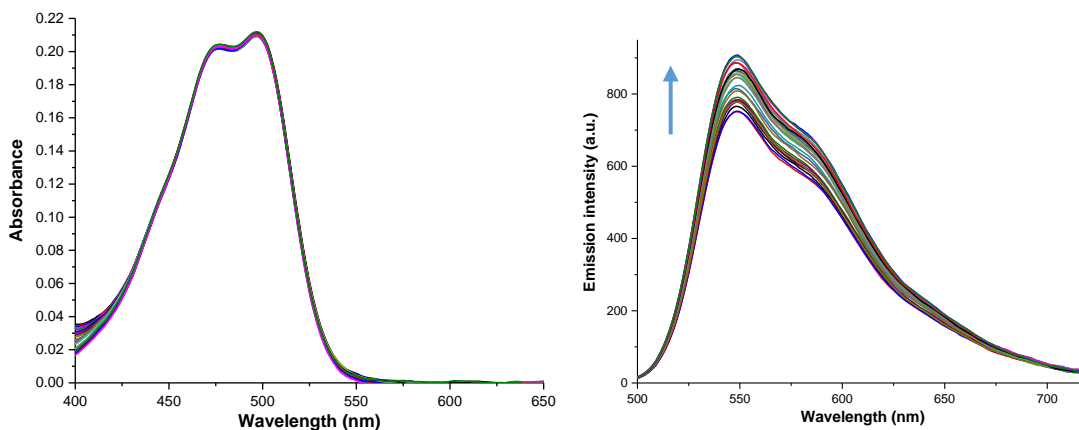


Fig. S4.27 Absorption and fluorescence spectra for **3PEG-Ru-py-per^{Im}** with increasing concentration of *t*BuNC.

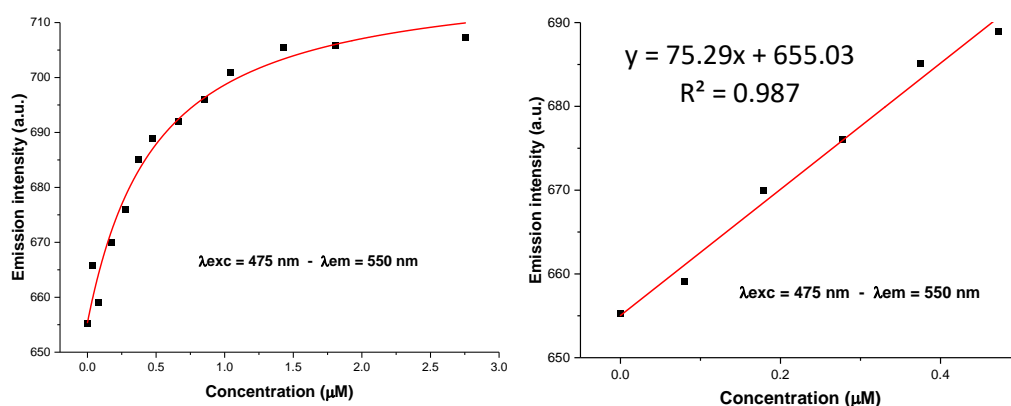
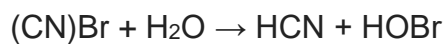


Fig. S4.28 Titration of **3PEG-Ru-py-per^{Im}** with increasing concentration of *t*BuNC. Fluorescence emission fitting for the calculation of the LOD.

The absorption spectra showed a band shift and the emission increased by 20% from 0 to 5 μM . The experimental LOD was **0.12 μM for *t*BuNC** with a 5% of false positive-negative.^{S4}

Additionally, the effect of adding cyanide in the form of BrCN was also tested (Figures S4.29 and S4.30) alongside the tests with the other vapours/gases. This

compound has a remarkable vapour pressure and is easily hydrolysed to form hydrogen cyanide:



As a consequence, the changes observed are different from adding other cyanide salts, being a mixture of a response to acid and cyanide properties.

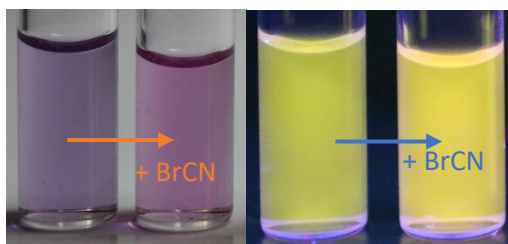


Fig. S4.29 A 5 μM Acetone solution of **3PEG-Ru-CH=CH-per^{lm}** before and after adding 2 mg of BrCN.

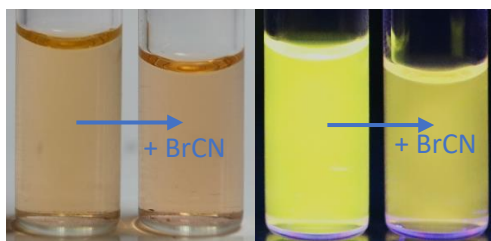


Fig. S4.30 A 5 μM Acetone solution of **3PEG-Ru-py-per^{lm}** before and after adding 2 mg of BrCN.

S4.5 Measurements of immobilised probes

The compounds **3PEG-Ru-CH=CH-per^{lm}** and **3PEG-Ru-py-per^{lm}** were absorbed onto silica supported on aluminium sheet (TLC plates with silica gel 60, Merck). The absorption was performed using 2 mg of compound dissolved in 25 mL toluene into which TLC plates (5x5 cm) were submerged and left overnight at 60 °C. The solution became colourless and the TLC absorbed the compound (Figure S4.31).

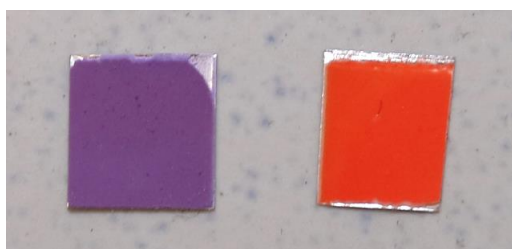


Fig. S4.31 Photograph of the TLC plates with absorbed **3PEG-Ru-CH=CH-per^{lm}** and **3PEG-Ru-py-per^{lm}**

For the supported probes the response was found to be different compared to the solutions. For the evaluations, the tests were performed following the procedure shown in Figures S4.32 and S4.33.



Fig. S4.32 Preparation and photos of the measurement vial using the immobilised probes.

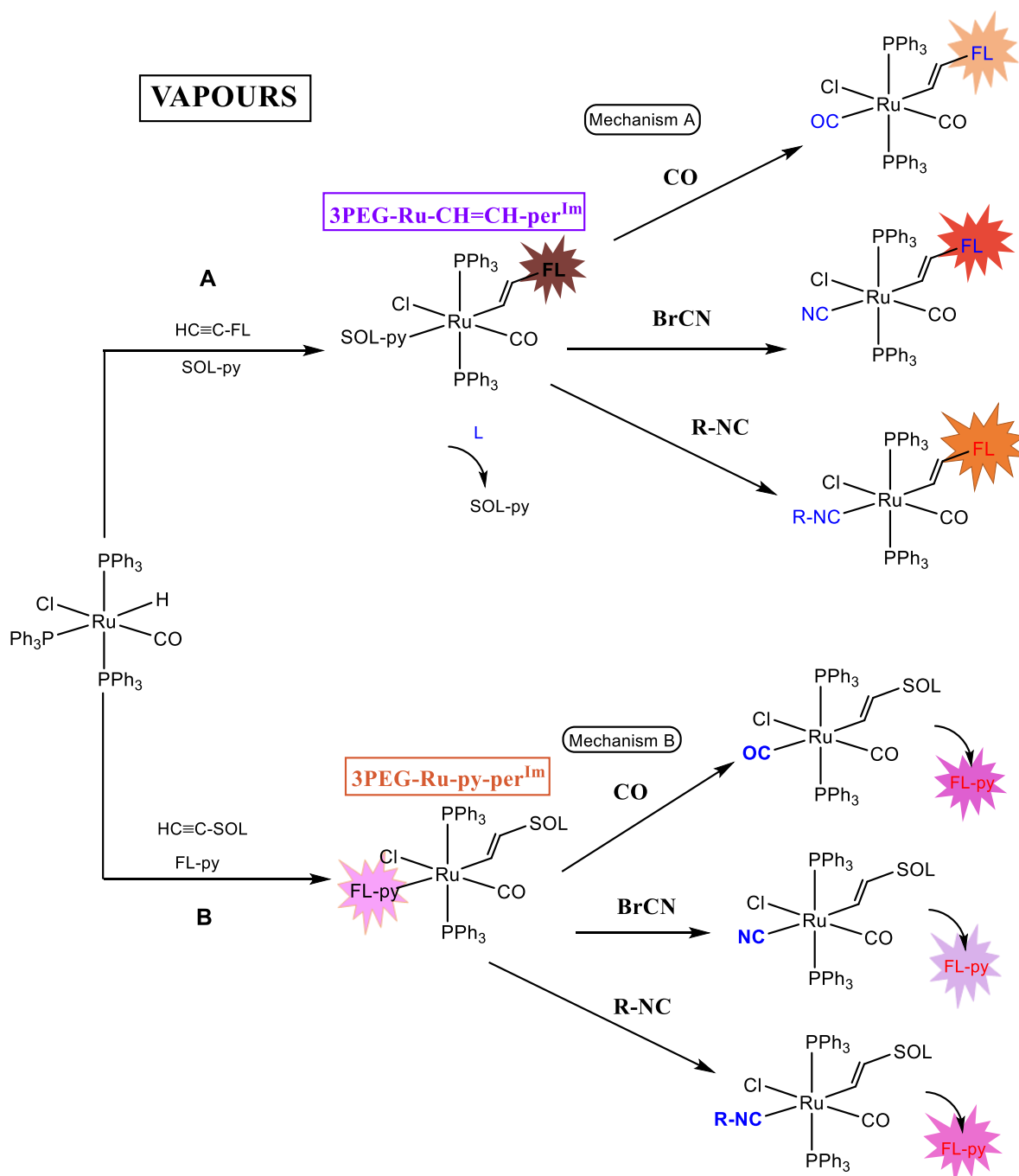


Fig. S4.34 Scheme showing the changes in fluorescence of the immobilised probes with absorbed **3PEG-Ru-CH=CH-per^{Im}** and **3PEG-Ru-py-per^{Im}** in presence of different gases.

The process was found to depend mainly on the vapour pressure of the substance/temperature and it could be followed by how it changed with time. First, the changes were studied qualitatively in presence of the different gases for 6 hours (Figures Fig. S4.35 and Fig. S4.36).

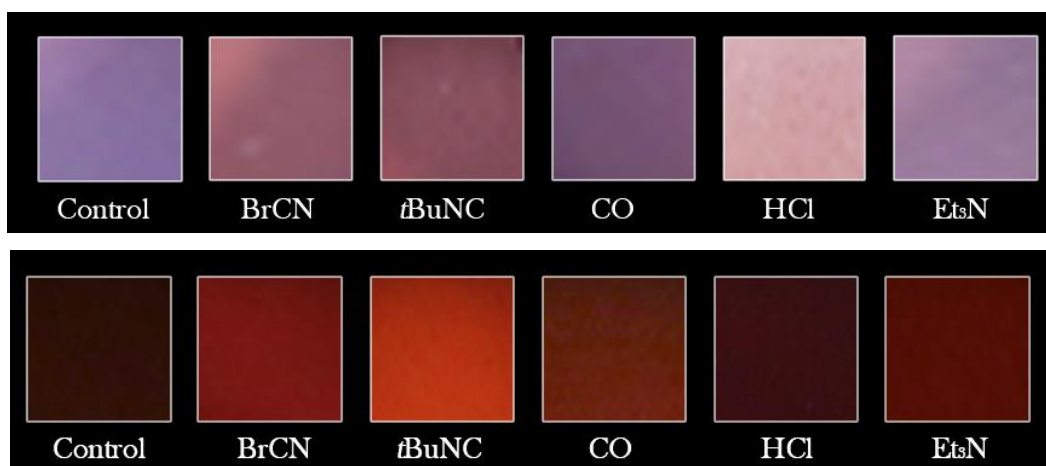


Fig. S4.35 Immobilised **3PEG-Ru-CH=CH-per^{lm}** under visible (above) and 366 nm UV light (below) after 6 hours exposed to different gases.



Fig. S4.36 Immobilised **3PEG-Ru-py-per^{lm}** under visible (above) and 366 nm UV light (below) after 6 hours exposed to different gases.

The process could be followed over time by measuring in an atmosphere saturated with these vapours at room temperature. The vials contained:

- 20 μ L of *t*BuNC
- 5 mg of BrCN

The effect of these vapours was measured after different time periods between several minutes to 5 hours to obtain changes in absorption/fluorescence.

Tests with BrCN

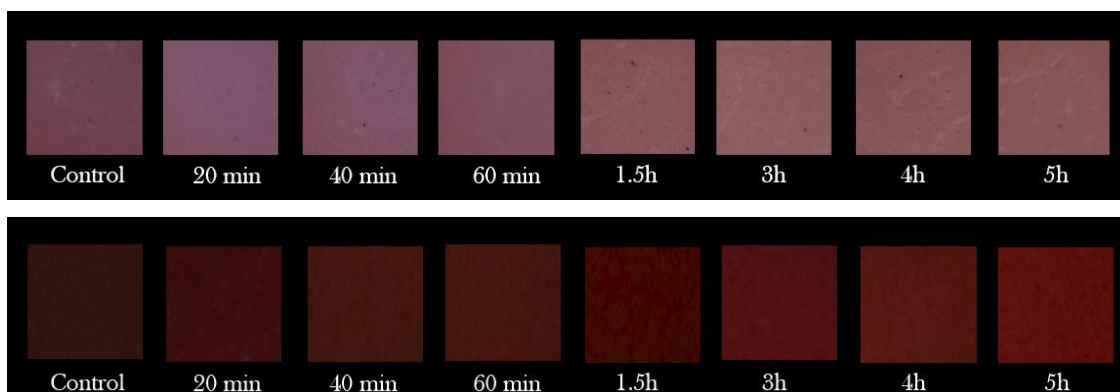


Fig. S4.37 Images of immobilised **3PEG-Ru-CH=CH-per^{Im}** in visible (above) and 366 nm UV light (below) after different time periods exposed to BrCN vapour.

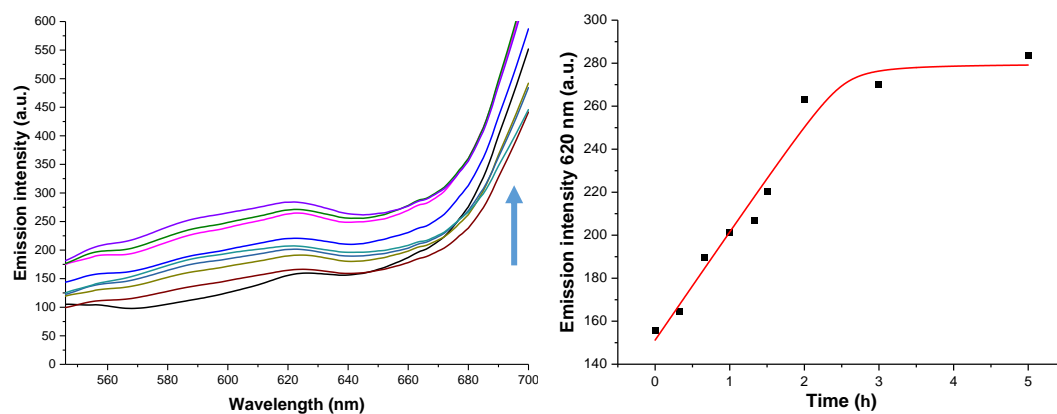


Fig. S4.38 Emission spectra ($\lambda_{\text{exc}} = 515 \text{ nm}$) of immobilised **3PEG-Ru-CH=CH-per^{Im}** after different time periods with BrCN vapour.

The fluorescence increases slightly, mostly in the IR region. The increase is noticeable after half an hour and reaches its maximum after 2 hours.

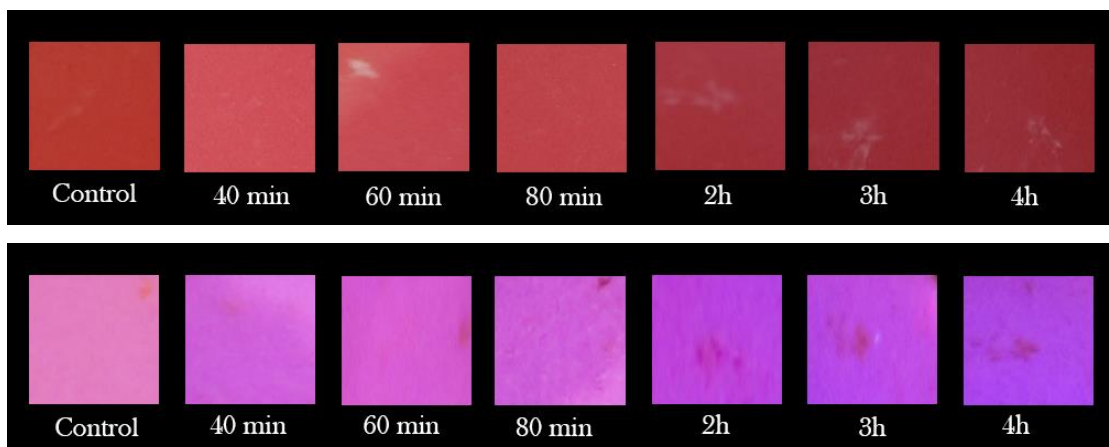


Fig. S4.39 Images of immobilised **3PEG-Ru-py-per^{Im}** in visible (above) and 366 nm UV light (below) after different time periods exposed to BrCN vapour.

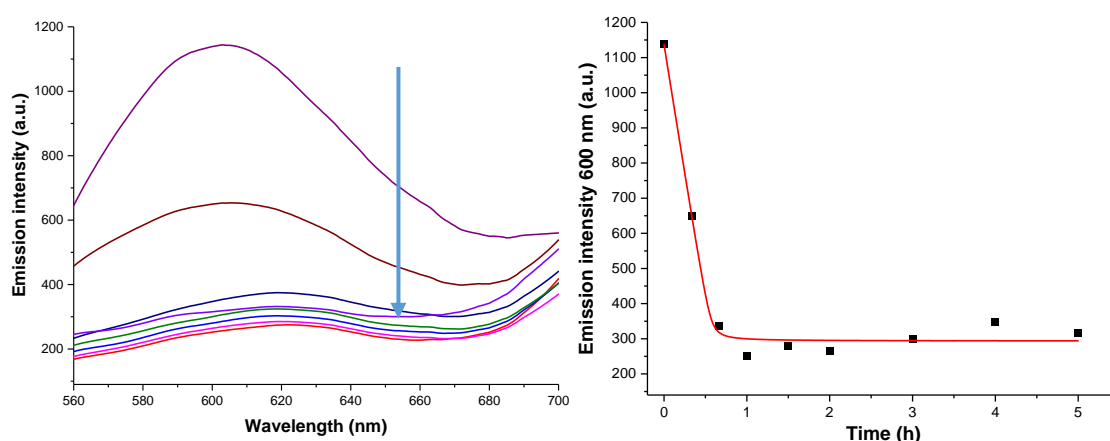


Fig. S4.40 Emission spectra ($\lambda_{exc} = 520$ nm) of immobilised **3PEG-Ru-py-per^{Im}** after different time periods with BrCN vapour.

For **3PEG-Ru-py-per^{Im}**, the fluorescence decreases substantially and rapidly. After 1 hour the fluorescence remained quenched and constant.

Tests with *t*BuNC

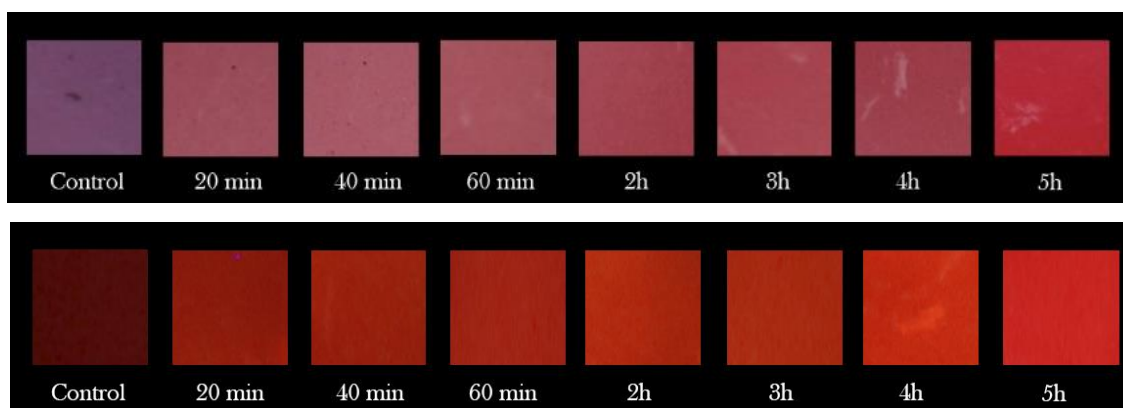


Fig. S4.41 Images of immobilised **3PEG-Ru-CH=CH-per^{Im}** in visible (above) and 366 nm UV light (below) after different time periods exposed to *t*BuNC vapour.

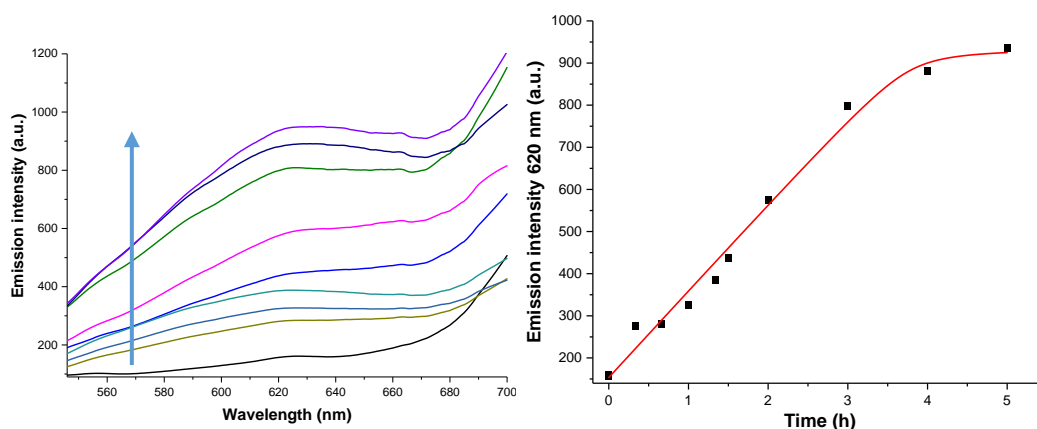


Fig. S4.42 Emission spectra ($\lambda_{\text{exc}} = 515 \text{ nm}$) of immobilised **3PEG-Ru-CH=CH-per^{Im}** after different time periods with *t*BuNC vapour.

The fluorescence was found to increase significantly. The increase is noticeable after half an hour and reaches its maximum after 3-4 hours.

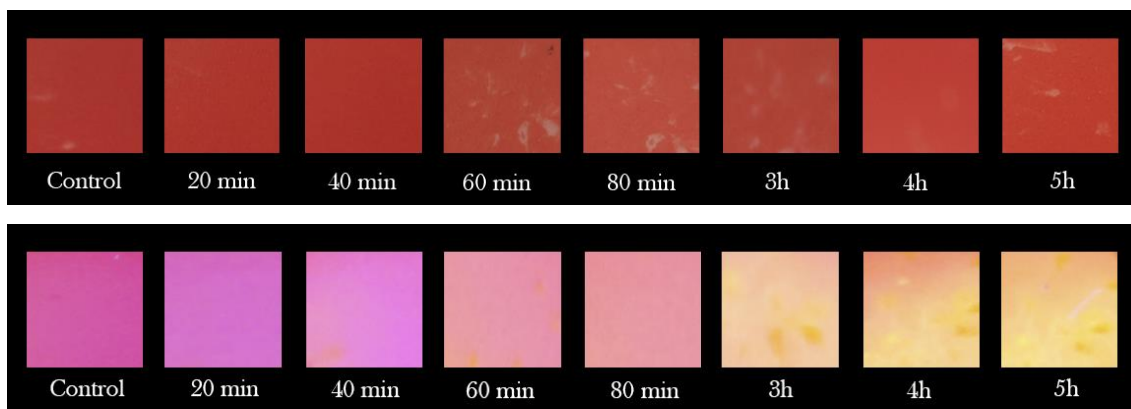


Fig. S4.43 Images of immobilised **3PEG-Ru-py-per^{lm}** in visible (above) and 366 nm UV light (below) after different time periods exposed to *t*BuNC vapour.

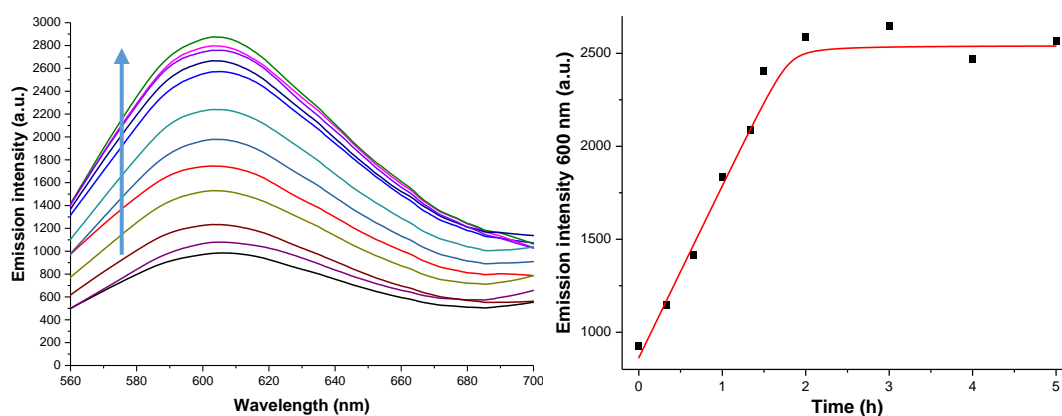


Fig. S4.44 Emission spectra ($\lambda_{\text{exc}} = 520 \text{ nm}$) of immobilised **3PEG-Ru-py-per^{lm}** after different time periods with *t*BuNC vapour.

The fluorescence increases substantially in the presence of *t*BuNC vapour. The increase is noticeable after half an hour and reaches its maximum after 2 hours.

Tests with carbon monoxide (CO)

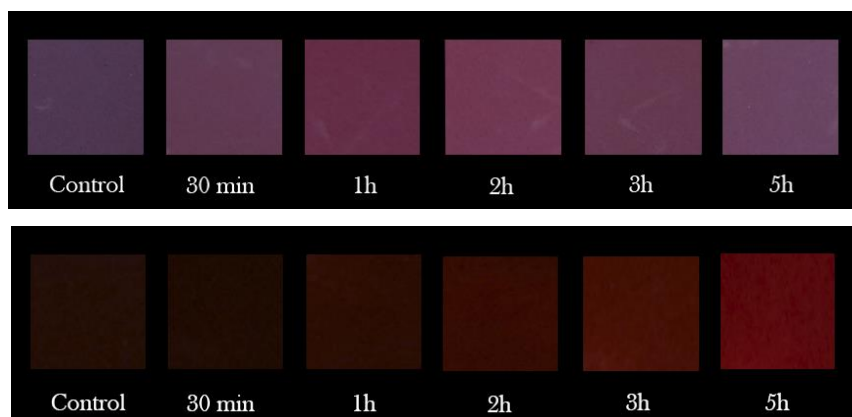


Fig. S4.45 Images of immobilised **3PEG-Ru-CH=CH-per^{lm}** in visible (above) and 366 nm UV light (below) after different time periods exposed to CO gas.

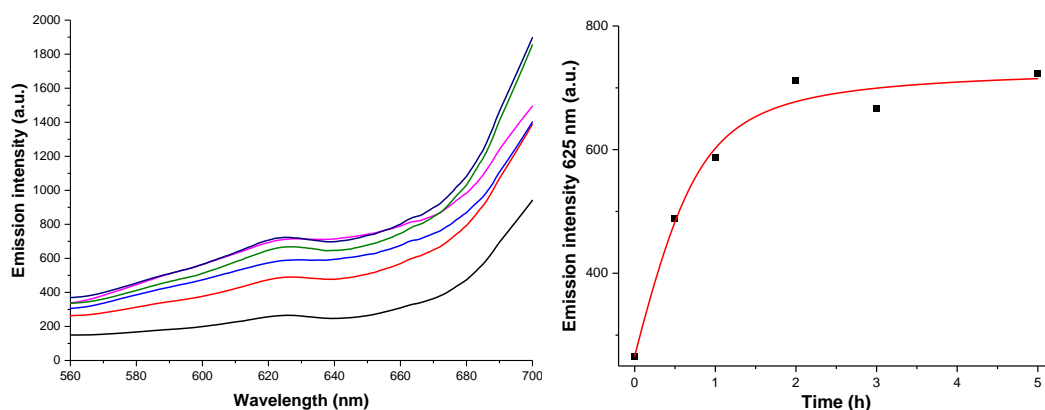


Fig. S4.46 Emission spectra ($\lambda_{\text{exc}} = 515 \text{ nm}$) of immobilised **3PEG-Ru-CH=CH-per^{lm}** after different time periods with CO gas.

The fluorescence increases slightly, mostly in the IR region. The increase is substantial in less than an hour and reaches its maximum 1 hour.

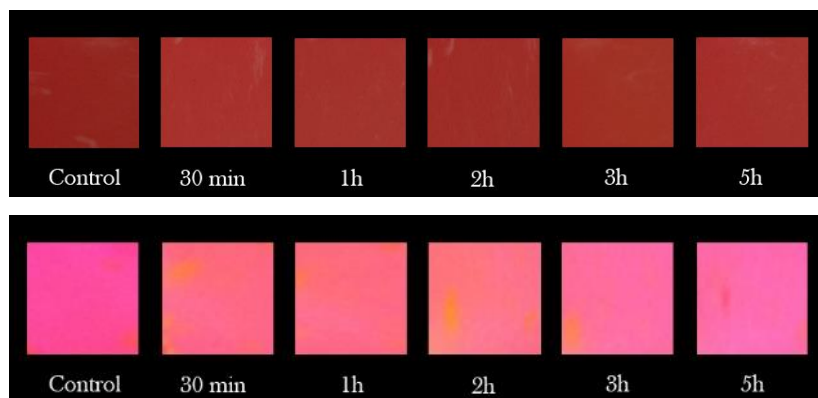


Fig. S4.47 Images of immobilised **3PEG-Ru-py-per^Im** in visible (above) and 366 nm UV light (below) after different time periods exposed to CO gas.

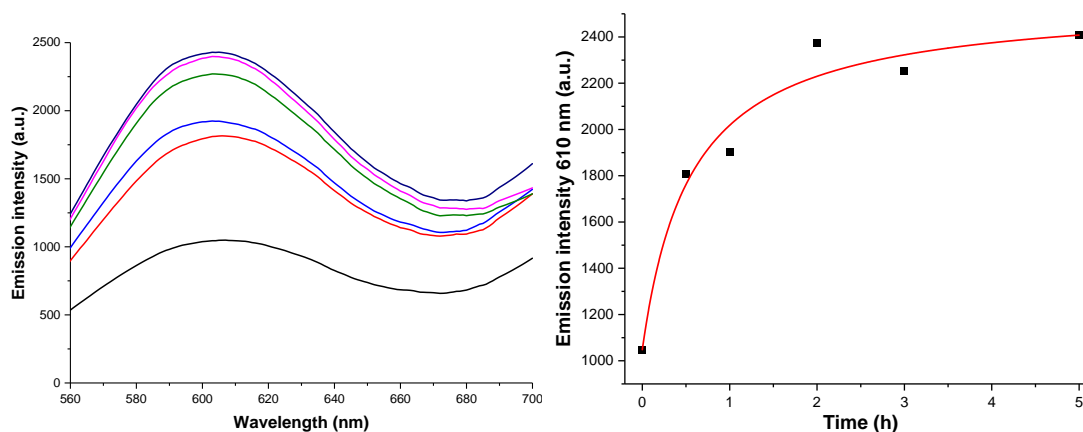


Fig. S4.48 Emission spectra ($\lambda_{exc} = 520$ nm) of immobilised **3PEG-Ru-py-per^Im** after different time periods with CO gas.

The fluorescence increases in the presence of CO gas. The increase is substantial within half an hour and reaches its maximum after 2 hours.

References

- S1. J. García-Calvo, P. Calvo-Gredilla, M. Ibáñez-Llorente, D. C. Romero, José V. Cuevas, G. García-Herbosa, M. Avella, T. Torroba, *J. Mater. Chem. A*, **2018**, 6, 4416–4423.
- S2. A. X. Zhang, R. P. Murelli, C. Barinka, J. Michel, A. Cocleaza, W. L. Jorgensen, J. Lubkowski, D. A. Spiegel, *J. Am. Chem. Soc.* **2010**, 132, 12711–12716.
- S3. a) D. K. Tosh, K. Phan, F. Deflorian, Q. Wei, L. S. Yoo, Z.-G. Gao, K. A. Jacobson, *Bioconjugate Chem.* **2012**, 23, 232–247. b) C. Deraedt, N. Pinaud, D. Astruc, *J. Am. Chem. Soc.* **2014**, 136, 12092–12098.
- S4. The calculation was performed using the software “R” v2.7. A least square regression was carried out and then the LODs were calculated by taking into account 5% or less possibilities of false positive-negative. The number was always within the range of the performed measurements, without considering the value at 0. In the same way than in other papers from the group: B. Díaz de Greñu, J. García-Calvo, J. Cuevas, G. García-Herbosa, B. García, N. Busto, S. Ibeas, T. Torroba, B. Torroba, A. Herrera, S. Pons, *Chem. Sci.*, **2015**, 6, 3757-3764.
- S5. a) K. R. Laing, W. R. Roper, *J. Chem. Soc. A* **1970**, 2149-2153; b) A. F. Hill, D. A. Tocher, A. J. P. White, D. J. Williams, J. D. E. T. Wilton-Ely, *Organometallics*, **2005**, 24, 5342-5355.
- S6. B. E. Cavit, K. R. Grundy and W. R. Roper, *J. Chem. Soc., Chem. Commun.*, 1972, 60.
- S7. M. E. Moragues, A. Toscani, F. Sancenón, R. Martínez-Máñez, A. J. P. White, J. D. E. T. Wilton-Ely; *J. Am. Chem. Soc.*, **2014**, 136, 11930–11933.